REPORT DOCUMENTATION PAGE

Form Approved
OMB No. 0704-0188

1. AGENCY USE ONLY (Leave blank)	2. REPORT DATE	3. REPORT TYPE AND DATES COVERED
		FINAL REPORT 01 Nov 92 - 30 Apr 96

4. TITLE AND SUBTITLE
Optoelectronic III-V Heterostructures by Gas-Source MBE

5. FUNDING NUMBERS
61102F
2305/FS

6. AUTHOR(S)
Professor Robinson

7. PERFORMING ORGANIZATION NAME(S) AND ADDRESS(ES)
Department of Electrical Engineering
Colorado State University
Fort Collins, CO 80523

8. PERFORMING ORGANIZATION REPORT NUMBER
AFOSR-TR-96
0402

9. SPONSORING / MONITORING AGENCY NAME(S) AND ADDRESS(ES)
AFOSR/NE
110 Duncan Avenue Suite B115
Bolling AFB DC 20332-0001

10. SPONSORING / MONITORING AGENCY REPORT NUMBER
F49620-93-1-0021

11. SUPPLEMENTARY NOTES

12a. DISTRIBUTION / AVAILABILITY STATEMENT
APPROVED FOR PUBLIC RELEASE: DISTRIBUTION UNLIMITED

12b. DISTRIBUTION CODE

13. ABSTRACT *(Maximum 200 words)*

The objective of this research program was to grow by molecular beam epitaxy (MBE) quantum well heterostructures of the alloy InGaAsP and related materials for use in high performance devices. The first task was to grow InGaAsP/GaAs and InGaAsP/InP structures for shallow quantum well (QW) optical modulators and other optoelectronics devices. The second task was to develop selective-area regrowth techniques for laternal definition of complex optoelectronic integrated devices. The method of growth was gas-source MBE, a technique which we have previously shown to produce high quality QW heterostructures containing alternating layers of III-V arsenide and phosphides.

14. SUBJECT TERMS

15. NUMBER OF PAGES

16. PRICE CODE

17. SECURITY CLASSIFICATION OF REPORT	18. SECURITY CLASSIFICATION OF THIS PAGE	19. SECURITY CLASSIFICATION OF ABSTRACT	20. LIMITATION OF ABSTRACT
UNCLASSIFIED	UNCLASSIFIED	UNCLASSIFIED	

DISCLAIMER NOTICE

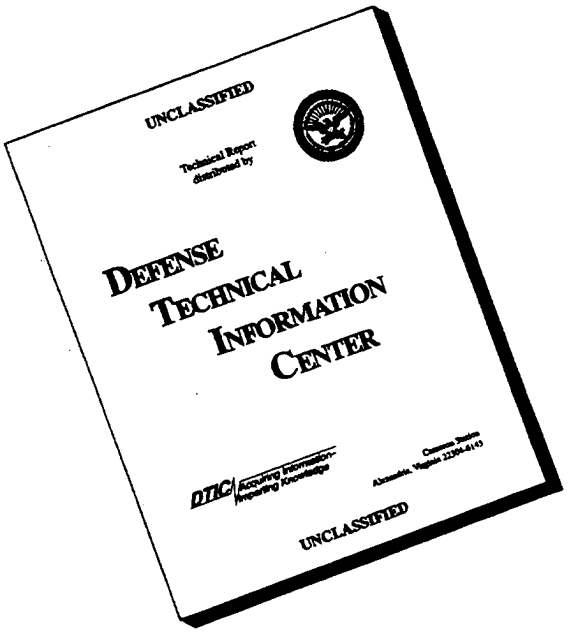

THIS DOCUMENT IS BEST QUALITY AVAILABLE. THE COPY FURNISHED TO DTIC CONTAINED A SIGNIFICANT NUMBER OF PAGES WHICH DO NOT REPRODUCE LEGIBLY.

afo_fr0.wp

Final Technical Report

AFOSR Contract # F49620-93-1-0021
1 November 1992 to 30 April 1996
USAF Office of Scientific Research

"Optoelectronic III-V Heterostructures by Gas-Source MBE"

Department of Electrical Engineering
Colorado State University
Fort Collins, CO 80523

PI: Gary Y. Robinson
Office: (970) 491-6575
FAX: (970) 491-2249
E-mail: gary@lance.ColoState.edu

Final Technical Report
1 November 1992 to 30 April 1996

"Optoelectronic III-V Heterostructures by Gas-Source MBE"

I. Research Objective

The objective of this research program was to grow by molecular beam epitaxy (MBE) quantum well heterostructures of the alloy InGaAsP and related materials for use in high performance devices. The first task was to grow InGaAsP/GaAs and InGaAsP/InP structures for shallow quantum well (QW) optical modulators and other optoelectronic devices. The second task was to develop selective-area regrowth techniques for lateral definition of complex optoelectronic integrated devices. The method of growth was *gas-source* MBE, a technique which we have previously shown to produce high quality QW heterostructures containing alternating layers of III-V arsenide and phosphides.

II. Major Accomplishments

Under this contract, we have concentrated on the development of several III-V material combinations for QW heterostructures in order to optimize optoelectronic device performance. Our major accomplishments for each material combination were as follows:

InGaP/InAlP and InGaP/InGaP Quantum Wells:

* Combined InGaP as the well material with InAlP as the barrier material and reported the *first* measurement of the band offset energies in this heterojunction system. InGaP/InAlP and InGaP/InGaAlP are grown on GaAs substrates and used in *visible* emitters, including edge emitting lasers (red) and LEDs (red, yellow, green).

* *First* report of L-band recombination in InGaP/InAlP QWs. Demonstrated that in unstrained narrow wells or in tensile-strained wide wells, the previously neglected L-band can dominate recombination and thus adversely affect laser operation.

* Extended our work, both theoretical and experimental, on the InAlP/InGaP system to include the introduction of controlled amounts of strain as a means to further tailor the heterostructure to meet device requirements.

* *First* results for optical modulators using $In_xGa_{1-x}P/In_yGa_{1-y}P$ ($x \neq y$) MQWs. In preliminary devices, transmission modulators on GaP substrates exhibited 15% modulation at 10V and 594 nm, and asymmetric reflection modulators on GaAs substrates showed 27% modulation at 20V at 605 nm, indicating suitability of InGaP QW MBE modulators for plastic optical fiber data transmission systems.

InGaAs/InGaP Quantum Wells:

* Reported the *first* strain-compensated QW heterostructures of the material combination InGaAs/InGaP, and obtained fewer defects than conventional InGaAs/GaAs modulators operating at a wavelength of 1 μm.

* Using Stark-effect red-shift modulators, obtained 42% modulation at 5V, and by using a superlattice, *first* observation of blue-shift modulation in the InGaAs/InGaP system.

* Careful measurements showed that the switching speed was slower and the modulation saturates at lower intensity levels in InGaAs/InGaP modulators than in conventional AlGaAs/GaAs structures, primarily because of the larger band offset energies.

InGaAsP/InGaAsP Quantum Wells:

* Demonstrated that GSMBE can produce atomically abrupt QW interfaces in the InGaAsP system; thus the randomness associated with composition does not limit the abruptness of heterointerfaces employing quaternary alloys.

Gas-Source MBE Technology

* Published a review of the gas-source MBE technology we developed under AFOSR sponsorship during the last 7 years.

Most of the work performed under this contract addressed the first task of our objective by obtaining a better understanding of the material properties of InGaP, InAlP, InGaAs, and InGaAsP heterostructures, and then used this improved understanding to design optical modulators for operation at given wavelength. The details of our work can be found in the reprints of the published papers included in this report.

For the second task as originally proposed, we fabricated lasers at 1.3 μm wavelength with the lowest yet reported threshold current for material grown by gas-source MBE. The lasers used InAsP/InGaAsP QWs, a material developed under a separate AF/DARPA contract (Hanscom Laboratory). The buried heterostructure growth process needed for the high performance lasers was to be developed under this contract, but we found the selectivity of the GSMBE growth process for the InGaAsP material was insufficient to produce the desired device structures. Instead, we carried out the growth of the critical InAsP/InGaAsP active region by GSMBE, and then had the buried heterostructure regrowth done by MOCVD, through a collaboration at Bell Laboratories. The resulting wafers were fabricated into lasers in our laboratories, and the device performance has been outstanding.

III. Publications Under AFOSR Sponsorship

(copies of publications are enclosed)

1. O. Buccafusca, J.A.L. Chilla, C.S. Menoni, J.J. Rocca, M.J. Hafich, L.M. Woods, and G.Y. Robinson, "Non-resonant Tunneling in InGaP/InAlP Asymmetric Double Quantum Wells", **Appl. Phys. Lett.** 62, 399 (25 Jan 1993).

2. J.W. Kim, C.W. Chen, T.J. Vogt, L.M. Woods, G.Y.Robinson, and D.L. Lile, "Strained Layer InGaAs/GaAs and InGaAs/InGaP Multiple Quantum Well Optical Modulators Grown by Gas-Source MBE," **IEEE Photonics Technol. Letters** 5 (9), 987 (September 1993).

3. C.W. Chen, J.W. Kim, P. Silvestre, M.J. Hafich, G.Y. Robinson, and D.L. Lile, "A Low Drive Voltage Electroabsorption Modulator Using an InGaAs/InP Superlattice," **J. Appl. Phys.** 74, 5895 (1 November 1993).

4. D. Patel, M.J. Hafich, G.Y. Robinson, and C.S. Menoni, "Direct Determination of the Band Discontinuities

in InGaP/InAlP Multiple Quantum Wells", Phys. Rev. B 48 (24), 18,031 (15 December 1993).

5. L.M. Woods, P.Silvestre, P. Thiagarajan, G.A. Patrizi, and G.Y. Robinson, "Photoluminescence and Interface Abruptness in InGaAsP/InGaAsP Quantum Wells", J. Electron. Materials 23 (11) 1229, (November 1994).

6. M.E. Watson, J.L.A.Chilla, J.J. Rocca, J-W Kim, D.L. Lile, T.J. Vogt, and G.Y. Robinson, "Saturation Intensity and time response of InGaAs/InGaP MQW modulators" IEEE J. Quantum Electron. 31 (2), 254-260 (February 1995).

7. G.Y. Robinson, "Gas-Source Molecular Beam Epitaxy", in the Handbook of Thin Film Process Technology: A Guide to Current Methods, D.A. Glocker, S.I. Shah, eds., Institute of Physics, Bristol and Philadelphia, 1995, pp A.2.2.1-A.2.2.22.

8. D. Patel, K. Interhozingher, P. Thiagarajan, G.Y. Robinson, and C.S. Menoni, "L-Band Recombination in InGaP/InAlP Multiple Quantum Wells", Physical Rev. B, 53 (19), 12633-12636 (15 May 1996).

9. J.W. Kim, Y.J. Lee, T.J. Vogt, G.A. Patrizi, G.Y. Robinson, and D.L. Lile, "Wannier-Stark localization in a strained InGaAs/InGaP superlattice", J. Appl. Phy. 79 (9), 7161-7163 (1 May 1996).

10. T.J. Vogt, P.Thiagarajan, and G. Y. Robinson, "MBE Growth of InGaP MQW Structures on GaP for Optical Modulators", accepted for publication in J. Vac. Sc. Technol., (May/June 1996).

11. C.M. Menoni, O.F. Buccafusca, M.C. Marconi, D. Patel, J.J Rocca, G.Y. Robinson, and S.M. Goodnick, "Effects of Indirect G-L and G-X Transfer on the Carrier Dynamics of InGaP/InAlP Multiple Quantum Wells", submitted to Appl. Phy. Letts., 1996.

IV. Conference Presentations and Invited Talks Under AFOSR Sponsorship

1. K. Mahalingam, N. Otsuka, M.J. Hafich, and G.Y. Robinson, "Correlation of Spontaneous Ordering in InGaAlP Alloys with Surface Reconstruction", APS Meeting, Seattle, March 1993.

2. J.W. Kim, C.W. Chen, T.J. Vogt, L.M. Woods, G.Y.Robinson, and D.L. Lile, "Strained Layer InGaAs/GaAs and InGaAs/InGaP Multiple Quantum Well Optical Modulators Grown by Gas-Source MBE," Fifth International Conference on Indium Phosphide and Related Materials, Paris, France, April 1993.

3. M. Prasad, O.E. Martinez, C.S. Menoni, J.J. Rocca, J.L.A. Chilla, M.J. Hafich, and G.Y. Robinson, "Transient Grating Measurements of Ambipolar Diffusion and Carrier Recombination in InGaP/InAlP MQWs and InGaP Bulk Material", Electronic Materials Conference, Santa Barbara, June 1993.

4. T.J. Vogt, J. K. Kim, L.M. Woods, G.A. Patrizi, D.L. Lile, and G.Y. Robinson, "Strain-Compensated InGaP/InGaAs Multiple Quantum Well Modulators Grown by Gas-Source MBE", Electronic Materials Conference, Santa Barbara, June 1993.

5. C.S. Menoni, D. Patel, M.J. Hafich, and G.Y. Robinson, "Band Offsets in InGaP/InAlP Quantum Wells Using High Pressure", presented at High Pressure Science and Technology Conference, Colorado Springs, June 1993.

6. M.E. Watson, J.L.A. Chilla, J.J. Rocca, J-W Kim, D.L. Lile, T.J. Vogt, and G.Y. Robinson, "Modulation-Saturation Measurements on InGaAs/InGaP MQW Modulators", IEEE LEOS Conference on

Lasers and Electro-optics, Anaheim, May 1994.

7. M.E. Watson, J.L.A. Chilla, J.J. Rocca, J-W Kim, D.L. Lile, T.J. Vogt, and G.Y. Robinson, "Saturation Intensity and Time Response of InGaAs/InGaP MQW Modulators", Electronic Materials Conference, Boulder, June 1994.

8. O. Buccafusca, J.E. Fouquet, G.A. Patrizi, L.M. Woods, C.S. Menoni, J.J. Rocca, and G.Y. Robinson, "Optical Properties of Lattice-Matched InGaP/InAlP Multiple Quantum Wells", Electronic Materials Conference, Boulder, June 1994.

9. L.M. Woods, P.Silvestre, P. Thiagarajan, G.A. Patrizi, G.Y. Robinson, K.M. Jones, and M. Al-Jassim, "Interface Abruptness in InGaAsP/InGaAsP Quantum Wells as Determined by Photoluminescence", North American Conference on Molecular Beam Epitaxy, Urbana, IL, October 1994.

10. G. Y. Robinson, "Band Offset Energies in InGaP/InAlP Quantum Wells" (invited talk) Center for Compound Semiconductor Microelectronics, University of Illinois, Champaign-Urbana, November 1994.

11. K. Interholzinger, D. Patel, C.S. Menoni, O. Buccafusca, P. Thiagarajan, T.J. Vogt, L.M. Woods, G.Y. Robinson, and J.E. Fouquet, "Band structure and band alignments of strained and lattice-matched InGaP/InAlP heterostructures", Electronic Materials Conference, Charlottesville, Virginia, June 1995.

12. O. Buccafusca, M.C. Marconi, D. Patel, C.S. Menoni, M. Prasad, J.J. Rocca, and G.Y. Robinson, "Effect of G-X coupling on carrier lifetime of InGaP/InAlP multiple quantum wells", Electronic Materials Conference, Charlottesville, Virginia, June 1995.

13. T.J. Vogt, P. Thiagarajan, and G.Y. Robinson, "Visible (λ=575nm) Multiple Quantum Well Modulators on GaP Substrates by Gas-Source MBE", North American Conference on Molecular Beam Epitaxy, College Park, MD, September 1995.

14. D. Patel, K. Interhozingher, P. Thiagarajan, G.Y. Robinson, and C.S. Menoni, "Direct Identification of the L-Band in InGaP/InAlP Multiple Quantum Wells", APS Meeting, St. Louis, MO, March 1996.

15. D. Patel, K. Interhozingher, P. Thiagarajan, G.Y. Robinson, and C.S. Menoni, "L-Band Recombination in $In_xGa_{1-x}P$/InAlP Multiple Quantum Wells", Electronic Materials Conference, Santa Barbara, CA, June 1996.

16. D. Patel, K. Interhozingher, P. Thiagarajan, G.Y. Robinson, and C.S. Menoni, "L-Band Recombination in $In_xGa_{1-x}P$/InAlP Multiple Quantum Wells", High Pressure Physics Conference, Schwabisch-Gmung, Germany, July 1996.

V. Awards

G. Y. Robinson, elected Fellow of IEEE, January 1996, for "contributions to the field of microelectronic materials".

VI. Technology Transfer

The first technology transfer under this contract was to Charles Cerny and Fritz Schuermeyer at Wright Labs and consisted of custom designed epitaxial InGaP wafers for p-channel FET fabrication. The FETs were to be evaluated for a use in a CMOS GaAs-based technology. At present, the wafers are being processed.

The second technology transfer was to Hewlett-Packard Laboratories where Julie Fouquet evaluated our InAlP/InGaP QW heterostructures by PLE. From our combined efforts to measure the band offsets, HP wanted to confirm how far the wavelength could be decreased in InGaAlP LEDs and still obtain sufficient light output. We are now examining the use of strain to further decrease the wavelength. Hewlett-Packard is the only American manufacturer of commercial LEDs.

VII. Personnel

Gary Y. Robinson, Professor, Principal Investigator

Gary A. Patrizi, Research Associate, MSEE from Colorado State University, US citizen (now at Philips Semiconductor, Albuquerque, NM).

Prabhu Thiagarajan, Graduate Student Research Assistant and Research Associate, Electrical Engineering, non-US citizen with green card.

Larry M. Woods, Graduate Student Research Assistant, US citizen, received MS in Electrical Engineering, December 1994 (now at Golden Photonics, Golden CO).

Tim J. Vogt, Graduate Student Research Assistant, Electrical Engineering, PhD candidate, US citizen (to be employed at Honeywell, Minneapolis, MN).

Joel Fastenau, Graduate Student Research Assistant, Electrical Engineering, PhD candidate, US citizen.

Daryl Pulver, Student Technician, US citizen.

VIII. Research Results

The majority of the results obtained under this contract have been published or have been accepted for publication in the near future. These results were summarized above and the details can be found in previous annual contract reports and in the reprints of our published papers provided in the next section. Here we will highlight our most recent research results which have yet to be published.

We have fabricated reflection modulators operating at near 600 nm, the wavelength for low loss transmission in plastic optical fibers, by growing InGaP QWs on "GaAsP substrates". The "GaAsP substrates" are commercially available GaAs wafers with thick epitaxial layer (about 100 μm) of $GaAs_{0.6}P_{0.4}$. We then grow a thick buffer layer of $In_{0.3}Ga_{0.7}P$ which lattice matches to the "GaAsP substrate" and avoids the generation of misfit dislocations obtained with growth directly on GaP and GaAs substrates. A MQW region is then grown on the buffer, with tensile-strained well layers of $In_{0.4}Ga_{0.6}P$ and compressively strained barrier layers of $In_{0.2}Ga_{0.8}P$. With the proper choice of well and barrier thickness, operation at the desired wavelength can be obtained with a MQW stack of zero net strain. This combination of materials has proved to be the most successful approach we have yet explored in attempting to obtain optical modulation at short wavelengths with the InGaP system.

As shown in the figure, the device consists of a pin diode, with the InGaP/InGaP MQW stack as the i-region and p^+ and n^+ InGaP layers used for ohmic contacts. To increase the contrast ratio of the reflection modulator, a Fabry-Perot optical cavity is formed between two mirrors, a distributed Bragg reflector (DBR) below the pin structure and the air-semiconductor interface above. The DBR consists of 19.5 pairs of λ/4 layers of $In_{0.3}Ga_{0.7}P$ and $In_{0.3}Al_{0.7}P$. The reflectivity spectra of the two mirrors are chosen to match the change in MQW absorption with bias resulting from the quantum confined

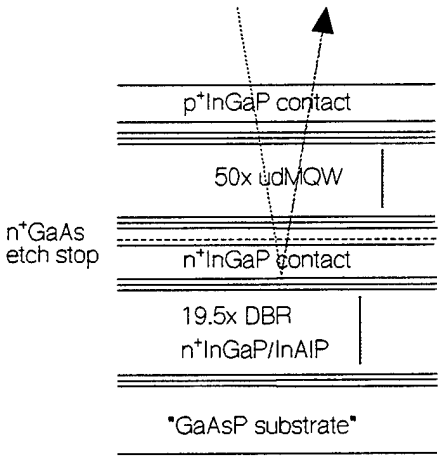

Stark effect. The device is an asymmetrical Fabry-Perot reflection modulator.

The measured reflection spectrum is shown in the figure. At a wavelength of 603 nm, the maximum change in reflectivity is 27% and the contrast ratio is 2.0 for a change in applied voltage of 20 V. This is the largest modulation yet achieved with the InGaP materials system, and is state-of-the-art performance for Stark-effect modulators in the 570-650 nm range. With improvements in the mirrors, we expect to achieve substantially larger contrast ratios. Such a device could then be used in short-haul plastic fiber data transmission systems by serving as both a photodetector for incoming signals and a modulator (by using some of the downstream light) for outgoing signals. Such two-way transmission networks using only one optical source and many optical modulators operating in reflection mode would minimize the use of low reliability and expensive components in robust networks.

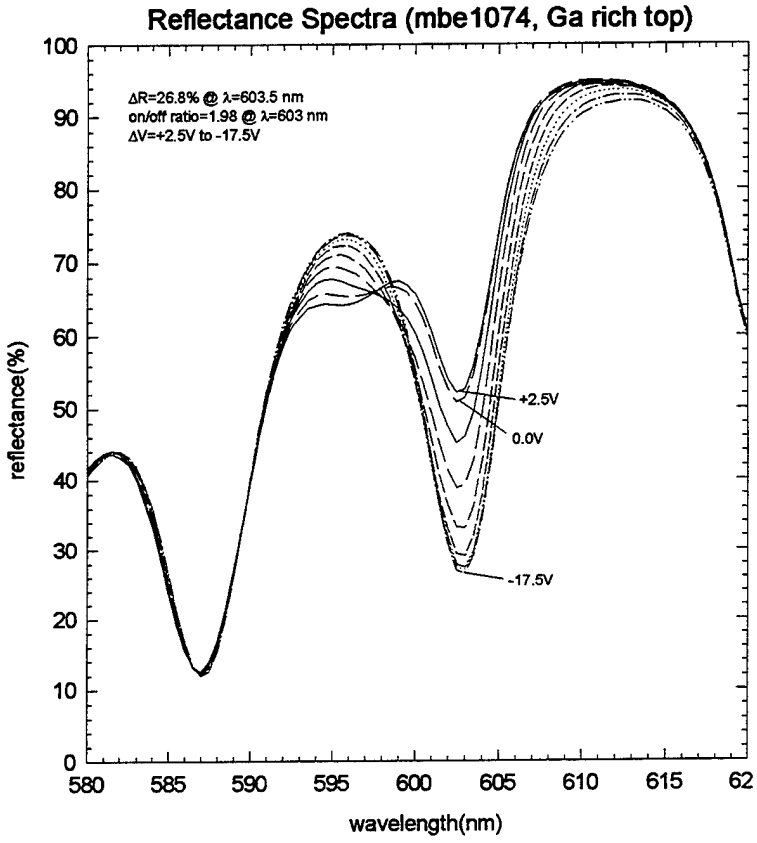

IX. Copies of Publications:

PHYSICAL REVIEW B VOLUME 48, NUMBER 24 15 DECEMBER 1993-II

Direct determination of the band discontinuities in $In_xGa_{1-x}P/In_yAl_{1-y}P$ multiple quantum wells

D. Patel, M. J. Hafich, G. Y. Robinson and C. S. Menoni
Center for Optoelectronic Computing Systems and Department of Electrical Engineering, Colorado State University, Fort Collins, Colorado 80523
(Received 20 July 1993)

The band structure of $In_{0.53}Ga_{0.47}P/In_{0.50}Al_{0.50}P$ multiple quantum wells grown by molecular-beam epitaxy has been determined from pressure-dependent-photoluminescence measurements at low temperature. The photoluminescence signals from the direct-gap well and the indirect barrier were monitored as a function of pressure up to 4 GPa. High pressure transformed the multiple quantum well from a type I to a staggered aligned, type II at 1.1 GPa. This transition was evidenced by the appearance of a photoluminescence signal due to the recombination of carriers separated in momentum and space. The simultaneous detection of this transition and that of the barrier material, allowed the direct determination of a valence-band offset energy of (0.24±0.05)eV, without requiring any information on parameters of the bulk materials. Considering that the total band-gap discontinuity for this heterostructure system is 0.50 eV at 20 K, an approximate band-gap splitting of 52:48 is determined to be the band lineup at the $In_xGa_{1-x}P/In_yAl_{1-y}P$ interface. Variations in the pressure coefficients of the indirect transitions in the barrier indicated that the valence band alignment changes with pressure at a rate of ≈18 meV/GPa, due to shifting of the heavy- and light-hole states with biaxial strain induced in the epilayers by applying pressure.

I. INTRODUCTION

The possibility of using quantum confinement to vary the effective band gap of $In_xGa_{1-x}P/In_yAl_{1-y}P$ heterostructures in the wavelength range 540–650 nm makes this system suitable for the engineering of optoelectronic devices which operate in the visible region of the optical spectrum. $In_xGa_{1-x}P$ heterostructures have been used as the wide-band-gap component of edge-emitting[1] and vertical-cavity-surface-emitting semiconductor lasers[2] and have also been employed in the design of heterojunction bipolar transistors.[3] In spite of the broad application of this material, basic knowledge of fundamental parameters such as the band discontinuities which are required for the design of efficient devices are still unknown.

We report the first, to our knowledge, direct determination of the band discontinuities in $In_xGa_{1-x}P/In_yAl_{1-y}P$ multiple quantum wells (MQW's) from low temperature photoluminescence (PL) measurements performed at high pressure. The valence band offset of this heterostructure was directly deduced from the PL signals corresponding to different transitions within the well and barrier obtained by excitation with three different lines of an argon ion laser.

High pressure photoluminescence measurements offer the possibility of determining the band-gap discontinuities in multiple quantum well structures which show a type-I alignment for the direct gap and a type-II alignment for the indirect X minima.[4] This method uses high pressure to modify the band structure of the heterostructure materials to obtain a band alignment in which the lowest conduction band state and the highest valence band state are separated in space. Under this condition indirect recombination of the spatially separated carriers is possible. Monitoring the variation with pressure of this indirect transition in addition to the recombination of carriers in the barrier material allows the determination of the energy of the barrier X minima at atmospheric pressure with respect to the well and barrier valence band, respectively. The valence band offset can then be directly calculated as the energy difference between these two transitions. The main advantage of the high pressure technique is that it does not require any assumptions concerning the bulk parameters nor does it require theoretical modeling or a special configuration of the sample as needed in some of the other techniques which have been used to determine the band offsets.[5–10] Using this technique the band alignment of several heterostructure systems such as $GaAs/Al_xGa_{1-x}As$,[4] $GaAs/In_xGa_{1-x}P$,[11] and more recently $GaAs/Ga_xAs_{1-x}P$ (Ref. 12) have been determined.

The rest of this paper is organized as follows: in Sec. II the sample characteristics and the high pressure photoluminescence experiments are described, the results are presented and discussed in Sec. III and Sec. IV summarizes the main findings of this work.

II. EXPERIMENTAL DETAILS

The $In_{0.53}Ga_{0.47}P/In_{0.50}Al_{0.50}P$ MQW samples were grown by gas-source molecular-beam epitaxy on a semi-insulating (100) GaAs substrate. The MQW's were composed of 30 periods of 8.5 nm wells and 22.5 nm barriers. An In-Al-P capping layer of 210 nm was also deposited. The samples were unintentionally n-doped with a background concentration of 10^{16} cm^{-3}. Transmission elec-

0163-1829/93/48(24)/18031(6)/$06.00

tron microscopy, and photoluminescence measurements indicated that the $In_xGa_{1-x}P$ material is mostly disordered. A detailed description of the growth and characterization of these samples is given in Ref. 13.

For the high pressure photoluminescence measurements, the GaAs substrate was removed by chemical etching and a small portion (100×150 μm) of the epilayer was placed in the gasketed diamond anvil cell (DAC).[14] A small piece of ruby was positioned next to the sample for the measurement of pressure, and a second ruby chip placed in the DAC body outside the pressure chamber was used as the zero pressure reference.[14] A sample of bulk $In_xGa_{1-x}P$ was also placed outside the pressure chamber for the measurement of the band gap of this material. Argon was used as the pressure transmitting medium. The choice of this pressure medium along with the reduced thickness of the sample were required to guarantee quasihydrostatic conditions at low temperature and at the highest pressure of 4 GPa achieved in these experiments. The DAC was cryogenically cooled to 20 K with a close-cycle He refrigerator. Using a specially designed cryostat chamber the pressure in the cell was changed while still at low temperature. Our ability to vary the pressure at low temperature avoided any hysteresis problems which may be encountered in systems requiring room temperature pressurization subsequent to cooling and measuring.

The PL from the multiple quantum wells was excited using three different lines from an Ar^+ laser, 514, 488, and 458 nm, each with a constant power of 3.5 mW. This variation in the wavelength allowed the excitation of different transitions in the well and barrier materials. The PL was dispersed using a 0.75 m spectrometer equipped with a 1200 g/mm grating and detected by a thermoelectrically cooled photomultiplier tube. Standard chopping techniques and a lock-in amplifier were used to analyze the signal.

III. RESULTS AND DISCUSSION

Typical PL spectra at different pressures obtained by excitation with the different Ar^+ lines are shown in Fig. 1. Curves *a*, *b*, and *c* were obtained with an excitation energy of 2.41 eV (514 nm). At low pressures the main PL feature, labeled E_1, corresponds to recombination in the well involving the $n = 1$ lowest confined conduction band state and the 1hh heavy hole valence band state. For pressures higher than 1.1 GPa a second much weaker and broader peak (E_2) appears at an energy of 2.09 eV. For pressures higher than 2.3 GPa another transition of characteristics similar to those of the E_2 peak is detected at an energy of 2.2 eV. This peak was labeled E_3. Both E_2 and E_3 were resolvable even at the highest pressure of 4 GPa. Excitation of the carriers with 2.54 eV (488 nm) photons resulted in PL spectra (not shown) with the same features as those shown in curves *a*–*c*.

When the PL was excited with 2.7 eV (458 nm) photons an additional broad peak at 2.35 eV is also observed. This peak, which was labeled E_4, is shown in Fig. 1, curve *d*, along with the E_1 peak and a much weaker peak

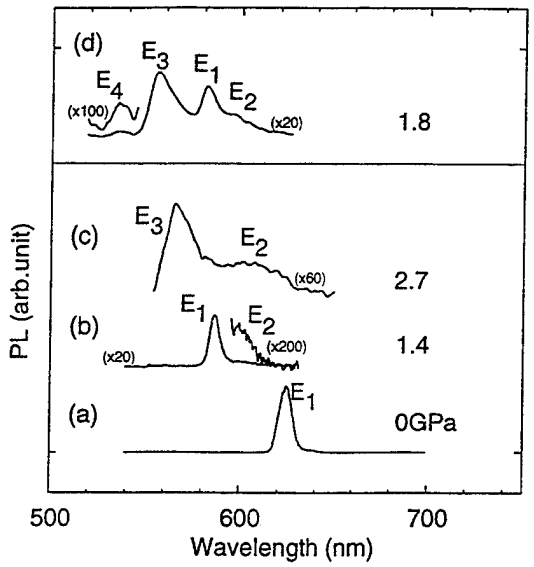

FIG. 1. Typical PL spectra of $In_xGa_{1-x}P/In_yAl_{1-y}P$ multiple quantum wells at different pressures at 20 K. Curves *a*–*c* were obtained with excitation of the carriers with a photon energy of 2.41 eV (514 nm) and curve *d* was obtained with an excitation of 2.7 eV (458 nm) photons.

at 2.27 eV which corresponds to the E_3 transition. For the highest excitation energy of 2.7 eV, it is possible to excite carriers in the well with sufficient excess energy to scatter to the indirect X level as well as to excite carriers within the barrier. The unique identification of these PL transitions, as shown below, requires the knowledge of the corresponding pressure coefficients.

A weak but resolvable peak at 1.94 eV is also observed in the PL spectra near zero pressure, for all three different excitation energies. Olsthoorn *et al.*[15] have speculated on the nature of this transition in $In_xGa_{1-x}P$ alloys as an isolated center whose PL was both temperature and excitation independent. The fact that this transition is only observable at very low pressures suggests that this transition is possible only when the $n = 1$ level is resonant with the center. Regardless, the origin of this PL peak remains speculative.

The measured energy variation with pressure of the $E_1 - E_4$ transitions is shown in Fig. 2. The energy of the E_1 transition shows the characteristic direct gap behavior, increasing with pressure at a rate of (92±3) meV/GPa. The remaining transitions, on the other hand, show negative pressure coefficients, a behavior which is characteristic of an X-like band. The highest energy transition E_4 is identified as that corresponding to recombination between electrons in the barrier X level (X_b) and holes in the barrier valence band. The atmospheric pressure value of the energy of these minima agrees very well with previous determination of the band structure of bulk $In_yAl_{1-y}P$.[16] At about 1.1 GPa the onset of the first direct-to-indirect crossover (E_1-E_2) occurs. The transition E_2 is identified as that involving states from the X_b level in the barrier and the 1hh valence band states in the well. This PL is the result of the recombination of carriers which are separated in momen-

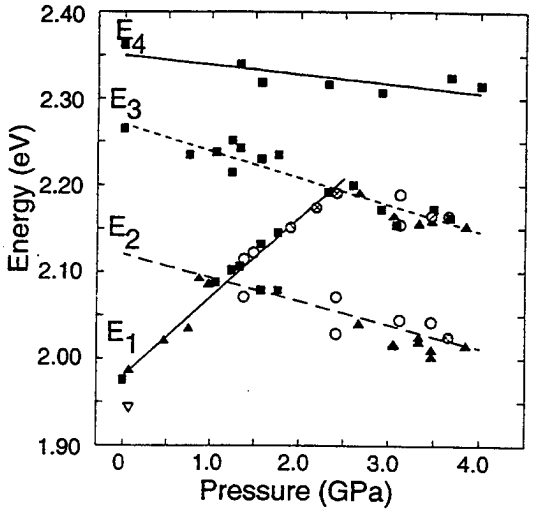

FIG. 2. Variation with pressure of the measured PL transition energies from $In_{0.53}Ga_{0.47}P/In_{0.5}Al_{0.5}P$ multiple quantum wells. Results of different excitations are indicated with different symbols: square, 458 nm; circle, 488 nm; and triangle, 514.5 nm. Four energy bands are clearly identified. The lines correspond to the least squares fit of the data from which the pressure coefficient and the energy at atmospheric pressure of each of the transitions were obtained.

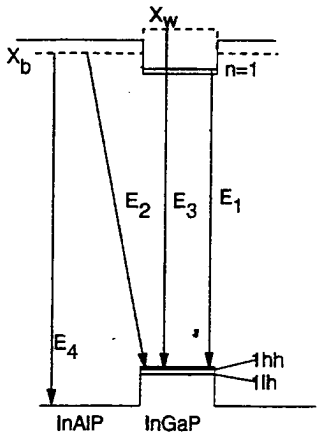

FIG. 3. Schematic diagram of the band structure of $In_xGa_{1-x}P/In_yAl_{1-y}P$ MQW's showing the PL transitions observed at 20 K at different pressures. The valence band offset can be directly determined from E_2 and E_4 with a small correction due to the heavy hole band confinement energy.

tum and space, that is, at this pressure the type-I MQW is transformed into a type-II staggered aligned system. A second direct-to-indirect crossover ($E_1 - E_3$) is observed at 2.3 GPa. This crossover, which is accompanied by the quenching of the E_1 PL signal, is assigned to the crossing of the $n = 1$ level and the well X minima (X_w). The corresponding crossover in bulk $In_xGa_{1-x}P$ at low temperatures occurs at 2.6 GPa.[17] The lower transition pressure of this direct-to-indirect crossover in the MQW is a consequence of the larger pressure coefficient of the direct gap of $In_xGa_{1-x}P$ in a confined structure when compared with bulk material.[17] Thus the transition E_3 is assigned to recombination of carriers from the X_w minima into the well valence band. Figure 3 schematically shows the different PL transitions observed in $In_xGa_{1-x}P/In_yAl_{1-y}P$ multiple quantum wells in these experiments.

Corroborative evidence of the $E_1 - E_2$ direct-to-indirect crossover was obtained by monitoring the PL intensity as a function of pressure. A sharp reduction in the E_1 PL peak intensity is observed at 1.1 GPa, as shown in Fig. 4. This behavior in the PL intensity is typical of a direct-to-indirect crossover and has been previously observed in other III-V materials.[18,19] Also shown in this figure is the PL peak intensity corresponding to the E_2 transition, which is approximately constant in the pressure range of these measurements.

Another feature which establishes our assignment of the E_2 transition was obtained by monitoring the dependence of the PL peak intensity of the indirect transitions on excitation power. Figure 5 shows the excitation power dependent PL at 2.4 and 3.12 GPa for the two indirect transitions E_2 and E_3. It is clear that the PL peak intensity from the indirect transition E_3 within the well is constant with excitation power; however, the indirect transition E_2 from the barrier into the well is excitation power dependent. The observed blueshift in the PL peak intensity of this transition is attributed to band bending due to an electric field created at the interface by the spatially separated carriers and has been previously observed in the GaAs/AlAs quantum well system[20] and in $GaAs/In_xGa_{1-x}P$ MQW's at high pressure.[21] The absence of any redshift in the peak intensity of the E_3 transition indicates negligible lattice heating.

The pressure coefficients of the different transitions were obtained from the slope of the least square fit to the data. The y intercept of these fits yielded the energy of the different electronic levels in the well and barrier at at-

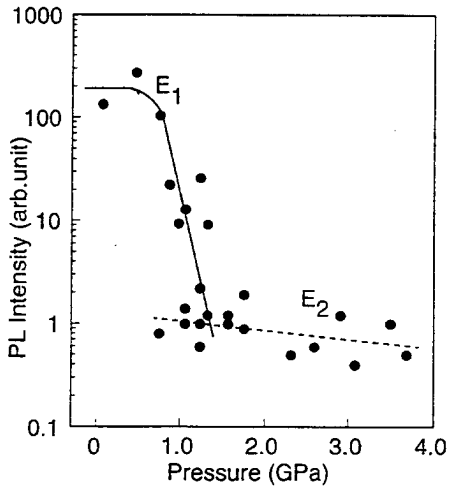

FIG. 4. Pressure dependence of the PL peak intensity from the main direct transition E_1 and that corresponding to the indirect transition E_2 between the barrier and the well. A two-orders-of-magnitude decrease in the peak intensity is observed at about 1 GPa due to the direct-to-indirect transitions between the barrier and the well. Lines through the data are only a guide to the eye.

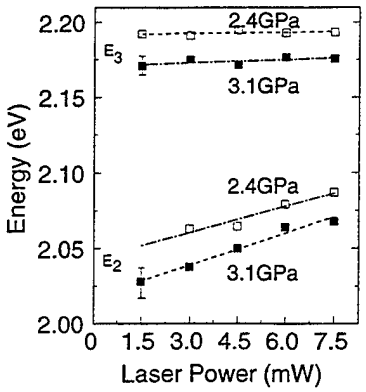

FIG. 5. Excitation power dependent PL at 2.4 and 3.1 GPa. The E_2 PL peak energy from the barrier is blueshifted with excitation power whereas the indirect transition within the well (E_3) is relatively constant with power. The blueshift is a consequence of band bending due to the electric field created by the spatially separated carriers.

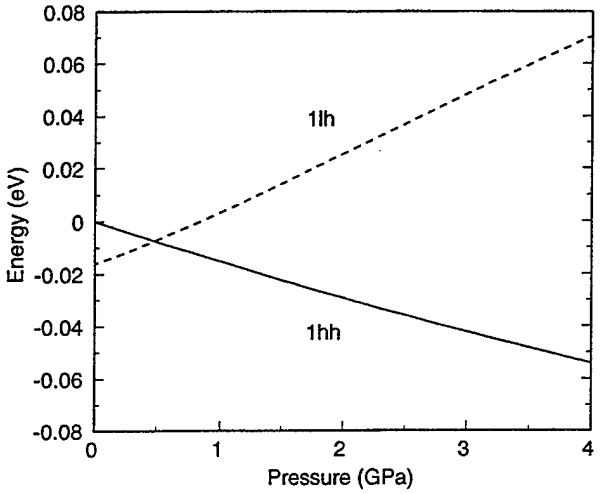

FIG. 6. Energy shift of the heavy and light hole bands in $In_xGa_{1-x}P$ as a function of pressure The shifts are calculated with respect to the average valence band energy using the solid-model approach (Ref. 24). Both bands were assumed to be separated by 16 meV at atmospheric pressure.

mospheric pressure. These parameters and the crossover pressures of the two direct-to-indirect transitions have been summarized in Table I.

Relevant information on the variation with pressure of the valence band offset can be obtained by comparing the pressure coefficients of the E_2 and E_4 transitions. Since both transitions originate at the same level X_b, their pressure coefficient should be the same. However, our results show that the E_2 transition decreases with pressure at about twice the rate of the E_4 transition. This difference in the pressure coefficients indicates that either the 1hh well valence band state or the barrier valence band are changing with pressure, possibly due to the presence of biaxial strain.

In two-dimensional systems the effect of hydrostatic pressure results in the generation of a biaxial strain in the growth plane due to the difference in the elastic constants of the well and barrier materials.[22] This biaxial strain is responsible for the shifting of the heavy and light hole bands and the splitting of the indirect conduction band minima.[23] We calculated the pressure induced strain for our sample using elastic theory and the corresponding shift of the heavy and light hole bands.[24] The elastic constants of both ternary materials were interpolated from the binary constituents[25] and were assumed to be constant in the pressure range of these experiments. These calculations show that as pressure is increased a biaxial tensile strain is induced in the $In_xGa_{1-x}P$ well and a compressive strain, less than half the value of that in the well, is generated in the $In_yAl_{1-y}P$ barrier. This difference in the magnitude of the strain in the well and barrier indicates that the changes in the band alignment are mostly due to the variation with pressure of the well valence band states. The corresponding shift in energy with pressure of the heavy and light hole well valence band states is shown in Fig. 6. The heavy hole band shifts with pressure at a rate of -13.5 meV/GPa while the light hole energy increases with pressure at a rate of $+21.5$ meV/GPa. Taking into account a separation of 16 meV between the heavy and light hole band as calculated from the envelope-approximation,[26] it is found that the two bands cross at 0.5 GPa. Therefore, in almost the entire pressure range of these experiments the light hole band is the top valence band state. Since this band has a positive pressure coefficient and the indirect transition E_2 has a negative pressure coefficient, then the measured rate is larger than that of the E_4 transition. A pressure rate for the light hole band of 18 meV/GPa is obtained from the difference between the measured pressure rates of the E_2 and E_4 transitions, in good agreement with the rate obtained in the calculations. The shifting of the light hole band is also responsible for the increased pressure coefficient of the E_3 transition. The lower crossover pressure of this transition when compared to bulk[17] is due to the splitting of the X_b minima with strain. In calculating the splitting of the well valence band states with strain we have ignored the variation in the confinement energies due to the change of the effective masses

TABLE I. Zero pressure energy band position, pressure coefficient, and crossover pressure of the different transitions observed in $In_xGa_{1-x}P/In_yAl_{1-y}P$ multiple quantum wells.

	E (eV) [at $P = 0$ GPa]	dE_g/dP (meV/GPa)	Transition pressure (GPa)
In-Ga-P (E_1)	1.984±0.004	92±3	
In-Ga-P/In-Al-P (E_2)	2.12±0.01	-28±5	1.1±0.2 ($E_1 - E_2$)
In-Ga-P (E_3)	2.272±0.007	-31±3	2.3±0.5 ($E_1 - E_3$)
In-Al-P (E_4)	2.35±0.01	-10±4	

with pressure and that due to the change in the well width with pressure. These corrections are very small, have opposite pressure coefficients, and therefore their effect on the confinement energy change with pressure is negligible. From our experimental results and calculations we find that in the $In_xGa_{1-x}P/In_yAl_{1-y}P$ system the valence band alignment cannot be assumed to remain constant with pressure as has been the case in the $GaAs/Al_xGa_{1-x}As$ system.[4] While this variation in energy of the valence band states modifies the pressure coefficients of the PL transitions, it does not alter the energy difference between the conduction and valence band states at atmospheric pressure.

The determination of the valence band offset of the $In_xGa_{1-x}P/In_yAl_{1-y}P$ heterointerface is straightforward knowing the energy of the different indirect transitions at atmospheric pressure. In reference to Fig. 3, the valence band offset is given by

$$\Delta E_v = E_4 - E_2 + E_{1hh} \quad (1)$$

where E_{1hh} is the confinement energy of the heavy hole band. In the envelope approximation, E_{1hh} is found to be equal to 9 meV when an $In_xGa_{1-x}P$ hole effective mass of $0.46m_0$ is used.[11] With this value of E_{1hh} a valence band offset of 0.24 eV is obtained from Eq. (1). This value of the band offset is smaller than that predicted by the model solid approach of Van de Walle.[24]

The calculation of the valence band offset using Eq. (1) assumes that the acceptor concentration is negligible in both the well and barrier materials, since our samples are n-type. However, in the presence of acceptor levels in either the well or barrier material, this expression needs to be modified to account for the binding energy of the acceptor level. We have calculated the valence band offset in this case considering two limiting situations, one in which an acceptor level with a binding energy of 50 meV is located in the well material, and the other in which the same acceptor level is located in the barrier. In the first case, the valence band offset is found to be 0.19 eV while in the second case a value of 0.29 eV for the valence band offset is obtained. Including the acceptor binding energy and the experimental uncertainties we find $\Delta E_v = (0.24 \pm 0.05)$ eV. To our knowledge, the only other reported measurement of the band offset energies for the In-Ga-P/In-Al-P interface has been made by Watanabe and Ohba using capacitance-voltage ($C-V$) carrier profiling.[27] They obtained a value at 300 K of 0.11 eV for ΔE_c for an $In_{0.5}Ga_{0.5}P/In_{0.5}Al_{0.5}P$ heterojunction grown by metal-organic chemical vapor epitaxy. Using a band-gap difference of 0.50 eV, their result indicates ΔE_v of 0.39 eV, considerably higher than our value of ΔE_v =(0.24±0.05) eV. The reason for this discrepancy may be the precision of the measurement techniques. The ΔE_c obtained by the $C-V$ method is now known to be strongly influenced by the structure (i.e., interfacial charge, doping, and compositional nonuniformities) and measurement conditions (i.e., frequency, temperature), and thus large errors in ΔE_c can easily occur.[28] In fact, Watanabe and Ohba note that a simulated carrier profile based on their ΔE_c value did not fit their measured profile.[27] In comparison, the pressure-dependent PL technique employed here measures energy levels directly and does not require additional knowledge of the bulk or interface properties. Thus, the value of $\Delta E_v = 0.24 \pm 0.05$ eV is free of the errors inherent in the $C-V$ technique.

The conduction band offset can be calculated from the measured value of the valence band offset and the band-gap energy difference of the well and barrier materials. The value of the direct band-gap of bulk $In_xGa_{1-x}P$ was determined from the maximum of the photoluminescence signal from the bulk sample corrected for the exciton binding energy. A value of 1.95 eV was obtained at 20 K. The band-gap of the barrier materials was taken equal to 2.45 eV from previous measurements on the band structure of In-Al-P.[16] The total band discontinuity for this heterostructure system is calculated to be 0.50 eV at 20 K. Therefore, the conduction band offset energy is 0.26 eV and a 52:48 band-gap splitting is determined to be the band lineup in the $In_xGa_{1-x}P/In_yAl_{1-y}P$ MQW. A schematic of the band structure diagram of this MQW is shown in Fig. 7. The only assumption made in this band diagram involves the energy of the barrier Γ minimum; however, this assumption does not play a role in determining the valence band offset as discussed above. The band diagram also shows the position of the indirect X levels in the well and barrier materials with respect to the well and barrier valence bands as obtained from the measurements. The 136 meV separation between the barrier X level and the lowest confined conduction band state in the well sets a lower limit for the well width of 16 Å for a type-I structure. This result agrees well with the measurements of Hafich *et al.*,[13] who observed the quenching of the photoluminescence in $In_xGa_{1-x}P/In_yAl_{1-y}P$ for well widths lower than 18 Å. Therefore the shortest wavelength that can be achieved with this heterostructure system is 563 nm. Shorter wavelengths would result in a type-II MQW which has been shown to have low radiative efficiency and radiative lifetimes up to several μsec.[29] These characteristics along with the low mobility of the carriers associated with the X valley are detrimental in device performance.

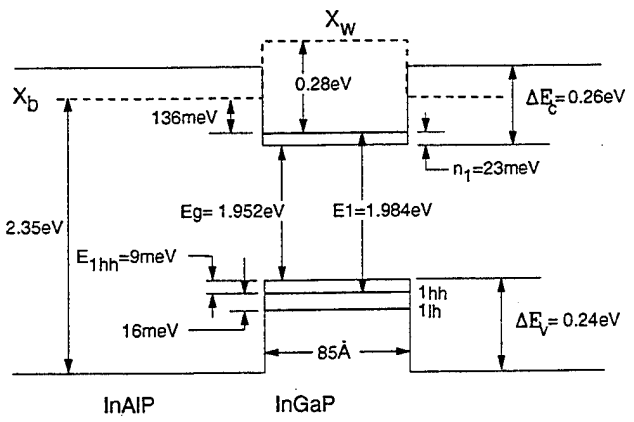

FIG. 7. Energy band diagram of $In_xGa_{1-x}P/In_yAl_{1-y}P$ at atmospheric pressure and 20 K . The values for the band-gap energies and energies of the barrier and well X minima are all obtained from the experiments.

IV. CONCLUSIONS

The band structure of $In_{0.5}Ga_{0.5}P/In_{0.5}Al_{0.5}P$ multiple quantum wells was determined from low temperature photoluminescence measurements at high pressure. Selective excitation of different transitions in the well and barrier materials allowed, to our knowledge, the first direct determination of the valence band offset at atmospheric pressure. This heterostructure system transformed from a type-I alignment to a type-II staggered-aligned system at 1.1 GPa. This direct-to-indirect crossover was accompanied by a sharp decrease in the intensity of the direct gap photoluminescence signal. The valence band alignment was found to vary with pressure due to pressure induced strains in the epilayers.

ACKNOWLEDGMENTS

The authors kindly acknowledge Professor M. Chandrasekar and B. Weinstein for stimulating discussions, Professor J. Mahan for lending us the close-cycle He refrigerator, and Professor D. Lile for the photomultiplier tube and cooled housing. This work was supported by the Center for Optoelectronic Computer Systems sponsored by the National Science Foundation/Engineering Research Center Grant No. ECD 9015128, the Colorado Advanced Material Institute, the State of Colorado, and the Air Force Office of Scientific Research (Contract No. F49620-93-1-0021).

[1] G. Hatakoshi, K. Itaya, M. Ishikawa, M. Okajima, and Y. Uematsu, IEEE J. Quantum Electron **QE-27**, 1476 (1991).
[2] R. P. Schneider, Jr., R. P. Bryan, J. A. Lott, G. R. Olbright, Appl. Phys. Lett. **60**, 1830 (1992).
[3] M. J. Mondry and H. Kroemer, IEEE Electron. Devices Lett. **EDL-6**, 175 (1985).
[4] D. J. Wolford, T. F. Kuech, and J. A. Bradley, J. Vac. Sci. Technol. B **4**, 1043 (1986).
[5] R. C. Miller, A. C. Gossard, D. A. Kleinman, and O. Munteamu, Phys. Rev. B **29**, 1329 (1984).
[6] W. I. Wang, Solid State Electron. **29**, 133 (1986).
[7] M. A. Haase, N. Pan, and G. E. Stillman, Appl. Phys. Lett. **54**, 1457 (1989).
[8] J. Batey and S. L. Wright, J. Appl. Phys. **59**, 200 (1986).
[9] M. A. Rao, E. J. Caine, H. Kroemer, S. I. Long, and D. I. Babic, J. Appl. Phys. **61**, 643 (1987).
[10] T. J. Drummond and I. J. Fritz, Appl. Phys. Lett. **47**, 284 (1985).
[11] J. Chen, J. R. Sites, I. L. Spain, M. J. Hafich, and G. Y. Robinson, Appl. Phys. Lett. **58**, 744 (1991).
[12] W. Shan, S. J. Hwang, and J. J. Song, H. Q. Hou, and C. W. Tu, Appl. Phys. Lett. **62**, 2078 (1993).
[13] M. J. Hafich, H. Y. Lee, G. Y. Robinson, D. Li, and N. Otsuka, J. Appl. Phys. **69**, 752 (1991).
[14] A. Jayaraman, Rev. Sci. Instrum. **57**, 1013 (1986), and references therein.
[15] S. M. Olsthoorn, F. A. J. M. Driessen, and L. J. Giling, J. Appl. Phys. **71**, 2423 (1992).
[16] D. P. Bour, J. R. Shealy, G. W. Wicks, and W. J. Schaff, Appl. Phys. Lett. **50**, 615 (1987).
[17] J. Chen, Ph. D. dissertation, Colorado State University, 1990.
[18] C. S. Menoni, H. D. Hochheimer, and I. L. Spain, Phys. Rev. B **33**, 5896 (1986).
[19] H. Müller, R. Troemmer, and M. Cardona, Phys. Rev. B **21**, 4879 (1980).
[20] G. Olbright, W. S. Fu, J. T. Klem, J. M. Gibbs, G. Khitrova, R. Pon, B. Fluegel, K. Meissner, N. Peyghambarian, R. Binder, I. Galbraith, and S.W. Koch, Phys. Rev. B **44**, 3043 (1991).
[21] J. Chen, D. Patel, J. R. Sites, I. L. Spain, M. J. Hafich, and G. Y. Robinson, Solid State Commun. **75**, 693 (1990).
[22] J. A. Tuchman and I. P. Herman, Phys. Rev. B **45**, 11 929 (1992).
[23] T. P. Pearsall, *Semiconductor and Semimetals* (Academic Press, Boston, 1990), p. 1.
[24] Chris G. Van de Walle, Phys. Rev. B **39**, 1871 (1989).
[25] T. Y. Wang, A. W. Kimball, G. S. Chen, D. Birkedal, and G. B. Stringfellow, J. Appl. Phys. **68**, 3356 (1990).
[26] G. Bastard, *Wave Mechanics Applied to Semiconductor Heterostructures* (Halsted Press, New York, 1988), p. 63.
[27] M. O. Watanabe and Y. Ohba, Appl. Phys. Lett. **50**, 906 (1987).
[28] L. Y. Leu and S. R. Forrest, J. Appl. Phys. **64**, 5030 (1988).
[29] J. Nunenkamp, K. Reimann, J. Kuhl, and K. Ploog, Phys. Rev. B **44**, 8129 (1991).

L-band recombination in $In_xGa_{1-x}P/In_{0.5}Al_{0.5}P$ multiple quantum wells

D. Patel, K. Interholzinger, P. Thiagarajan, G. Y. Robinson, and C. S. Menoni
Department of Electrical Engineering, Colorado State University, Fort Collins, Colorado 80523
(Received 19 January 1996)

We report the direct observation of recombination from the L_{1c} band in $In_xGa_{1-x}P/In_{0.5}Al_{0.5}P$ multiple quantum wells. The indirect L_{1c} transition is observed in unstrained structures with narrow wells and in tensile strained structures, using high-pressure photoluminescence measurements. L_{1c} recombination is characterized by a pressure coefficient of 60 ± 5 meV/GPa, considerably smaller than that of the direct gap Γ_{1c} states. In the same experiments we also identify heterostructure states associated with Γ_{1c} and X_{1c} from which we determine the separation among the conduction minima in unstrained bulk $In_xGa_{1-x}P$ for $x\leq 0.48$. [S0163-1829(96)06620-9]

$In_xGa_{1-x}P$ is one of the most attractive materials for the development of semiconductor lasers emitting in the yellow-red region of the optical spectrum.[1] Current visible laser diode technology uses multiple quantum wells (MQW's), with $In_xGa_{1-x}P$ wells and $In_{0.5}Al_{0.5}P$ or $In_x(Al_yGa_{1-y})_xP$ barriers. This heterostructure combination coupled with the possibility of varying well width and composition offers large flexibility in the selection of the operating wavelength as well as for tailoring of the output characteristics. Successful design and optimization of advanced laser structures is based on a complete understanding of the band structure and band alignments of the heterostructure materials composing the laser. Normally knowledge of the direct energy band gap is sufficient for the selection of the operating wavelength. However, for specific requirements such as the reduction of the laser threshold current, it is necessary to know the separation among the conduction-band minima, so as to avoid any detrimental influences in the laser operation from the higher effective mass, indirect L_{1c} and X_{1c} valleys.

The band structure of bulk $In_xGa_{1-x}P$ has been investigated previously.[2–7] It is known that $In_xGa_{1-x}P$ is a direct-gap material for In compositions $x>0.32$ and that it becomes indirect, with L_{1c} being the lowest conduction-band minima, for In compositions $x<0.32$.[3,7] Decreasing the In composition further reveals the X_{1c} extrema that become the conduction-band minima for $x<0.2$.[2,3,7] The proximity of the L_{1c} and X_{1c} transitions has made difficult the identification of L_{1c}. Previous optical studies in alloys with varying compositions did not show any evidence of the L_{1c} band.[2] The L-like behavior was also absent in optical measurements at high pressure conducted on In-rich alloys.[4–6] Evidence of L_{1c} was obtained from modulated piezoreflectance measurements[3] and high-pressure mobility measurements[7] from which the energy separation among the conduction-band extrema of $In_xGa_{1-x}P$ alloys was not obtained directly. The proximity of the Γ_{1c}, L_{1c}, and X_{1c} extrema for $x<0.48$ places restrictions in the design of $In_xGa_{1-x}P$ MQW's, as indirect well structures can be obtained by tailoring the separation among the conduction-band states by means of varying the composition and the well width.

In this paper we report the observation of recombination from the L_{1c} states in $In_xGa_{1-x}P/In_{0.5}Al_{0.5}P$ MQW's. The L-like behavior of the conduction-band minima was identified in narrow lattice matched MQW's, and also confirmed on tensile strained MQW's, from pressure-dependent photoluminescence (PL) measurements at low temperature. Carrier recombination from L_{1c} was characterized by a reduced pressure coefficient compared to that measured for the lowest confined Γ_{1c} state. The identification of the MQW states associated with Γ_{1c} and X_{1c} in the same experiments made possible the calculation of the separation among the conduction-band extrema in $In_xGa_{1-x}P$ for compositions $x\leq 0.48$.

The combination of using hydrostatic pressure and MQW's with different well width and compositions was essential for the unique determination of the L_{1c} transition in $In_xGa_{1-x}P/In_{0.5}Al_{0.5}P$ MQW's. With hydrostatic pressure the relative position of the conduction-band extrema was modified and the indirect states were revealed as they became the lowest conduction-band minima. The Γ_{1c}, L_{1c}, and X_{1c} minima were distinctly identified as they shifted with pressure at rates of about 100, 60, and -20 meV/GPa, respectively, typical of other semiconductor materials.[8] Since both Γ_{1c} and L_{1c} have positive pressure coefficient, obtaining a band alignment in which L_{1c} becomes the conduction-band minimum at high pressures, requires the Γ_{1c}-L_{1c} separation to be considerably smaller than that of Γ_{1c}-X_{1c} at atmospheric pressure. This condition was achieved in the $In_xGa_{1-x}P/In_{0.5}Al_{0.5}P$ MQW's, by decreasing the well width and in a separate experiment by decreasing the In composition x.

The $In_xGa_{1-x}P/In_{0.5}Al_{0.5}P$ MQW samples used in these studies were grown by gas-source molecular beam epitaxy on (100) GaAs substrates with nominally lattice matched composition for the barrier material. The growth of the $In_xGa_{1-x}P/In_{0.5}Al_{0.5}P$ MQW's was carried out at 530 °C at 1.0 μm/h, conditions that produced a disordered, random alloy in bulk samples as previously determined by photoluminescence, photoluminescence excitation (PLE), and transmission electron diffraction measurements.[9] Each sample contained a buffer layer of GaAs of 0.5-μm thickness, followed by an $In_{0.5}Al_{0.5}P$ buffer layer 0.035 μm thick, the MQW region and an $In_{0.5}Al_{0.5}P$ cap layer 0.1 μm thick. All layers were unintentionally doped. The MQW's consisted of 50 periods of 50-Å wells and 150-Å barriers. The well composition x was selected equal to 0.48, 0.41, and 0.37 corre-

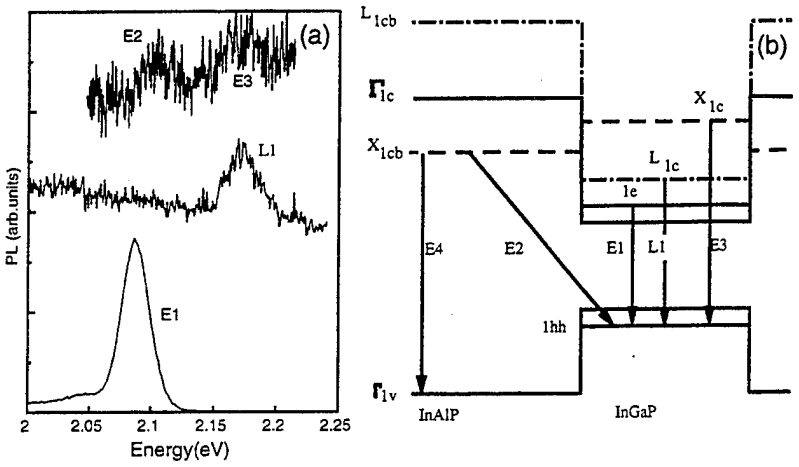

FIG. 1. (a) PL spectra from the −0.57% tensile strain MQW, corresponding to transitions associated with Γ_{1c}, L_{1c}, and X_{1c}. (b) Schematic diagram of the band structure of $In_xGa_{1-x}P/In_{0.5}Al_{0.5}P$ MQW's showing the various photoluminescence transitions observed in the experiments.

sponding to 0, −0.57%, and −0.87% tensile strain. For the unstrained composition a second structure consisting of 50 periods of 30-Å wells and 150-Å barriers was also grown. The high-pressure photoluminescence measurements were conducted at 50 K. Details of these experiments have already been described in Ref. 10.

Typical PL spectra originating from well states associated with Γ_{1c}, L_{1c}, and X_{1c} are shown in Fig. 1(a). The full width at half maximum of the PL signal corresponding to the direct transition was measured to be ~17 meV. The PL signals of the indirect transitions were broader and weaker compared to the direct transition. We notice that since the L_{1c} states are confined in the well, their PL is more intense and narrower than that of X_{1c}. As shown next, the identification of the PL transitions was made strictly on their pressure rate of change. Their labeling is shown in the band diagram of Fig. 1(b) and is consistent with our previous work on this material system.[10]

Figure 2 shows the pressure dependence of the PL transitions measured in the unstrained $In_{0.48}Ga_{0.52}P/In_{0.5}Al_{0.5}P$ MQW's investigated. The pressure behavior of both the 50-Å and the 30-Å MQW's is qualitatively similar. Four PL transitions were identified, one with a positive pressure coefficient (dE/dp) and three PL transitions with negative slope, characteristic of an X band. Among the three X-like transitions, two were observed over the whole pressure range of the experiments. These PL transitions, labeled $E3$ and $E4$, correspond to the indirect recombination of photoexcited carriers from the X_{1c} minima in the well (X_{1c}- 1hh) and in the barrier, respectively (X_{1cb}-Γ_{1v}). The third indirect transition ($E2$) was only observed at high pressures after the lowest confined conduction-band state becomes resonant with the barrier X_{1cb} states. $E2$ corresponds to the indirect, in real and k space, (X_{1cb}-1hh) recombination. As expected, the onset of $E2$ occurred at lower pressures in the 30-Å MQW's as the separation between the lowest confined Γ_{1c} state ($1e$) and X_{1cb} is reduced with increased carrier confinement.

The PL transitions characterized by a positive dE/dp showed a distinct behavior. In the 50-Å MQW, this transition labeled $E1$ was characterized by $dE/dp = 92 \pm 3$ meV/GPa, a value typical of a Γ-like behavior.[8] We associate $E1$ with the recombination between the conduction- and valence-band ground states ($1e$-1hh). By contrast, dE/dp in the 30-Å MQW's was measured to be 60 ± 5 meV/GPa. Although an ~6% reduction in the pressure coefficient of $E1$ is expected from the variation in the well width,[11] this effect cannot explain the almost 50% decrease measured in the narrow MQW's. The lower value of dE/dp indicates that in the 30-Å MQW's recombination takes place from a conduction-band state with an L-like behavior. L_{1c}-1hh recombination, labeled $L1$ in Fig. 1(b), is observed in the narrow well structures since $E1$ is shifted above L_{1c} due to the increased carrier confinement. The calculated pressure dependence of $E1$ in the 30-Å MQW is represented by the solid line in Fig. 2(b). In the 50-Å MQW the $L1$ transition was not observed, as it occurred at higher pressures where the indirect $E2$ transition becomes dominant. The $L1$ behavior in the 50-Å MQW, calculated assuming the same pressure coefficient

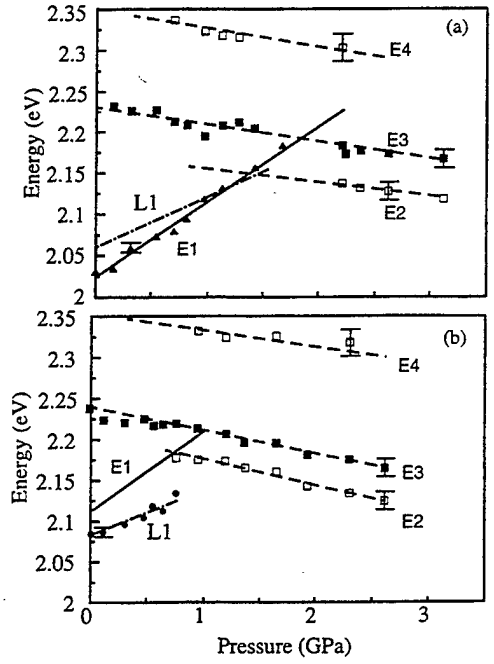

FIG. 2. Pressure dependence of the photoluminescence transitions of unstrained $In_{0.48}Ga_{0.52}P/In_{0.5}Al_{0.5}P$ multiple quantum wells of (a) 50-Å well width and (b) 30-Å well width. The pressure behavior of all transitions has been fitted using a least-square routine from which their pressure rate of change and the atmospheric pressure values are determined.

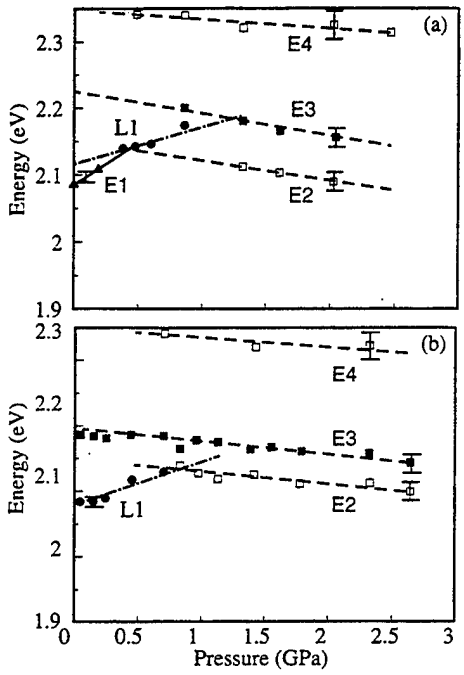

FIG. 3. Energy-pressure diagram for tensile strained MQW's with (a) -0.57% strain and (b) -0.87% strain.

as that measured in the 30-Å MQW, is shown by the dash-dotted line in Fig. 2(a).

To confirm our assignment of L_{1c}, we examined the results of the tensile strained MQW's. The L-like behavior should also be apparent in these structures as the separation between L_{1c} and Γ_{1c} decreases with decreasing In composition.[3] Figure 3 shows the energy-pressure data of the $In_xGa_{1-x}P/In_{0.5}Al_{0.5}P$ MQW's with well compositions $x=0.41$ and 0.37, corresponding to -0.57% and -0.87% strain, respectively. Hereafter, we discuss the behavior of the transitions with positive dE/dp, as the indirect transitions are equivalent to those observed in the unstrained MQW's. In the -0.87% strain MQW's, dE/dp was measured to be 60 ± 5 meV/GPa, identical to that of $L1$ in the 30-Å unstrained MQW's. In the -0.57% strain MQW's the PL transition with positive dE/dp showed at first glance a distinct behavior. Below 0.5 GPa it shifted at a rate $dE/dp=110\pm5$ meV/GPa and above 0.5 GPa at a slower rate $dE/dP=60\pm5$ meV/GPa, as shown by the solid and dash-dotted lines of Fig. 3(a). This change in the slope indicates that a pressure-induced $E1$-$L1$ crossover takes place at 0.5 GPa. The low pressure at which this crossover occurred shows that $E1$ and $L1$ are separated approximately 35 meV at ambient conditions. With increased tensile strain, the $E1$-$L1$ separation was decreased and $L1$ became the lowest conduction-band state, as observed in the -0.87% strained MQW.

The identification of the MQW states associated with the Γ_{1c}, L_{1c}, and X_{1c} extrema in the $In_xGa_{1-x}P$ wells allowed the calculation of the energy separation among the conduction-band extrema in $In_xGa_{1-x}P$ for $x\leq 0.48$. In reference to Fig. 1(b), the Γ_{1c}-L_{1c} separation was calculated from the difference of $L1$ and $E1$ at atmospheric pressure and by adding the $1e$ confinement energy.[12] We neglected the $L1$ electron confinement energy since it is small due to the large effective mass of the L_{1c} band.[13] The Γ_{1c}-X_{1c} separation was determined from the difference between $E3$ and $E1$ at atmospheric pressure and by adding the $1e$ confinement energy[12] and the strain-induced splitting of X_{1c}, calculated using the model solid theory.[14] The values of $E1$ in the MQW's with composition $x=0.37$ and $x=0.48$ (30 Å well width), in which this transition was not observed, were determined from PLE measurements.[15]

In unstrained bulk $In_{0.48}Ga_{0.52}P$, L_{1c} was calculated to be 0.1 ± 0.02 eV above Γ_{1c} and 0.18 ± 0.04 eV below X_{1c}. Decreasing the In composition x decreased the Γ_{1c}-L_{1c} separation to 0.08 ± 0.02 and 0.03 ± 0.02 eV for $x=0.41$ and 0.37, respectively. The L_{1c}-X_{1c} separation was detremined to be 0.21 ± 0.05 eV for $x=0.48$. For the lower In compositions its value was equal to 0.175 ± 0.05 eV. The insensitivity of our results for determining the separation of X_{1c} relative to the other conduction-band extrema arises from the uncertainties involved in calculating the strain-induced shift of X_{1c}. From the measured variation of the Γ_{1c}-L_{1c} energy separation with In composition and assuming a linear behavior in the range of compositions investigated, we determined that L_{1c} becomes the conduction-band minima at $x=0.3$. A similar value was predicted by Bugaski, Kontkiewicz, and Mariette[13] and also determined from Hall measurements at high pressure[7] and piezomodulated measurements.[3] Although the agreement in the Γ_{1c}-L_{1c} crossover composition with previous work[3,7] is very good, the values of the Γ_{1c} band gap used as reference in this work are found to be approximately 60 meV smaller than that reported by Merle *et al.*[3] While ~20 meV can be accounted for by the localization energy, the rest is likely to arise from differences in the growth conditions.[16]

In conclusion, we have identified the L_{1c} band in narrow unstrained and in tensile strained $In_xGa_{1-x}P/In_{0.5}Al_{0.5}P$ MQW's and determined from these results the separation of the conduction-band extrema in $In_xGa_{1-x}P$ for In compositions $x\leq0.48$.

We would like to acknowledge encouraging discussions with Dr. J. Fouquet, Dr. J.L. Chilla, Osvaldo Buccafusca, and Professor S.L. Lee. This work was supported NSF Grants No. DMR 9321422, ECS-9502888, and AFOSR Contract No. F49620-93-1-0021.

[1] D. P. Bour, R. S. Geels, D. W. Treat, T. L. Paoli, R. L. Thornton, B. S. Krusor, R. D. Bringans, and D. F. Welch, IEEE J. Quantum Electron. **30**, 593 (1994).

[2] A. Onton, M. R. Lorenz, and W. Reuter, J. Appl. Phys. **42**, 3420 (1971); C. J. Nuese, A. G. Sigai, M. S. Abrahams, and J. J. Gannon, J. Electrochem. Soc. **120**, 956 (1973).

[3] P. Merle, D. Auvergne, H. Mathieu, and J. Chevallier, Phys. Rev. B **15**, 2032 (1976).

[4] S. W. Tozer, D. J. Wolford, J. A. Bradley, D. Bour, and G. B. Stringfellow, in *Physics of Semiconductors*, edited by W. Zawadski (Polish Academy of Sciences, Warsaw, 1988), p. 881.

[5] D. Patel, J. Chen, I. L. Spain, J. H. Quigley, M J. Hafich, and G.

Y. Robinson, Phys. Rev. B **38**, 13 206 (1988).
[6]D. Patel, J. Chen, S. R. Kurtz, J. M. Olson, J. H. Quigley, M J. Hafich, and G. Y. Robinson, Phys. Rev. B **39**, 10 978 (1989).
[7]G. D. Pitt, M. K. R. Vyas, and A. W. Mabbitt, Solid State Commun. **14**, 621 (1974).
[8]I. L. Spain, Contemp. Phys. **28**, 523 (1987).
[9]K. Mahalingam, N. Otsuka, M. J. Hafich, and G. Y. Robinson, Bull. Am. Phys. Soc. **38**, 737 (1993).
[10]D. Patel, M. J. Hafich, G. Y. Robinson, and C. S. Menoni, Phys. Rev. B **48**, 18 031 (1993).
[11]U. Venkateswaran, M. Chandrasekhar, H. R. Chandrasekhar, B. A. Vojak, F. A. Chambers, and J. M. Meese, Phys. Rev. B **33**, 8416 (1986).
[12]The electron and hole confinement were calculated at the finite well approximation using a value of $\Delta E_c/\Delta E_v = 70/30$ for the band discontinuities of the unstrained system. Values of $\Delta E_c/\Delta E_v = 62/38$ and 60/40 were used for the -0.57% and -0.87% strained structures, respectively. These band offset ratios were calculated from the measured valence-band discontinuity and using a value of 2.6 eV for the direct band gap of $In_{0.5}Al_{0.5}P$ determined from absorption measurements in our samples. Changes of the effective masses with strain were calculated using the model solid theory.
[13]M. Bugaski, A. M. Kontkiewicz, and H. Mariette, Phys. Rev. B **28**, 7105 (1983).
[14]C. G. Van de Walle, Phys. Rev. B **39**, 1871 (1989).
[15]J. E. Fouquet (private communication).
[16]J. H. Quigley, M. J. Hafich, H. Y. Lee, R. E. Stave, and G. Y. Robinson, J. Vac. Sci. Technol. B **7**, 358 (1988).

Accepted for publication in J. Vac. Sci. Technol., 9/95.

MBE Growth of InGaP MQW Structures on GaP for Optical Modulators

T. J. Vogt, P. Thiagarajan, and G. Y. Robinson
Department of Electrical Engineering, Colorado State University, Fort Collins, Colorado 80523

Abstract

The epitaxial growth and characterization of multiple quantum well (MQW) optical modulators on GaP substrates is reported. The devices were fabricated using graded composition InGaP strain relieving buffer layers and strain-compensated InGaP MQWs. The devices operate in the 570 nm to 620 nm wavelength range with a maximum transmission change of 15% occurring at 594 nm for an applied bias of -10 V. The composition range required for the target wavelength range is near the indirect-direct crossover point for the InGaP material system and the corresponding effects on photoluminescence and absorption data is presented.

The current interest in plastic optical fibers, displays, and optical storage has spurred interest in optical devices operating in the visible wavelength range. The wavelength range from 550 nm to 670 nm is of particular interest for plastic fiber communications since the lowest fiber absorption occurs at 570 and 650 nm. In addition, two-way transmission networks using only one optical source and many optical modulators operating in reflection mode have been proposed to minimize the use of low reliability and costly components in robust networks [1]. To date visible modulators have been fabricated in both the III-V and II-VI semiconductors at wavelengths ranging from 506 nm to 660 nm [2-9]. Recently, Blum et al. reported observation of the quantum confined Stark effect (QCSE) in surface normal InGaAlP/InGaP multiple quantum well structures grown on GaAs by metal-organic vapor phase epitaxy and operating at 645 nm [2]. In addition, Goosen et al. reported MQW modulators operating at 575 nm using indirect AlAs/AlGaAs in the active region grown on GaAs [10]. Here we report the fabrication, by gas source molecular beam epitaxy (GSMBE), of multiple quantum well (MQW) optical modulators for operation near 570 nm. The modulators consist of strain-compensated $In_zGa_{1-z}P$(well)/$In_yGa_{1-y}P$(barrier) MQWs grown on a thick $In_xGa_{1-x}P$ buffer layer, where y<x<z, all of which were grown on a transparent GaP substrate using a buffer layer of graded composition.

A graded buffer layer was used to reduce the density of misfit dislocations in the MQW region. Several graded buffer schemes were evaluated, on both GaP and GaAs substrates, using double crystal X-ray diffraction (DCXD) and photoluminescence (PL). Constant-composition, step-graded, linear-graded, and superlattice-graded buffers were tested with the step-graded scheme producing marginally better results than the linear-graded scheme and significantly better than the superlattice-graded approach. The graded buffer layers grown on GaP were consistently of higher structural and optical quality than those on GaAs.

The MQW-PIN device structure under study is shown in Fig. 1 and was grown on a (100) n^+GaP substrate using thermally cracked PH_3. The In mole fraction in the thick buffer layer of constant composition, denoted as x, was varied systematically in a series of growths. The composition of the wells z and the barriers y were varied along with x such that $z = x+0.15$ and $y = x-0.10$. The GaP substrates were degreased and etched in a 4:4:5 HCL:HNO_3:H_2O solution at 25 °C for 2 minutes and then soaked for 10 minutes in H_2O to prepare the surface prior to growth. Surface oxide was desorbed at 700 °C for 30 minutes under a PH_3 flow of 8 sccm. Reflection high energy electron diffraction (RHEED) gave a characteristic (2x4) pattern. An improved

(i.e., more streaked) RHEED pattern was typically observed after depositing a few monolayers of Ga and annealing at 660°C for 30 seconds under the phosphorous flux. The step-graded buffer layer consisted of three layers of InGaP of different composition, each 200-nm thick, followed by a 2.0-μm thick constant composition $In_xGa_{1-x}P$ layer. The MQW active region consisted of 50 periods of 7.5-nm $In_yGa_{1-y}P$ wells and 11-nm $In_zGa_{1-z}P$ barriers. Compensating strain in the wells and barriers was used to avoid introduction of additional defects that may result from the strain in the MQWs. The devices were etched mesas of $400x400\mu m^2$ with Au-Sn-Au and Ti-Au ohmic contacts for the n^+ and p^+ layers, respectively.

One of the issues in using the alloy InGaP for devices operating in the 550-670 nm range is the crossover in the conduction band from indirect to direct for In mole fractions greater than about 0.30 [12]. For the range of x used in this study ($0.25<x<0.35$), the wells were direct ($0.40<z<0.50$) and the barriers were indirect ($0.15<y<0.25$). The well composition and thickness was chosen to match the target wavelength, including any strain and confinement effects as determined from the model solid theory [11]. The barrier composition was chosen to balance the strain in the well, giving an average lattice constant for the MQW stack equal to that of the buffer layer. The buffer layer composition was chosen so as to allow the least amount of strain required in the well while at the same time minimizing absorption in the buffer at the wavelength of interest.

A typical PL spectra is shown in Fig. 2(a) for the modulator structure. Two peaks are observed: one at 565 nm corresponding to emission from the cap and buffer layers with x=0.28 and one at 595 nm for emission from the QWs. The peak locations are in agreement with the calculated energies. The effect of the direct-indirect crossover was evident in the variation of PL intensity as x was varied from sample to sample. Fig. 2(b) shows a strong decrease in PL intensity with decreasing wavelength as the composition of the buffer layer approaches the crossover point. This effect is consistent with a decrease in the number of electrons available for radiative recombination due to the indirect valley becoming more populated as x decreases. Likewise, the PL intensity from the QWs decreases at shorter wavelengths. The variation in the QW PL intensity could result from the electrons in the well occupying the indirect minima in the well. Since our calculations suggest that the $In_yGa_{1-y}P/In_zGa_{1-z}P$ interface is a type-II heterojunction, electrons in the well could also transfer to the indirect minima *in the barrier*. Based on our calculations, the slopes of the curves in Fig. 2(b) for the bulk and QW luminescence are expected to differ if transfer to the barrier indirect minima is the dominating effect for the QWs. Since the slopes are the same within the experimental uncertainty, it appears that an increasing occupation of the indirect minima in the well is the dominant mechanism for the decrease of PL intensity as x decreases.

Optical transmission data was taken to estimate the absorption coefficient in the MQW region and to determine the feasibility of InGaP on GaP for normal-incident optical modulators. Since the GaP substrate is transparent for wavelengths >545 nm, the transmission measurement was made without removal of the substrate. The absorption spectra at room temperature for three different modulators are shown in Fig. 3(a). Each exhibits features characteristic of QW excitonic absorption, with the peak at 594 nm in the sample with x=0.30 due to the 1e-hh transition, as based on our calculations. A shoulder in the spectra at ~12 nm below the 1e-hh transition corresponds to the expected position of the 1e-lh transition. The strong absorption edge observed ~30 nm below the 1e-hh peak corresponds to that expected for the buffer layer. Fig. 3(b) shows absorption coefficient data for the same samples at low temperature (10 K). Measurements at low temperature confirmed carrier confinement in the well and provided estimates of the half width of the excitonic resonance. Half widths for the 1e-hh resonance at 10 K were typically 15 to 20 meV for the range of wavelengths covered by the samples grown, with the narrowest peak found for the sample operating at 594 nm at room temperature.

The smaller 1e-hh peak amplitude in Fig. 3 for the sample with x=0.25 compared to that for x=0.30 may result from the direct-indirect crossover. Not only is the well material closer to indirect at shorter wavelengths, but calculations suggest that the indirect barrier conduction band edge is near or below the direct confined energy level in the well. Such a condition would result in a reduction of exciton lifetime [3] and a broadening of the excitonic absorption peak, in agreement with our observations. We would then expect the sample with x=0.35 to show a more pronounced exciton absorption peak than for x=0.30; as is evident from Fig. 3, this is not the case. Alternatively, the material quality could

suffer as x is increased because of a larger defect density produced by the increased mismatch with the GaP substrate. We suspect that the material quality is not the dominant effect causing the weakening and broadening of the excitonic resonance at longer wavelengths, since additional efforts to improve the material quality by changing the buffer layer produced improved DCXD linewidths but gave no significant improvement in the absorption data.

Voltage dependent absorption and transmission data are shown in Fig. 4(a) for a device with x=0.30, which corresponds to room temperature modulation at 594 nm. The excitonic absorption peak shows a weakening, broadening, and a red shift with increasing reverse bias. The shift in the peak to longer wavelengths was most distinct for the 594-nm device and was consistent with that expected for the QCSE. A change in the absorption coefficient of 1700 cm^{-1} was measured for devices operating at 594 nm. Differential transmission data is shown in Fig. 4(b). A maximum change in transmission of 15% at -10V bias was measured at 594 nm.

In summary, the growth and operating characteristics of MQW modulators in the InGaP material system fabricated on transparent GaP substrates is reported for the first time. Using GSMBE the devices were grown on graded composition buffer layers and employed strain compensation in the MQW region. PL intensity variation with composition showed clear evidence of the direct-to-indirect crossover in the InGaP QWs designed to operate in the 570-620 nm range. The best devices produced a transmission change of 15% with a modest 10 V bias at a wavelength of 594 nm. Operation at shorter wavelengths was observed but with weaker excitonic effects.

The authors gratefully acknowledge the support of the Air Force Office of Scientific Research and the National Science Foundation.

References

[1] T. H. Wood, E. C. Carr, B. L. Kasper, R. A. Linke, C. A. Burrus, and K. L. Walker, Electron. Lett. **22**, 529 (1986)

[2] O. Blum, I. J. Fritz, R. J. Shul, R. P. Schneider, Jr. and A. J. Howard, Electron. Lett. **30**, 1885 (1994)

[3] P. Pezeshki, S. M. Lord, T. B. Boykin, B. L. Shoop, J. S. Harris, Electron. Lett. **27**, 1971 (1991)

[4] P. Pezeshki, D. Lui, S. M. Lord and J. S. Harris, Electron Lett. **28**, 1170 (1992)

[5] R. J. Egan, A. Clark, C. Jagadish, and J. S. Williams, Electron. Lett. **31**, 1270 (1995)

[6] A. Partovi, A. M. Glass, D. H. Olson, R. D. Feldman, R. F. Austin, D. Lee, A. M. Johnson, and D. A. B. Miller, Appl. Phys. Lett., **58**, 334 (1991)

[7] M. A. Hasse, D. K. Misemer, L. C. Olsen, and G. D. Vernstrom, Appl. Phys. Lett., **60**, 2054 (1992)

[8] S. Y. Wang, Y. Kawakami, J. Simpson, H. Stewart, K. A. Prior, and B. C. Cavenett, Appl. Phys. Lett., **62**, 1715 (1993)

[9] M. A. Hasse, H. Cheng, D. K. Misemer, T. A. Strand, and J. M. DePuydt, Appl. Phys. Lett., **59**, 3228 (1991)

[10] K. W. Goosen, R. H. Yan, J. E. Cunningham, and W. Y. Jan, Appl. Phys. Lett., **59**, 1829 (1991)

[11] C. G. Van de Walle, Phys. Rev. B, **39** 1871 (1989).

[12] Semiconductors - Group IV Elements and III-V Compounds, Springer-Verlag Series *Data in Science and Technology*, edited by O. Madelung, (Springer-Verlag, Berlin Heidelberg, 1991), pg. 153.

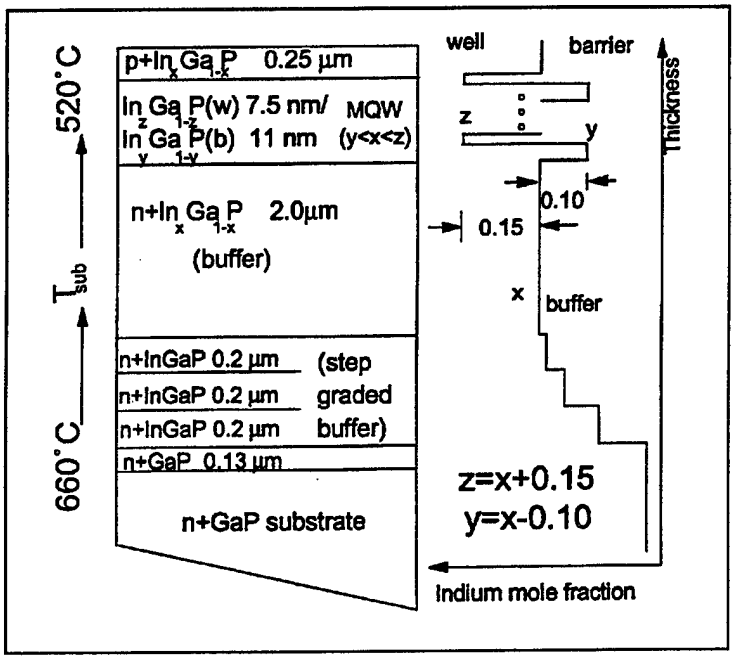

FIG. 1. Schematic representation of the *p-i-n* diode layer structure used in this study. An InGaP step composition graded buffer was used to reduce dislocation densities in the MQW active region.

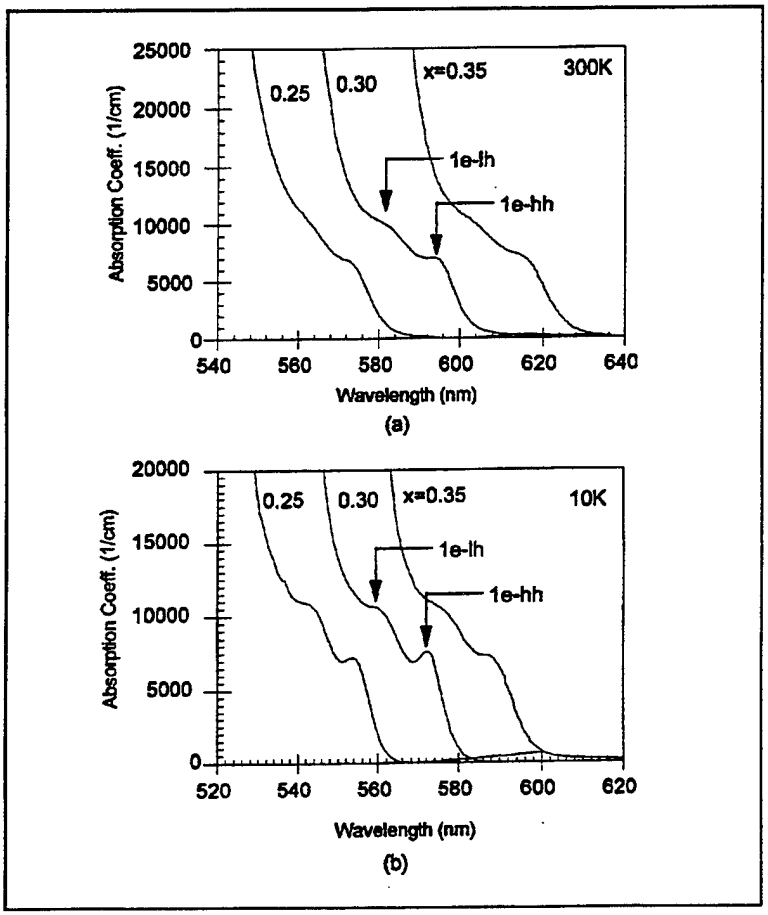

FIG. 2. Measured (PL) data for the MQW samples in this study. (a) PL spectra for the device with a nominal buffer composition of x=0.30. Luminescence from the bulk cap layer and MQW is observed. (b) Variation in PL intensity at different wavelengths for both the cap layer and MQW. The decrease in intensity with decrease in wavelength is expected as the composition approaches the indirect-direct crossover.

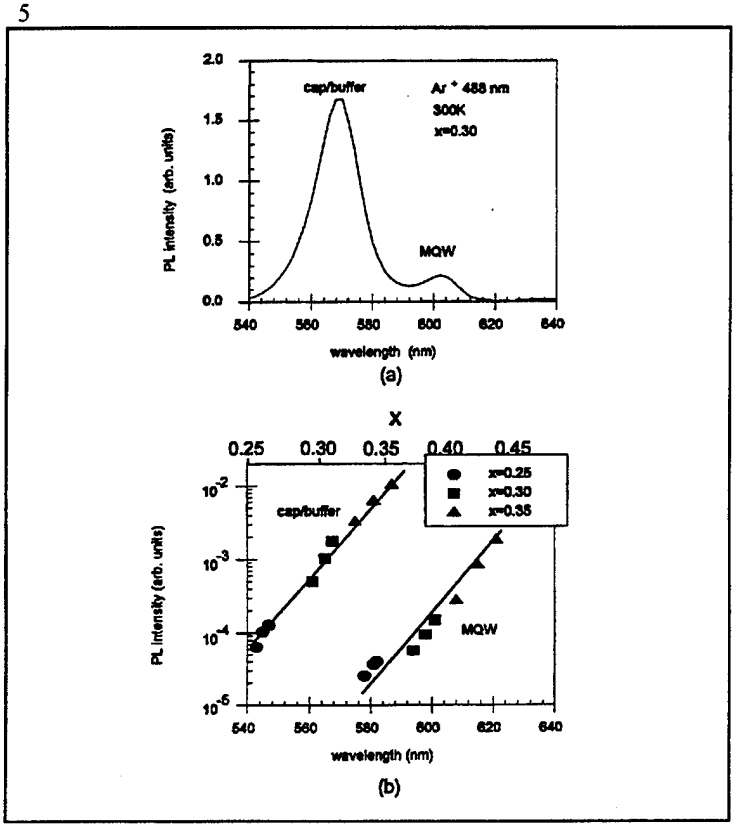

FIG. 3. Absorption coefficient spectra for samples of different nominal composition at (a) room temperature, and at (b) 10K.

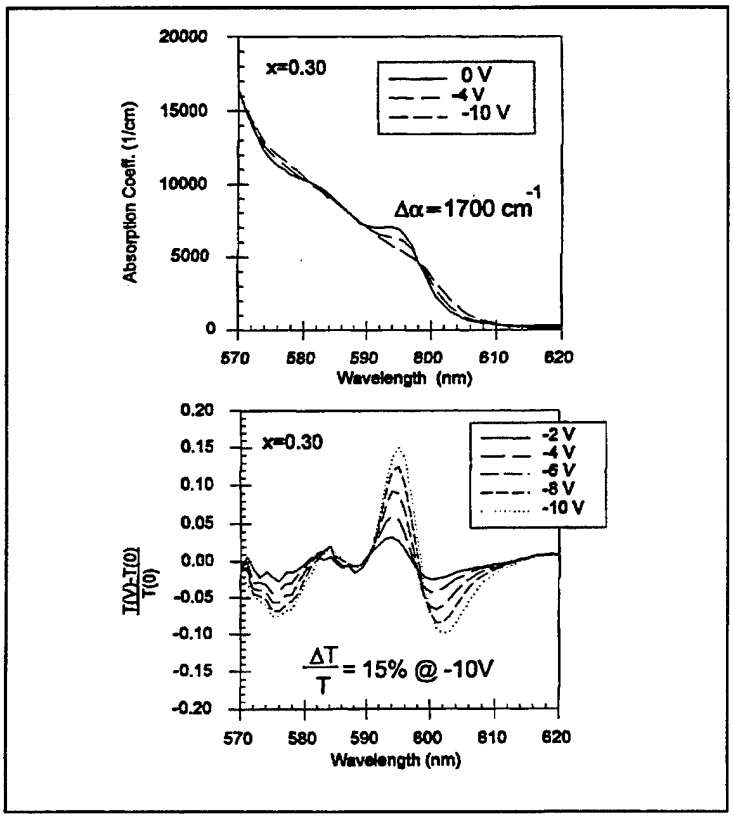

FIG. 4. Bias dependence of (a) absorption coefficient and (b) transmission for the sample with x=0.30, where the transmission at voltage V is T(V).

Nonresonant tunneling in InGaP/InAlP asymmetric double quantum wells

O. Buccafusca, J. L. A. Chilla, C. S. Menoni, J. J. Rocca, M. J. Hafich, L. M. Woods, and G. Y. Robinson
Center of Optoelectronic Computing Systems and Department of Electrical Engineering, Colorado State University, Fort Collins, Colorado 80523

(Received 6 August 1992; accepted for publication 9 November 1992)

Nonresonant tunneling rates have been measured in InGaP/InAlP asymmetric double quantum-well structures for which optical phonon assisted tunneling is energetically forbidden. For an initial photoexcited carrier density of 2.4×10^{11} cm^{-2}, tunneling times of 220, 60, and less than 9 ps have been measured in samples with barrier thickness 4.5, 3.0, and 1.5 nm, respectively. The tunneling times were found to be strongly dependent on carrier density. The measured tunneling times and their dependence on carrier density are compatible with impurity scattering being the dominant mechanism assisting the tunneling.

Tunneling phenomena in semiconductor structures is being actively investigated for fundamental reasons and possible device applications.[1,2] Recently, resonant and nonresonant carrier tunneling has been studied in GaAs based asymmetric double quantum-well (ADQW) structures[3–11] in part motivated by their potential use in optical switching and computing.[9,10] Herein, we report the first tunneling measurements in InGaP/InAlP asymmetric double quantum wells which are suitable for the design of modulators that operate in the visible region of the spectrum. In this work, nonresonant carrier tunneling was investigated in ADQW structures where optical phonon assisted tunneling is energetically forbidden. Steady state and time resolved photoluminescence (PL) measurements were conducted on samples with different barrier thicknesses as a function of carrier density and temperature.

The samples studied, grown by gas source MBE, were unintentionally n doped and consisted of 15 periods of ADQW structures separated by an InAlP layer of 15 nm. Each period consists of InGaP wells of 6 and 12 nm widths, separated by an InAlP barrier having a different width for each sample: 1.5, 3.0, 4.5, and 15 nm. The layer thicknesses are nominal values with an error of less than 10%. The structure with a 15 nm barrier, for which no carrier tunneling is expected to occur, was used as a control sample.

The epitaxial structures were grown on (100) $n+$GaAs substrates at approximately 1 μm/h at 500 °C using thermally cracked AsH_3 and PH_3, conditions that have previously been shown to produce abrupt interfaces and high quality quantum wells.[12,13] Each sample consisted of a GaAs layer (0.25 μm thickness) followed by 15 periods of the ADQW structure and capped by an InAlP layer (0.5 μm thickness). At each heterointerface of the ADQWs, the growth was paused for 18 s without interruption of the PH_3 flow. X-ray diffraction indicated the alloy compositions to be $In_{0.48}Ga_{0.52}P$ and $In_{0.47}Al_{0.53}P$, with lattice match to the GaAs substrate to within 500 ppm. Previous measurements indicate an impurity concentration of $(2–5)\times10^{16}$ cm^{-3} in the InGaP wells.[13]

In the PL measurements, the samples were excited by a train of 2 ps pulses produced by a Rhodamine 560 dye laser synchronously pumped by a frequency doubled mode-locked Nd-YLF laser at a repetition rate of 76 MHz. The excitation energy, around 2.14 eV, was selected to excite both wells simultaneously and to be sufficiently separated from the photon energies corresponding to the PL of the two quantum wells to facilitate detection. The laser beam was focused on the sample with a spot diameter of approximately 36 μm. Steady state PL spectra were taken with a 0.75 m focal length spectrometer and a Hamamatsu R2228 photomultiplier using standard lock-in techniques. The time resolved PL was measured by a synchroscan streak cameras (Hamamatsu M1955) coupled to a thermoelectrically cooled two-dimensional CCD array detector. The streak camera was attached to the exit of a 0.3 m focal length spectrometer provided with a 150 g/mm grating. The time resolution of the system was determined to be 9 ps. The samples were mounted in a closed cycle refrigerated cryostat for low-temperature measurements.

Figure 1 shows the steady state PL signal corresponding to the four ADQW structures with different barrier thicknesses obtained at 11 K. All spectra show two peaks: the stronger one, at lower energy, corresponds to radiative recombination in the wide well and the weaker peak, at higher energy, to the same process in the narrow well. The decreasing PL intensity for the narrow well with decreasing barrier thickness suggests that carriers tunnel from the narrow well to the wide well. This is confirmed by the time resolved PL measurements which, as discussed below, show a strong dependence of the time decay of the narrow well PL with barrier thickness.

From the steady state PL data of Fig. 1 and the values for effective masses, the band gap from Ref. 13 and the band offset given in Ref. 14, we estimated the energy difference between levels in the wells. For all the samples in which tunneling can occur, these calculations yield a difference between the first energy levels in the conduction band of the two wells of less than 34 meV. This energy difference is more than 10 meV below the LO phonon energy for InGaP having the same composition as in our samples.[15] This implies that, in these samples, LO phonon emission is not energetically available to assist the tunneling process. Next, we discuss the results of time resolved PL measurements.

Time resolved PL signals obtained at 11 K are shown

 0003-6951/93/040399-03$06.00

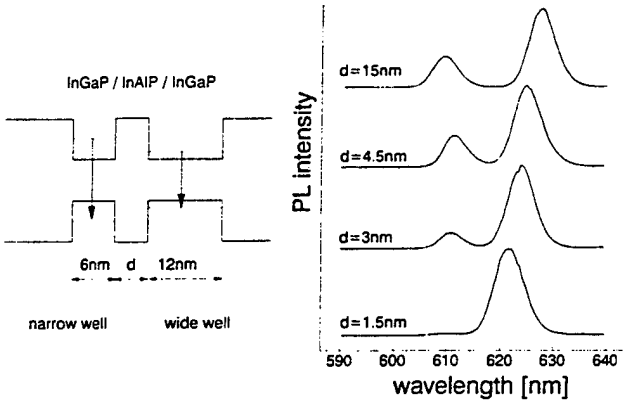

FIG. 1. CW PL at 11 K of ADQWs with different barrier thickness, d. A significant drop in the intensity of the PL peak associated with the narrow well is observed when the barrier thickness is reduced.

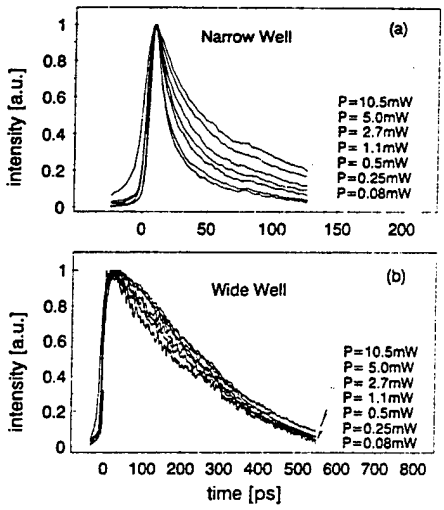

FIG. 3. Low temperature (11 K) time resolved PL signals for the ADQW with a 3 nm barrier as a function of excitation intensity for both the narrow well (a) and the wide well (b).

in Fig. 2 as a function of barrier thickness. Figures 2(a) and 2(b) illustrate the temporal evolution of the PL peak corresponding to the narrow and the wide well, respectively. For the sample with the 15 nm barrier, the time decay of the PL from the narrow well is only slightly shorter than that corresponding to the wide well, which is about 300 ps. As the barrier thickness is decreased, the decay time of the narrow well PL is observed to be consistently shorter. Values of 130, 50, and less than 9 ps (the time resolution of our system) were measured for the ADQWs with barriers of 4.5, 3.0, and 1.5 nm, respectively. In contrast, the decay time of the wide well PL was found to be independent for all the samples, except for the ADQW with a 1.5 nm barrier that showed a shorter decay, probably due to a variation in sample quality.

The decay time of the wide well PL is due to both radiative and nonradiative recombination. In the narrow well, however, carriers can also relax through tunneling to the wide well. The tunneling time can then be calculated from the measured values of the narrow well PL decay

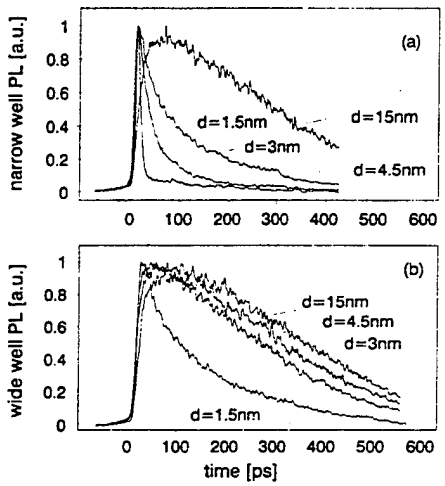

FIG. 2. Time resolved PL signals corresponding to the PL peak wavelength of the narrow well (a) and the wide well (b) for ADQWs with different barrier corresponding to an initial photoexcited sheet carrier density of 2.4×10^{11} cm^{-2}. The measurements were conducted at 11 K.

time and the narrow well recombination time. To calculate the narrow well recombination time, we measured the decay rate of the corresponding wide well and corrected this value for the difference in well thickness according to the ratio of the PL decay times from both wells in our control sample. For an initial photoexcited carrier concentration of 2.4×10^{11} cm^{-2}, the tunneling times were calculated to be approximately 220, 60, and less than 9 ps for the samples with 4.5, 3.0 and 1.5 nm barriers, respectively. These relatively long tunneling times are consistent with the fact that LO phonon assisted tunneling is not available in these samples. Acoustic phonon scattering can also be ruled out as the dominant mechanism assisting the tunneling. Analysis of the time resolved PL spectra shows that the intraband carrier relaxation time due to acoustic phonon scattering is of tens of picoseconds. The associated interwell transfer time is expected to be several orders of magnitude larger due to the reduced overlap of the wave functions.

In the absence of phonon assisted tunneling, the scattering mechanisms that may contribute to tunneling are electron-electron, acoustic phonon, impurity, interface-roughness, and alloy disorder. To gain additional information on the role of different scattering mechanisms, we measured the tunneling rate dependence on carrier density and temperature. Time dependent PL measurements were performed for laser intensities ranging from 0.08 to 10.5 mW corresponding to sheet carrier densities between 8×10^{9} and 1×10^{12} cm^{-2}. Figure 3 shows the measured dependence of the PL decays for the ADQW with a 3 nm barrier as a function of excitation intensity. For the wide well, the PL decay was relatively independent of carrier density. In contrast, the narrow well PL decay time increased approximately four times as the intensity was increased in the range mentioned above. A similar, but weaker, dependence on excitation intensity was measured in the narrow well PL decay of the sample with the 4.5 nm barrier. For the sample with the 1.5 nm barrier the time decay of the narrow well PL remained below the temporal

resolution of our detection system for intensities below 6.5 mW and for intensities above this value the PL decay was also observed to increase. Local heating of the samples caused by the increased intensity may affect PL decay measurements. However, this effect can be ruled out as a possible cause of an increase in carrier lifetime because measurements done as a function of temperature showed the opposite behavior: the PL decay of the wide well was observed to decrease slightly as a function of temperature. Hence, we conclude that the scattering processes that assist tunneling are carrier density dependent.

A possible cause of the observed decrease of the tunneling rate with the increased photoexcited density is space-charge buildup caused by the significantly larger tunneling rates for electrons compared to that of holes, due to their large difference in effective mass. This difference in tunneling rates can cause a charge buildup between the two wells, producing an electric field which increases the potential barrier between the two wells, opposing tunneling. We have calculated that the maximum potential change for our largest carrier density power to be 5 meV. In this calculation we assumed the extreme case in which all of the electrons and none of the holes have tunneled. Since, in practice, the change in the potential barrier is much smaller than this limit value, which is small compared with the energy separation between the initial and final states, we conclude that space-charge effects are not responsible for the observed density dependence. An analysis of the shape of the measured PL decay as a function of time for difference excitation intensities also shows no evidence of space-charge effects.

The increase of the tunneling time with carrier density rules out electron-electron scattering a the dominant tunneling mechanism. The remaining three processes have a dependence on carrier density which is compatible with our observations. However, calculated tunneling times due to alloy scattering, using the potential given by Mukhopadhyay and Nag,[16] resulted in times larger than 1 ns. Tunneling times due to interface roughness, calculated by Ferreira and Bastard,[17] were found to be between one and two orders of magnitude larger than for impurity scattering when the concentration of scatterers is the same as that of impurities. We have calculated the nonresonant tunneling rate for impurity scattering following the procedure outlined by Ferreira and Bastard.[17] Assuming a density of impurities of 5×10^{16} cm^{-3}, and that these impurities are localized mostly at the interfaces, we calculated nonresonant electron tunneling times of 450, 70, and 12 ps for barrier widths 4.5, 3.0, and 1.5 nm, respectively. These calculated values are very similar to the measured tunneling times. This suggests that the mechanism assisting the tunneling is likely to be impurity scattering. A similar decrease of the nonresonant tunneling rate as a function of the density of photoexcited carriers was recently observed in GaAs/AlGaAs ADQW's.[11] The measured tunneling dependence in that experiment was found to be compatible with impurity assisted interwell scattering, and it was also suggested that excitons may tunnel as a single entity.

In summary, we have measured for the first time nonresonant tunneling times in InGaP/InAlP ADQW in which LO phonon assisted tunneling is not allowed. The tunneling times were found to increase as a function of the photoexcited carrier density. The magnitude of the tunneling times and their dependence on carrier density are compatible with impurity scattering being the dominant tunneling mechanism.

The authors wish to acknowledge Professor J. Mahan for lending the closed cycle refrigeration system, Dr. D. Patel and M. Prasad for their assistance in the experiment, and Dr. K. Bhattacharyya for helpful discussions. This work was supported by the Center for Optoelectronic Computer Systems through National Science Foundation Grant ECD 9015128 and by the Colorado Advanced Technology Institute. C. S. Menoni acknowledges here support by the Engineering Foundation AFOSR Research Initiation Grant RI-B-91-16.

[1] F. Capasso, K. Mohammed, and A. Y. Cho, IEEE J. Quantum Electron. **QE-22**, 1853 (1986).
[2] S. Luryi, Superlattices Microstructures **5**, 475 (1989).
[3] T. Tada, A. Yamagushi, T. Ninomiya, H. Uchiki, T. Kobayashi, and T. Yao, J. Appl. Phys. **63**, 5491 (1988).
[4] S. Muto, T. Inata, A. Tacheuchi, Y. Sugiyama, and T. Fujii, Appl. Phys. Lett. **58**, 2393 (1991).
[5] M. Nido, M. G. W. Alexander, W. W. Ruhle, T. Schweizer, and K. Kohler, Appl. Phys. Lett. **56**, 355 (1990).
[6] D. Y. Oberli, J. Shah, T. C. Damen, C. W. Tu, T. Y. Chang, D. A. B. Miller, J. E. Henry, R. F. Kopf, N. Sauer, and A. E. DiGiovanni, Phys. Rev. B **40**, 3028 (1989).
[7] K. Leo, J. Shah, E. O. Gobel, T. C.Damen, S. Schmitt-Rink, W. Schafer, and K. Kohler, Phys. Rev. Lett. **66**, 201 (1991).
[8] N. Sawaki, R. A. Hopfel, E. Gornik, and H. Kano, Appl. Phys. Lett. **55**, 1996 (1989).
[9] C. Tanguy, B. Deveaud, A. Regreny, D. Hulin, and A. Antonetti, Appl. Phys. Lett. **58**, 1283 (1991).
[10] A. Tackeuchi, S. Muto, T. Inata, and T. Fujii, Appl. Phys. Lett. **58**, 1670 (1991).
[11] D. H. Levi, D. R. Wake, M. V. Klein, S. Kumar, and H. Morkoç, Phys. Rev. B **45**, 4274 (1992).
[12] M. J. Hafich, J. H. Quigley, R. E. Owens, G. Y. Robinson, D. Li, and N. Otsuka, Appl. Phys. Lett. **54**, 2686 (1989).
[13] M. J. Hafich, H. Y. Lee, G. Y. Robinson, D. Li, and N. Otsuka, J. Appl. Phys. **69**, 752 (1991).
[14] M. O. Watanabe and Y. Ohba, Appl. Phys. Lett. **50**, 906 (1987).
[15] M. Zachau and W. T. Masselink, Appl. Phys. Lett. **60**, 2098 (1992).
[16] S. Mukhopadhyay and B. R. Nag, Appl. Phys. Lett. **60**, 2897 (1992).
[17] R. Ferreira and G. Bastard, Phys. Rev. B **40**, 1074 (1989).

Strained Layer $In_xGa_{1-x}As/GaAs$ and $In_xGa_{1-x}As/In_yGa_{1-y}P$ Multiple-Quantum-Well Optical Modulators Grown by Gas-Source MBE

J. W. Kim, C. W. Chen, T. J. Vogt, L. M. Woods, G. Y. Robinson, and D. L. Lile

Abstract—**The first results on low-power p-i-n diode modulator structures using strained multiple quantum wells (MQW's) of InGaAs/InGaP grown by gas-source molecular beam epitaxy (MBE) on GaAs are presented. A comparison of transmission, reflection, and photocurrent spectra for these nonresonant devices with those fabricated from InGaAs/GaAs indicates larger modulation, with a maximum change in reflection of > 42% observed at 5-V bias at a wavelength of 0.96 μm.**

I. Introduction

With advances in crystal growth techniques such as molecular beam epitaxy (MBE) and metalorganic deposition (MOCVD), multiple-quantum-well (MQW) structures based on a variety of III-V semiconductor materials have attracted considerable attention for their potential use in high-speed optoelectronic devices. In particular, and starting with the work of Wood *et al.* in GaAs/AlGaAs, [1] many groups have used MQW structures to investigate optical modulation based on the quantum confined Stark effect (QCSE). To date most of this research has relied upon GaAs/AlGaAs MQW p-i-n diode structures, lattice matched on GaAs substrates, which operate at wavelengths around 0.85 μm [2]. Since the GaAs is opaque at these operating wavelengths, cascadability for optical interconnects, switching, or signal processing applications requires removal of the substrate. $In_{0.53}Ga_{0.47}As/InP$ structures, operating at ~ 1.5 μm, avoid this problem, but at the cost of reduced constrast [3]. Another possibility is strained-layer $In_xGa_{1-x}As/GaAs$ QWs on GaAs [4], which, in addition to having a transparent substrate, also possess a relatively low potential barrier in the conduction and valence bands, with the resulting potential for improved speed and reduced saturation via faster carrier sweep-out times and smaller voltage, lower power operation [5]. Similar advantages would be expected to attend the $In_xGa_{1-x}As/In_yGa_{1-y}P$ system except that, in addition, and like $In_xGa_{1-x}As/AlGaAs$ [6], the barrier composition, strain, and related barrier height can also be varied. Strain compensation can also be provided through the use of the ternary barrier—as demonstrated by Cunningham *et al.* [7] in InGaAs/GaAsP structures—thereby permitting the growth of thicker modulators with a minimum of strain induced defects. Lasers have already been demonstrated in these materials [8] and, operating in the 0.95- to 1.1-μm range, these strained materials combinations are compatible with operation at wavelengths at which Si is absorbing, hence allowing for optical interconnects in hybrid III-V/Si systems [9].

In this paper we present results obtained on strained-layer MQW modulators made from $In_xGa_{1-x}As/GaAs$ and $In_xGa_{1-x}As/In_yGa_{1-y}P$ grown by gas source MBE. These are the first results for the $In_xGa_{1-x}As/In_yGa_{1-y}P$ materials system by any growth technique and suggest that, in addition to providing greater material flexibility, the ternary barrier may lead to an improvement in modulator performance.

II. Device Structure

The $In_xGa_{1-x}As/GaAs$ and $In_xGa_{1-x}As/In_yGa_{1-y}P$ MQW p-i-n structures were grown by gas source MBE at 500°C on n^+ (100) GaAs substrates [10]. Two samples, one for each material system, were grown with essentially the same structure. This consisted of a 0.5-μm n^+ GaAs buffer layer followed by an n^+ InGaP etch-stop layer, and 24.5 periods of undoped strained $In_xGa_{1-x}As$ quantum wells, separated by ~ 150-A-thick barriers of either GaAs or InGaP. The structure was completed by growing an undoped GaAs or InGaP buffer layer and a p^+ GaAs or InGaP cap. The nominal thickness and In mole fraction x of the $In_xGa_{1-x}As$ wells were ~ 100 A and 0.15, respectively, and the In mole fraction y of the $In_yGa_{1-y}P$ barriers was ~ 0.5. Individual devices were fabricated in both samples by etching mesas of size 360 μm × 510 μm and e-beam evaporating Au/Ti to make ohmic contact to the n- and p-type GaAs and InGaP regions. The resulting devices exhibited good electrical behavior with breakdown voltages > 20 V for both types of samples. For optical measurements the back side of the devices was chemomechanically polished, and then both surfaces were antireflection coated using SiO_2. For reflection measurements

Manuscript received April 5, 1993; revised June 10, 1993. This work was supported by the NSF and CATI, a funding agency of the State of Colorado.

The authors are with the Optoelectronic Computing Systems Center and the Department of Electrical Engineering, Colorado State University, Fort Collins, CO 80523.

IEEE Log Number 9211419.

the SiO_2 on the rear surface was replaced by an evaporated Au layer.

III. Results and Discussion

Photocurrent, transmission, and reflection spectra of the individual modulators were measured using a monochromator and conventional lock-in techniques. Fig. 1 shows absorption spectra versus reverse bias for an $In_xGa_{1-x}As/GaAs$ device. Photocurrent spectra were very similar in shape. The absorption coefficient values were calculated from the transmission spectra using a total QW layer thickness of 0.61 μm. From these data we see that the excitonic resonances in this sample are relatively broad, resulting presumably from strain-induced defects as well as alloy disordering. Visual inspection using a Nomarski microscope revealed relatively weak, though certainly discernable, cross hatchings across the entire wafer, indicating the presence of misfit dislocations resulting from strain relief. On application of bias, the shift in the absorption peaks to larger wavelength resulting from the QCSE is clearly evident. In particular, the change in the absorption coefficient at the zero-bias heavy hole peak at 9880 A is 2743 cm^{-1} for 7 volts of reverse bias corresponding to a contrast ratio (CR) of 1.16. Due to the small difference in the bandgap energy of the InGaAs well material, estimated in our case to be 1.27 eV, and the GaAs (1.42 eV) barrier, we would expect rapid dissociation of the excitons at low applied voltages due to field-assisted tunneling. This is evidenced in Fig. 1 by both the rapid distortion of the spectra at low biases and the associated marked broadening of the excitons. Noteworthy for low-power modulator applications is the almost complete extinguishing of the exciton resonance at voltages as low as 5 V, resulting presumably from the shallow wells in this structure [7].

In Fig. 2 we show the photocurrent and equivalent absorption data to Fig. 1, but for an $In_xGa_{1-x}As/In_yGa_{1-y}P$ device, where we have normalized the photocurrent curves to the same value at 0.90 μm to more clearly show the progression of the exciton peaks with bias. The inset shows the fit between the experimental and theoretical shift of the heavy hole peak with bias. The theoretical curve in this figure was calculated using a second-order perturbation theory [11], using values for the well width of 90A, obtained from TEM cross sections [12], and effective mass values of 0.0627 m_0 and 0.444$_0$ for the electron and heavy hole, respectively. These mass values were chosen to effect the best fit with the data and are similar to those reported earlier by others [13], [14]. It is clear in both the sets of data in Fig. 2, but most pronounced in the photocurrent curves, that in contrast to the GaAs barrier sample, where weak transitions at higher energies completely disappear with applied field, increasing reverse bias leads to the appearance of strong higher order peaks. These are somewhat reminiscent of the spectra observed by Pezeshki *et al.* [6] on InGaAs/AlGaAs and may result in both cases from strain. Although uncertainties in barrier heights and strain in this material system make the calculations of exciton energies somewhat imprecise, reasonable estimates for these quantities lead to resonance values not inconsistent with those in the data in Fig. 2, as indicated by the arrows which show the calculated positions of the 1*ehh*, 1*e2hh*, and 1*elh* peaks using the same mass values as above. Presumably the absence of higher energy excitons in the spectra of Fig. 1 results from the extreme shallowness of the wells and their inability to confine other than the $n = 1$ level. Exciton full width at half maximum (FWHM), obtained from a Lorentzian fit with the 1*ehh* transition at zero bias in Fig. 2(b), gives a value of 10.5 meV, slightly smaller than the value of 14 meV reported for the InGaAs/AlGaAs MQW system [15].

Reflection spectra and the associated transmission and reflection modulation behavior of the InGaP barrier device are shown in Figs. 3–5. From the last two figures we see that the majority of the modulation takes place for the

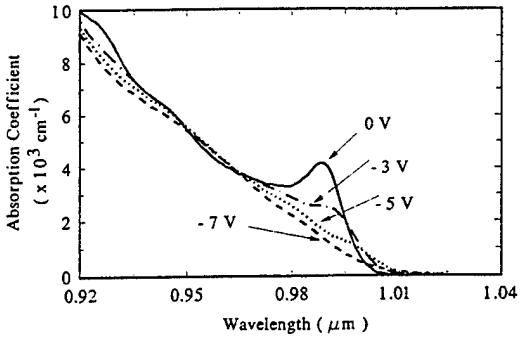

Fig. 1. Absorption spectra of an InGaAs/GaAs device.

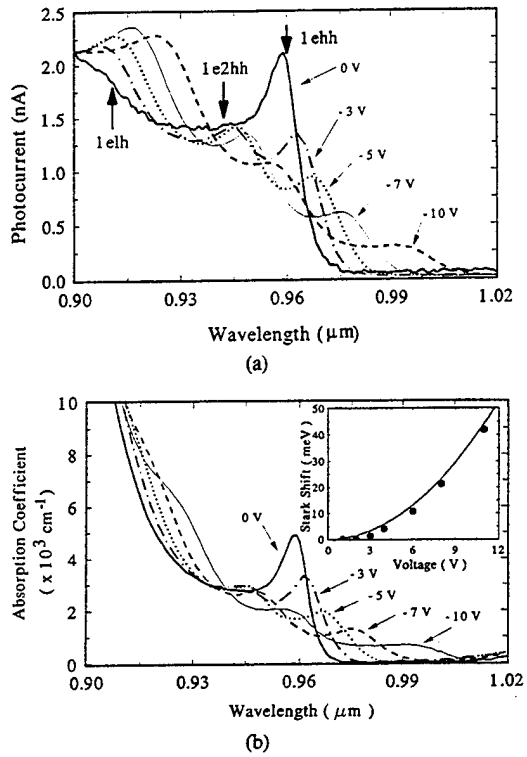

Fig. 2. (a) Photocurrent spectra of an InGaAs/InGaP device. The arrows show the calculated positions of the first three exciton peaks. (b) Absorption spectra of an InGaAs/InGaP device. The inset shows experimental (dotted) and theoretical (solid) Stark shifts of the 1*ehh* exciton versus reverse bias.

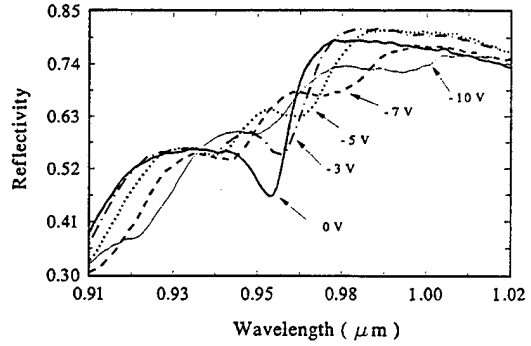

Fig. 3. Reflection spectra of an InGaAs/InGaP MQW modulator measured at various values of reverse bias.

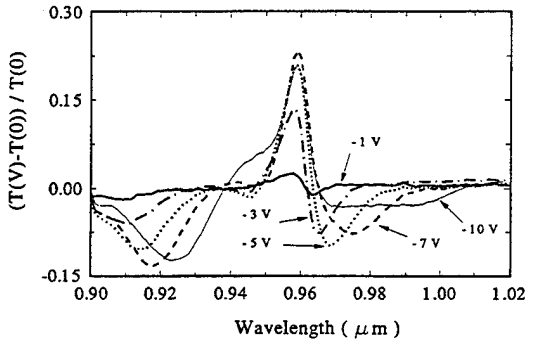

Fig. 4. Transmission modulation spectra of an InGaAs/InGaP MQW device.

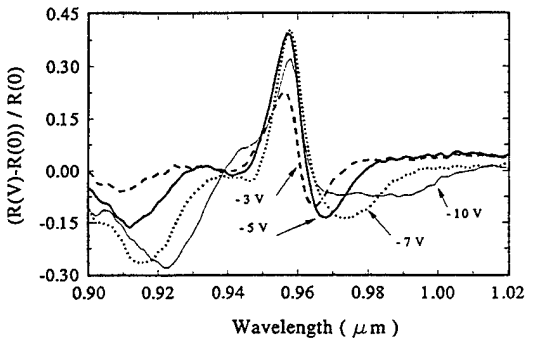

Fig. 5. Reflection modulation spectra of an InGaAs/InGaP MQW device.

first 7 volts of applied bias. From the transmission data, and at the peak wavelength of 0.959 μm, we obtain an absorption coefficient change of 3511 cm^{-1}, corresponding to a 9% change in absolute transmission and a fractional change of 24% for 7-V bias. This gives a CR of 1.24, which should be compared to the value of 1.16 obtained under the same conditions in the GaAs barrier structures. In reflection, because of the double pass through the optically active QW stack, we observe a larger effect with $> 42\%$ change in the optical signal. These results suggest that InGaP may result in some significant advantages over GaAs when employed with InGaAs for MQW modulator applications. Certainly, the variable composition of barrier and well means that band offsets and strain can be varied independently to optimize the electrooptic effect. From our results it is evident that the increased barrier height, compared to that with GaAs, has enhanced the excitonic effects at zero bias and increased the resistance to rapid deterioration of the excitonic resonance with increasing applied biases. This is similar to results achieved by adding aluminum to the barrier regions in the InGaAs/AlGaAs material system to enhance electroabsorption [6]. Another advantage is the flexibility the ternary barrier allows for the growth of a sample with a balanced strain, where biaxial compressive strain induced in the InGaAs well due to a larger lattice constant can be balanced with a tensile strain occurring in the InGaP barrier [7], [16]. Thus, in principle, a sample with InGaP barriers ($y < 0.48$) and InGaAs wells can be grown with no net strain accumulation, resulting in no lattice relaxation and a low density of dislocations. In this way a greater number of wells can be grown so as to increase the optical interaction distance and thereby enhance the modulation.

REFERENCES

[1] T. H. Wood *et al.*, "High-speed optical modulation with GaAs/GaAlAs quantum wells in a p-i-n diode structure," *Appl. Phys. Lett.*, vol. 44, p. 16, 1984.

[2] T. K. Woodward *et al.*, "Operation of a fully integrated GaAs-$Al_xGa_{1-x}As$ FET-SEED: A basic optically addressed integrated circuit," *IEEE Photon. Technol. Lett.*, vol. 4, p. 614, 1992.

[3] J. Thompson *et al.*, "The growth and characterization of InP-based multiquantum wells and multilayer structures," *J. Electron. Materials*, vol. 19, p. 323, 1990.

[4] Li Chen, K. C. Rajkumar, and A. Mahukar, "Optical absorption behavior of strained $In_xGa_{1-x}As/GaAs(100)(\times < 0.25)$ multiple quantum well structures grown via molecular beam epitaxy," *Appl. Phys. Lett.*, vol. 57, p. 2478, 1990.

[5] L. Buydens, P. Demeester, Z. Yu, and P. Van Daele, "High contrast/low voltage normally-on InGaAs/AlGaAs asymmetric Fabry–Perot modulator," *IEEE Photon. Technol. Lett.*, vol. 3, p. 1104, 1991.

[6] B. Pezeshki, S. M. Lord, and J. S. Harris, Jr., "Electroabsorptive modulators in InGaAs/AlGaAs," *Appl. Phys. Lett.*, vol. 59, p. 888, 1991.

[7] J. E. Cunningham, K. W. Goosen, M. Williams, and W. Y. Jan, " Pseudomorphic InGaAs-GaAsP quantum well modulators on GaAs," *Appl. Phys. Lett.*, vol. 60, p. 727, 1992.

[8] N. Yamada and J. S. Harris, Jr., "Strained InGaAs/GaAs single quantum well lasers with saturable absorbers fabricated by quantum well intermixing," *Appl. Phys. Lett.*, vol. 60, p. 2463, 1992.

[9] C. Cameri-Ginestet, Y. W. Kim, N. M. Jokerst, M. G. Allen, and M. A. Brooke, "Three dimensional integrated circuits: Epitaxial lift-off GaAs photodetectors integrated directly on top of silicon circuits," presented at the *IEEE Lasers and Electro-Optics Society Topical Meeting on Smart Pixels*, Santa Barbara, CA, Aug. 1992.

[10] J. H. Quigley, M. J. Hafich, H. Y. Lee, R. E. Stave and G. Y. Robinson, "Growth of InGaP on GaAs using gas-source MBE," *J. Vac. Sci. Technol.*, vol. B7, p. 358, 1989.

[11] F. M. Fernandez and E. A. Castro, "Hypervirial-perturbational treatment of a particle in a box in the presence of an electric field," *Physica*, vol. 111A, p. 334, 1982.

[12] K. Mahalingam and N. Otsuka, Private communication.

[13] D. J. Arent, K. Deneffe, C. Van Hoof, J. De Boeck, and G. Borghs, "Strain effects and band offsets in GaAs/InGaAs strained layered quantum structures," *J. Appl. Phys.*, vol. 66, p. 1739, 1989.

[14] G. Ji, D. Huang *et al.*, "Optical investigation of highly strained InGaAs/GaAs multiple quantum wells," *J. Appl. Phys.*, vol. 62, p. 3366, 1987.

[15] K. Fujiwara, K. Kawashima, K. Kobayashi and N. Sano, "Electro-optical bistability in strained $In_xGa_{1-x}As/Al_{0.15}Ga_{0.85}As$ multiple quantum wells," *Appl. Phys. Lett.*, vol. 57, p. 2234, 1990.

[16] T. K. Woodward, T. H. Chiu, and Theodore Sizer II, "Multiple quantum well light modulators for the 1.06 μm range on InP substrates: $In_xGa_{1-x}As_yP_{1-y}/InP$, $In_yGa_{1-y}P/InP$, and coherently strained $InAs_yP_{1-y}/In_xGa_{1-x}P$," *Appl. Phys. Lett.*, vol. 60, p. 2846, 1992.

Wannier–Stark localization in a strained-layer $In_xGa_{1-x}As/In_yGa_{1-y}P$ superlattice

J. W. Kim, Y. J. Lee, T. J. Vogt, G. A. Patrizi,[a] G. Y. Robinson, and D. L. Lile
Center for Optoelectronic Computing Systems and Department of Electrical Engineering, Colorado State University, Fort Collins, Colorado 80523

(Received 28 November 1995; accepted for publication 17 January 1996)

We present an observation of the Wannier–Stark effect in a strained InGaAs/InGaP superlattice grown on a GaAs substrate. A blueshift of the effective absorption edge is observed in room and low-temperature photocurrent and transmission measurements. A ~2000 cm^{-1} absorption change due to the transition of the absorption edge from a broad to a sharp quantum well-like excitonic shape was obtained for as little as a 2 V change in bias voltage. © *1996 American Institute of Physics.* [S0021-8979(96)02409-2]

INTRODUCTION

In recent years, there has been growing interest in electroabsorption modulators based on Wannier–Stark localization in superlattice (SL) structures because of their potential for low voltage, and, hence, low power, operation in optical interconnect and switching systems applications.[1] In contrast to a quantum well (QW) structure, a superlattice consists of alternating semiconductor layers where the barrier layer is sufficiently thin to allow appreciable tunneling and a strong resonant coupling between adjacent quantum wells. Due to this coupling, the discrete energy levels found in QWs broaden into minibands of widths ΔE and ΔH in the conduction and valence bands, respectively. By applying an electric field the resonant condition of aligned energy levels in adjacent wells can be easily destroyed so that the initially delocalized SL wave functions become localized over a few adjacent QWs, leading to a blueshift of the effective absorption edge of the order $(\Delta E+\Delta H)/2$.[2] Since this Wannier–Stark localization can occur at a relatively small electric field, typically in the range of a few tens of kV/cm, a low drive voltage electroabsorption modulator can in principle be realized using the SL structure. To date the Wannier–Stark effect has been mostly observed in the GaAs/AlGaAs and InP-based material systems lattice matched on GaAs and InP substrates, respectively.[3–7] A 22 000 cm^{-1} absorption change for 6.8 V voltage swing in a GaAs/AlGaAs SL[5] and a reflection change of 32% for 4 V of bias in an InGaAs/InP SL modulator[7] are examples of results reported to date. More recently, with advances in crystal growth techniques, strained-layer InGaAs/GaAs SLs have also been fabricated.[8,9] In this paper, we report for the first time observation of a blueshift in a superlattice made from strained $In_xGa_{1-x}As/In_yGa_{1-y}P$, a materials system which has been previously employed for low power multiple QW modulators.[10]

EXPERIMENT

The $In_xGa_{1-x}As/In_yGa_{1-y}P$ SL $p-i-n$ structures used in this study were grown by gas source molecular beam epitaxy (MBE) on n^+(001) GaAs substrates at 500 °C. The sample consisted of a 0.6 μm thick n^+ GaAs buffer layer followed by an undoped 300 Å GaAs layer, and 49.5 periods of an undoped 60 Å $In_{0.13}Ga_{0.87}As$ well/20 Å $In_{0.48}Ga_{0.52}P$ barrier SL of residual carrier concentration $n\sim10^{16}$ cm^{-3}. The structure was completed by growing an undoped 300 Å thick GaAs layer and a p^+ GaAs cap layer as shown schematically in Fig. 1. Individual devices were fabricated by wet etching mesas of size 360×510 μm^2 Ohmic contacts were made by e-beam evaporating Ti/Au on both the n- and p-type GaAs regions. Typical I–V characteristics of the $p-i-n$ diodes showed low reverse leakage currents of <100 nA and breakdown voltages >15 V. For optical measurements the back side of the substrate was polished and antireflection coated using SiO_2. Photocurrent and transmission measurements were then performed at room and low temperatures (~20 K) using a monochromator and conventional lock-in techniques.

RESULTS

Figure 2 shows typical photocurrent (PC) spectra obtained as a function of reverse bias voltage at 300 K and 20 K. At low bias, the spectra show no significant excitonic features, consistent with the presence of minibands and delocalization of the carriers. In Fig. 2(a) we observe two bumps, identified by the arrows, near 1.319 eV and 1.366 eV, which are presumably associated with miniband transitions from the ground-state electron to heavy hole (HH) and light hole (LH) excited states, respectively. For a quantitative analysis, the SL band structure was calculated using a simple Kronig–Penney model. Values of the material parameters were estimated by linearly interpolating between the binary parent compounds.[11] The band offsets at the heterojunction in the presence of strain were determined using the model-solid theory of Van de Walle.[12] Although x-ray diffraction indicates dislocations are distributed throughout the superlattice, for purposes of calculation, we assumed that misfit dislocations were confined only to the interface between the multilayer and the substrate and thus that the superlattice tends to the average lattice constant of the unsupported multilayer structure.[13] The calculated band-offset values are 197, 418, and 352 meV for the electron, HH, and LH, re-

[a]Present address: Sandia National Laboratories, Alburquerque, NM.

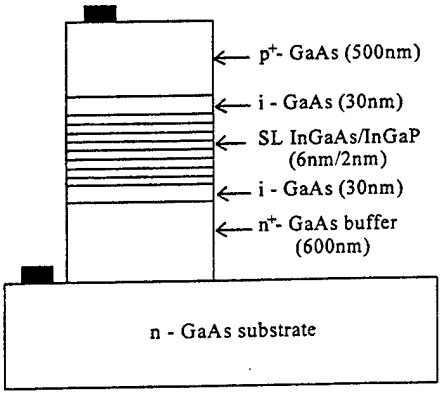

FIG. 1. Schematic diagram of the strained InGaAs/InGaP superlattice structure.

spectively. Corresponding fractional conduction band offsets for the electron-heavy-hole and the electron-light-hole system are 0.32 and 0.36, respectively. With these values, the carrier miniband widths were computed; 35, 0.1, and 16 meV for the electron, HH, and LH, respectively. As the applied reverse bias increases, the absorption edge evolves from that appropriate to a 3D SL to a 2D QW-like excitonic line shape due to the Wannier–Stark localization. A relatively small electric field induces carrier wave function localization and thus increases the excitonic binding energy and the excitonic oscillator strength. This can be seen in Fig. 2(a) where a well-resolved excitonic peak appears at 1.310 eV, in good agreement with a calculated value of 1.308 eV

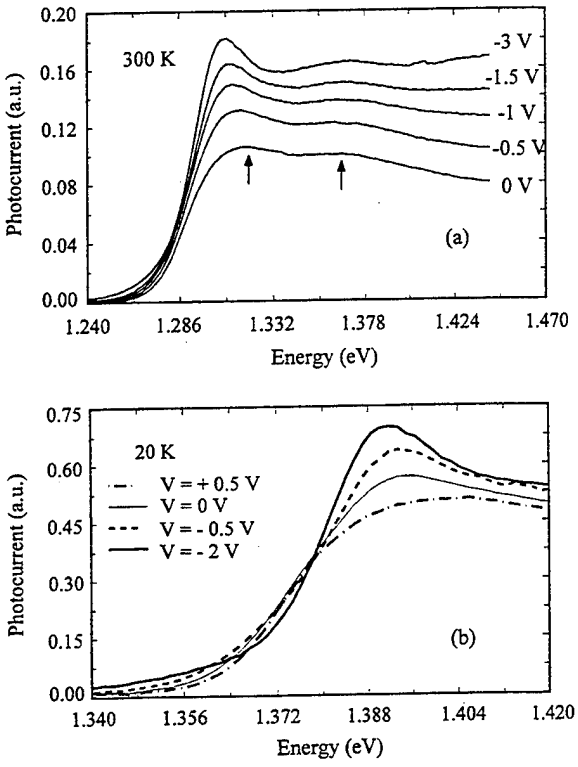

FIG. 2. Photocurrent spectra taken at (a) 300 K and (b) 20 K for various values of reverse bias.

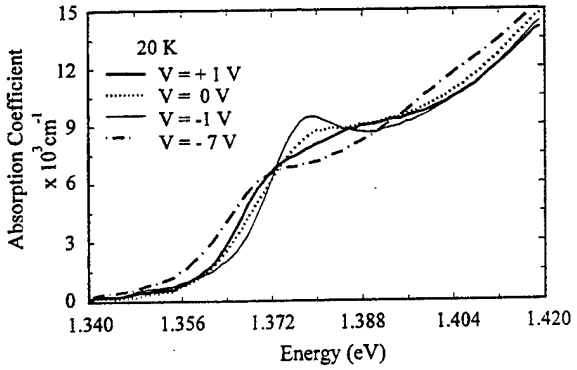

FIG. 3. Low temperature absorption spectra of sample in the presence of various applied biases.

we obtained using a QW exciton binding energy of 8 meV.[9] The 20 K PC spectra shown in Fig. 2(b) are similar to those at 300 K, but show more clearly a blueshift of the effective absorption edge at ~1.364 eV. In addition, a weak absorption variation is also observed below the SL band edge in Fig. 2(b), possibly caused by the appearance of the low-energy oblique transitions due to the carriers localized in different wells. Nevertheless, in this sample a pronounced Stark ladder was not observed, possibly as a result of generation of misfit dislocations due to strain relaxation and the electric field inhomogeneity due to the large residual doping.

Transmission measurements were performed to directly study electroabsorption properties of the SLs. Figure 3 shows absorption spectra at 20 K in the presence of various applied biases. The absorption coefficient values were calculated from the transmission spectra using a total SL layer thickness of 0.4 μm. We obtain a positive absorption coefficient change of ~2000 cm^{-1} at the QW-like excitonic peak at 1.393 eV for only 2 V bias swing and, due to the blueshift of the effective absorption edge, a negative change of 1565 cm^{-1} at wavelengths close to 1.375 eV. At high reverse biases $\gtrsim$3 V, the oscillator strength of the QW exciton tends to saturate, corresponding to full localization of the carriers, and the exciton peak starts to redshift due to the quantum confined Stark effect (QCSE), giving rise to an absorption change of 2770 cm^{-1} for applied voltages of -1 V to -7V at 1.393 eV. The field-induced Wannier–Stark shifts of the SL, corresponding to a blueshift of the absorption edge can

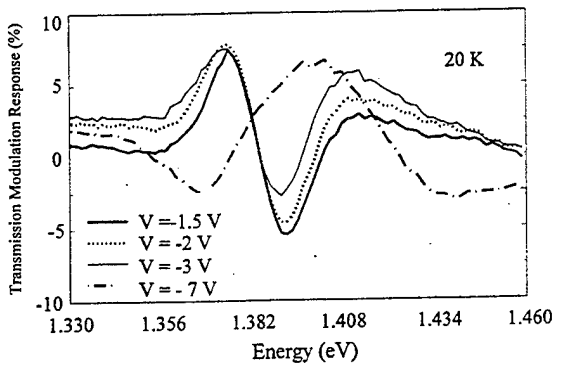

FIG. 4. Transmission modulation spectra measured at 20 K. The relative transmissions were calculated with respect to the transmission T_0 at +1 V.

be used in a "normally off" electroabsorptive modulator to achieve high modulation ratios at moderately low bias voltages. A contrast ratio greater than 130:1 from this mechanism was reported using GaAs/AlGaAs SL asymmetric Fabry–Perot modulators.[14]

Figure 4 shows the transmission modulation response ($\Delta T/T_0$) where T_0 is the transmission at +1 V. From the data we see that the majority of the modulation occurs for the first 2 volts of applied bias. Maximum fractional modulation at −2 V is ~8% at 1.375 eV. Our results suggest that the InGaAs/InGaP SL can have application as a low-drive voltage optical modulator. The relatively low values of modulation could presumably be enhanced, as has been accomplished in other materials systems, using reflection or resonant structures. In addition, the use of the ternary binary InGaP provides the flexibility to tailor the electronic properties of the SL layer through changes in the barrier composition, and further allows for the growth of samples with balanced strain in both the well and barrier, possibly resulting in an enhancement in modulator performance.

ACKNOWLEDGMENT

This work was supported by the Air Force Office of Scientific Research (Contract No. F 49620-93-1).

[1] E. Bigan, M. Allovon, M. Carre, C. Braud, A. Carenco, and P. Voisin, IEEE J. Quantum Electron. **QE-28**, 214 (1992).

[2] E. E. Mendez, F. Agullo-Rueda, and J. M. Hong, Phys. Rev. Lett. **60**, 2426 (1988).

[3] I. Bar-Joseph, K. W. Goossen, J. M. Kuo, R. F. Kopf, D. A. B. Miller, and D. S. Chemla, Appl. Phys. Lett. **55**, 340 (1989).

[4] R. H. Yan, R. J. Simes, H. Ribot, L. A. Coldren, and A. C. Gossard, Appl. Phys. Lett. **54**, 1549 (1989).

[5] G. R. Olbright, T. E. Zipperian, J. Klem, and G. R. Hadley, J. Opt. Soc. Am. B **8**, 346 (1991).

[6] J. Bleuse, P. Voisin, M. Allovon, and M. Quillec, Appl. Phys. Lett. **53**, 2632 (1992).

[7] C. W. Chen, J. W. Kim, P. Silvestre, M. J. Hafich, L. M. Woods, G. Y. Robinson, and D. L. Lile, J. Appl. Phys. **74**, 5895 (1993).

[8] B. Soucail, N. Dupuis, R. Ferreira, P. Voisin, A. P. Roth, D. Morris, K. Gibb, and C. Lacelle, Phys. Rev. B **41**, 8568 (1990).

[9] G. Ji, D. Huang, U. K. Reddy, T. S. Henderson, R. Houdre, and H. Morkoc, J. Appl. Phys. **62**, 3366 (1987).

[10] J. W. Kim, C. W. Chen, T. J. Vogt, L. M. Woods, G. Y. Robinson, and D. L. Lile, IEEE Photon. Technol. Lett. **5**, 987 (1993).

[11] Landolt–Borstein, *New Series Group III* (Springer, Berlin, 1982), Vol. 17a.

[12] C. G. Van de Walle, Phys. Rev. B **39**, 1871 (1989).

[13] Jianhua Li, Zhenhong Mai, Shufan Cui, Junming Zhou, and Wei Feng, Appl. Phys. Lett. **63**, 3327 (1993).

[14] K.-K. Law, R. H. Yan, L. A. Coldren, and J. L. Merz, Appl. Phys. Lett. **57**, 1345 (1990).

Saturation Intensity and Time Response of InGaAs–InGaP MQW Optical Modulators

M. E. Watson, J. L. A. Chilla, J. J. Rocca, J.-W. Kim, D. L. Lile, T. J. Vogt, and G. Y. Robinson, *Senior Member, IEEE*

Abstract—**We report modulation saturation and time response measurements on InGaAs–InGaP MQW modulators. The measurements yield a saturation intensity of (3.7 ± 0.1) kW/cm^2 for a 0–10 V swing and switching times between 10 and 90 ns, depending on the bias voltage and incident light intensity. The observed dependence indicates that field screening due to carrier build-up is the dominant physical mechanism determining both the speed and the saturation intensity. This conclusion is supported by results of theoretical calculations.**

I. Introduction

INCREASING demands for high-speed optical switching devices has sparked considerable interest in the area of addressable optical modulators. Much success has come from work on multiple quantum well modulators utilizing the quantum confined Stark effect (QCSE). Material systems which have been studied for this purpose include GaAs–AlGaAs [1]–[3] InGaAs–AlGaAs [4], [5], InGaAs–GaAs [6]–[8], and InGaAs–GaAsP [9]. Recently, p-i-n modulators based on strained layers of InGaAs–InGaP grown on GaAs have also been demonstrated [10]. The InGaAs–InGaP modulators, which offer the advantage of a transparent GaAs substrate, were shown to require low bias voltages ($\sim$ 5 V) for operation, and hence reduced power dissipation. Modulation of the absorption at the wavelength of the excitonic peak up to 25% has been obtained for a single transmission pass. However, two important device parameters for its utilization in applications: the saturation intensity and time response had not been studied.

In this paper, we report the results of a study of saturation intensity and time response for nonresonant InGaAs–InGaP MQW modulators and analyze the dominant physical mechanisms responsible for the observed device performance. The MQW modulators used in the experiments are p-i-n diodes with the intrinsic region comprised of 24.5 periods of undoped, strain compensated $In_xGa_{1-x}As$–$In_yGa_{1-y}P$ quantum wells fabricated using gas source MBE [10]. The mole fractions used were $x = 0.15$ and $y = 0.5$. The top and bottom of the modulators have InGaP buffer layers 0.5 μm thick. The quantum well thickness is 10 nm and the barrier thickness is 15 nm. The barrier thickness was chosen to provide adequate tensile strain to compensate the compressive strain of the mismatched well layers, and thus avoid the formation of misfit dislocations. The devices were grown with 360 μm × 510 μm active areas, Au–Ti contacts, and SiO_2 anti-reflection coatings. The samples used were from an array of modulators on the same region of a wafer which was configured for transmission measurements.

The next section discusses the saturation intensity measurements and Section III the results of the time response measurements. Finally, Section IV presents a simple model for the carrier sweep-out that describes well the observed intensity and voltage dependence of the transmission of the devices and gives values of the saturation intensity and time response of the modulation which are similar to those obtained experimentally.

Manuscript received April 29, 1994; revised August 10, 1994. This work was supported by the National Science Foundation, Center for Optoelectronic Computer Systems through NSF Grant ECD 9015128, by the Colorado Advanced Technology Institute Grant 1537757 and by the Air Force Office of Scientific Research (Contract F49620-93-1).

The authors are with the Center for Optoelectronic Computing Systems and Department of Electrical Engineering, Colorado State University, Fort Collins, CO 80523 USA.

IEEE Log Number 9407803.

II. Measurements of the Saturation Intensity

The performance of modulators at high intensity is affected by several phenomena caused by the high density of photogenerated carriers including phase space filling [3], field screening due to charge build-up [11], [12], and thermal effects [13]. To determine the saturation intensity, we measured the transmission of the modulator at the excitonic wavelength as a function of incident light intensity. For this measurement we used a tunable CW Ti:Sapphire laser pumped by a CW argon ion laser as the light source. The light detection was done using p-i-n silicon photodiodes and standard lock-in detection techniques. To minimize heating of the sample, the output of the laser was modulated using a specially constructed optical chopper to achieve pulses of $\sim$4 μs duration with a repetition rate of $\sim$3.5 kHz. The beam was focused on the sample utilizing a 5 cm focal length lens and the sample was positioned at the focal plane. The beam profile was measured to be approximately Gaussian and circular, with a $1/e$ intensity radius of 10 μm at the focus. The power density on the sample was adjusted by selecting the power of the laser using a variable neutral density filter.

Fig. 1 shows the transmission spectra of the InGaAs–InGaP modulators for applied voltages of 0 and 6 V of reverse bias for two different optical powers. For low intensity (75 W/cm^2) and no bias applied to the device, the excitonic resonance is clearly visible as an absorption peak at 960 nm. Applying 6 V to the device, the excitonic peak shifts and broadens due to the quantum confined Stark effect, resulting in a net change in transmission at the excitonic wavelength that allows the use of this device as a modulator at that wavelength. With a 10 V swing in applied bias, the contrast ratio is 1.25 which could be increased by configuring the device for reflection operation [10]. Fig. 1(b) shows the effect of high intensity (2.5 kW/cm^2) on the transmission spectrum of the device. The 0 V data still

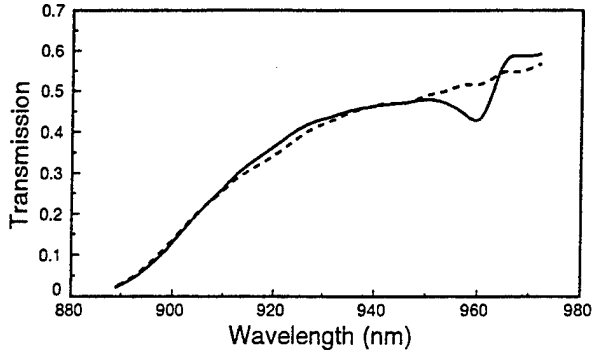

(a)

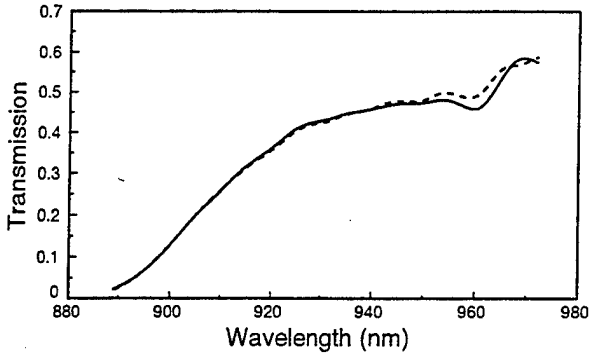

(b)

Fig. 1. Transmission spectra of the modulator measured at two different intensities, 75 W/cm^2 (a) and 2.5 kW/cm^2 (b), and applied voltages, 0 (solid line) and 6 V (dashes).

shows the excitonic peak, although not as distinct as in the low intensity case. The change in transmission with applied voltage is also smaller at high intensity, thus reducing the contrast ratio of the device.

From a technological point of view, and regardless of the physical origin of this saturation, it is necessary to define a parameter that characterizes the dependence of the contrast ratio CR with incident intensity I. As done in [14], we will define the modulation saturation intensity I_{sat} according to the following expression

$$\mathrm{CR}(I) = 1 + \frac{\mathrm{CR}(0) - 1}{1 + I/I_{sat}}. \quad (1)$$

The measured dependence of the contrast ratio with incident power density was fitted with expression (1) for voltage swings ranging from (0–3 V) to (0–10 V). Fig. 2 shows the change in contrast ratio corresponding to a 0–10 V bias swing for four different devices for input intensities between 0.1 and 60 kW/cm^2. As can be observed in the figure, the dependence of the contrast ratio as a function of the light intensity is well described by expression (1) (solid line) for all four devices. The fitted value of saturation intensity for a 0–10 V swing is (3.7 ± 0.1) kW/cm^2.

Fig. 3 shows the resulting dependence of modulation and saturation intensity with voltage. At low power, the modulation saturates at about 6 V (Fig. 3(a)). This is consistent with the fact that the excitonic absorption is washed out for voltages greater than ~6 V [10]. For higher power, the modulation remains linear with voltage within the 0–10 V range studied, but its maximum decreases due to saturation. The saturation

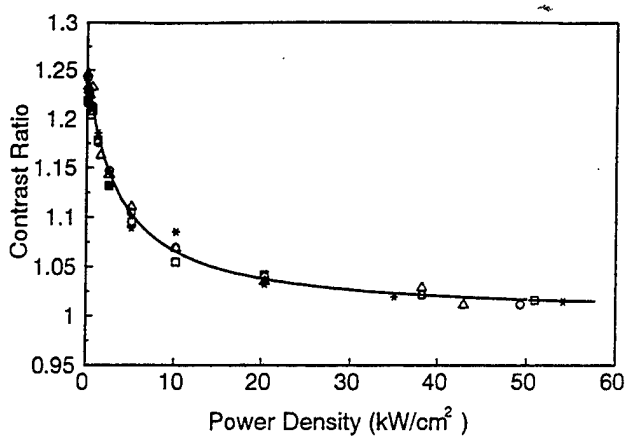

Fig. 2. Contrast ratio versus incident intensity for a 10 V change in applied voltage. The symbols represent different devices in the same wafer, the solid curve is a least squares fitting.

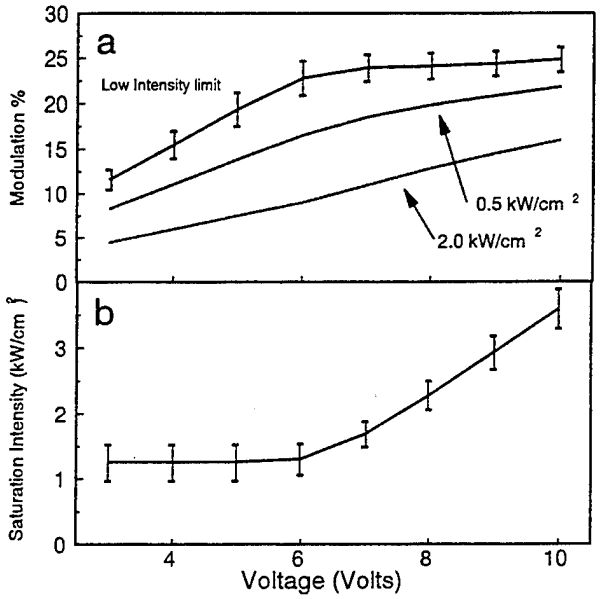

Fig. 3. Dependence of modulation (a) and saturation intensity (b) as a function of operating voltage.

intensity as a function of applied voltage is shown in Fig. 3(b). The saturation intensity is relatively constant with a value of (1.3 ± 0.1) kW/cm^2 up to ~6 V where the saturation begins to increase linearly with voltage to reach (3.7 ± 0.1) kW/cm^2 at 10 V. This saturation intensity value is relatively small when compared with that of similar devices constructed utilizing other material systems [3], [14], [15].

A physical mechanism affecting the performance of modulators at high light intensities is the saturation of the excitonic absorption [3]. Our measurements indicate that in these devices, this is not the dominant physical mechanism responsible for the observed saturation of the modulation. This can be concluded from Fig. 4. Fig. 4(a) shows the differential transmission spectra for a 0–6 V swing both at low and high intensity. The operating wavelength is indicated by a vertical dotted line in the figure. It is evident that degradation of the modulation occurs at high intensity. Fig. 4(b) shows the corresponding transmission spectra at 0 and 6 V for low and high intensity. The transmission at the operation wavelength

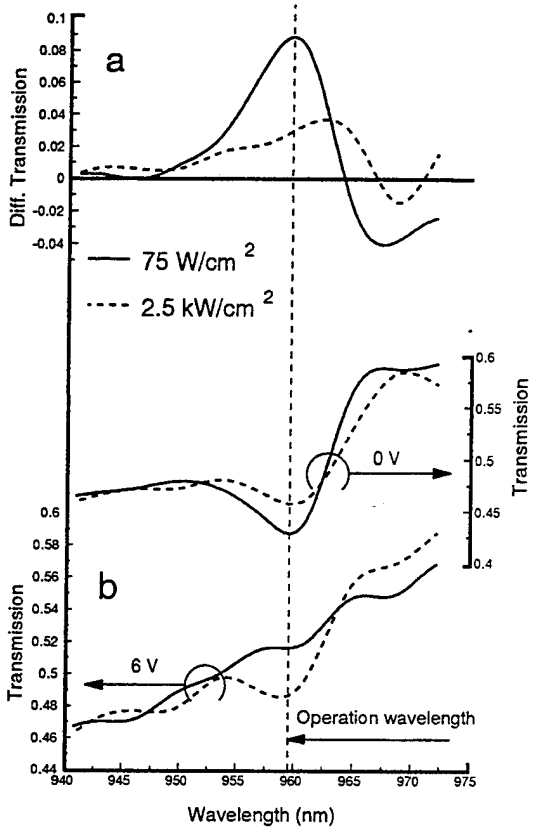

Fig. 4. (a) Differential transmission spectra at low and high intensities for a 0–6 V voltage swing. (b) Transmission spectra at 0 and 6 V for the same intensities as in (a).

drops noticeably at high intensity for the 6 V data, contrary to what would be produced by saturation of the excitonic absorption. We note that most of the saturation observed in the modulation is due to the change in transmission at 6 V, suggesting that field screening due to charge build-up [11], [12] and/or thermal effects caused by ohmic heating associated with the photocurrent [13] are responsible for the observed saturation of the modulation. The role of these mechanisms will be discussed in the following sections.

As discussed in [3], there is a close relationship between the sweep out time of the carriers and the value of the saturation intensity. For that reason, time response measurements on the modulators not only have a value of their own in characterizing device performance, but also provide further evidence that allows the attribution of the observed saturation to field screening effects. The results of time response measurements are discussed in the following section.

III. Time Response Measurements

The time response of the device was characterized by measuring the change in transmission at the excitonic wavelength produced by fast (<4 ns risetime) electrical bias pulses applied to the device. Simultaneous measurement of the current shows that the capacitance of the device (~30–50 pF) is not a limitation for its speed in this range. The transmitted light was detected with a silicon photodetector having a response time of approximately 1 ns. The signal was amplified by a fast (3 ns risetime) amplifier and was measured with a 250 MHz

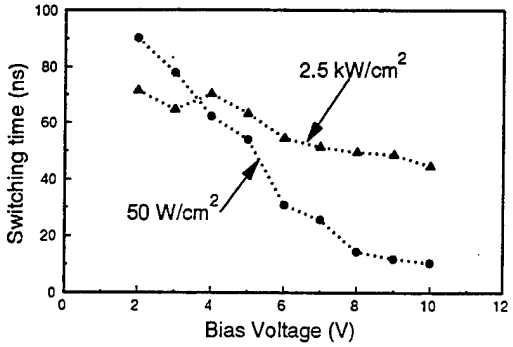

Fig. 5. Switching time (10%–90%) versus operating voltage measured for 50 W/cm^2 and 2.5 kW/cm^2. The lines are only intended to guide the eye.

oscilloscope. The overall resolution of the system thus allows us to measure changes in transmission occurring in times of approximately 4 ns.

We measured the switching of the transmission for different voltages and incident light intensities. The results are summarized in Fig. 5, where we plot the switching times (for 10% to 90% change in transmission) for applied voltages from 2 to 10 V, at low and high incident intensities of 50 W/cm^2 and 2.5 kW/cm^2, respectively. For low intensity there is a significant reduction in the switching time from 90 ns at 2 V to 10 ns at 10 V as applied bias increases. In contrast, for high intensity the switching time remains relatively constant for all applied voltages. As discussed below, the observed dependence with voltage and intensity is consistent with the presence of field screening and rules out heating as the dominant mechanism. Let us note here that the measured switching times are slower than other devices previously reported in the literature [1], [11], which is consistent with a lower saturation intensity [3].

Heating effects were studied for AlGaAs/GaAs p-i-n modulators [13]. As thermal properties are similar for all III–V materials, we would expect comparable results for a similar structure in the InGaP/InGaAs material system. As shown in [13], when heating is the dominant mechanism the time response of the transmission has two components, one fast corresponding to the onset of the applied field, and one slow corresponding to the change in transmission due to heating. As heat is produced mainly by ohmic dissipation caused by the photocurrent [13], the power to the device increases with applied voltage, making the slow component of the signal more noticeable as voltage increases. The decay time of the slow component was determined [13] to be close to 50 ns and should be independent of the applied voltage.

Although the measured switching times for our devices are in that range, our experiments do not show any of the features that can be attributed to heating, as can be observed in Fig. 6, which shows the temporal evolution of the transmission of the device for different conditions of incident intensity and bias voltage. All curves have been normalized to the steady state modulation for ease of comparison. Curves a and b were measured with 50 W/cm^2 of incident intensity, while curves c and d correspond to 2.5 kW/cm^2. The applied voltage changes from 0 to 10 V (a,c) and 0 to 4 V (b,d). The two component rise of the transmission is not observed in any of the curves, while the change in switching speed is evident.

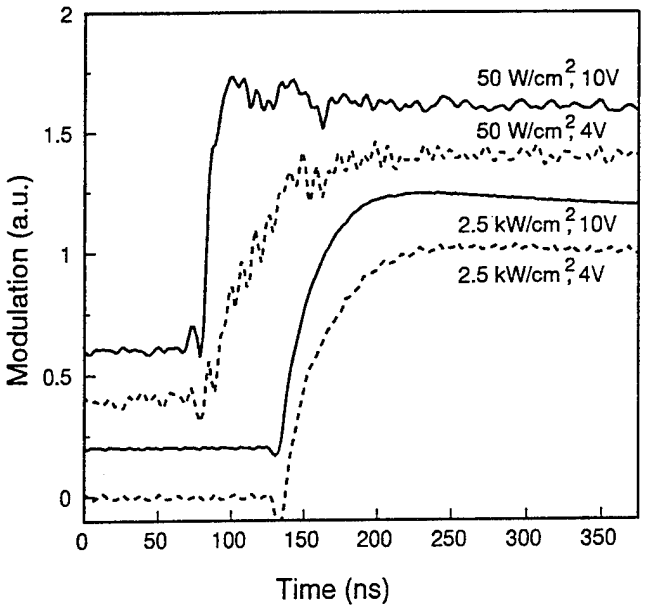

Fig. 6. Measured temporal evolution of the transmission of the device normalized to the steady state modulation. The applied voltage changes from 0 to the voltage in the figure with a risetime of 4 ns, the intensity of the laser is also indicated in the figure.

Fig. 4 provides further evidence against the hypothesis of thermal effects because heat absorbed in the sample would produce a localized increase in lattice temperature which would shift the band gap and accompanying excitonic resonance towards lower energy. This shift would move the excitonic absorption out of the operation wavelength of the device, thus increasing the transmission, contrary to the behavior of the transmission shown in Fig. 4.

Field screening effects [11], [12] occur due to charge build-up of one of the photogenerated carriers: either electrons or holes. Carriers may escape from the quantum wells through thermionic emission or tunneling through the barrier. As it is likely that electrons escape much more rapidly than holes due to the difference in effective masses, accumulation of holes results in charge build-up. Tunneling escape probability is negligible because the barriers are 15 nm thick [3], leaving thermionic emission as the only escape process. The thermionic emission rate for holes [16] is given by

$$\frac{1}{\tau} = \left(\frac{k_B T}{2\pi m_{hw} L_w^2}\right)^{1/2} \exp\left(-\frac{H(F)}{k_B T}\right). \tag{2}$$

In this expression T is the lattice temperature, m_{hw} is the effective mass for holes in the well, k_B is Boltzmann constant and L_w is the well width. The barrier height H depends on the field F through

$$H(F) = Q\Delta E_g - E_h - |e|FL_w/2 \tag{3}$$

where Q is the fraction of discontinuity in the valence band, ΔE_g is the difference in band gaps between the well and barrier material, e is the electron charge and E_h is the energy of the $n = 1$ level for holes. Although measurements in AlGaAs/GaAs [12] showed that the escape time is not accurately predicted by expression (2), it gives the correct qualitative behavior and is a good approximation for a simple model. Calculations assuming 60% [17] of the ~0.67 eV of bandgap difference [18] occurs in the valence band offset reveal that the hole thermionic lifetime varies between a few ns and 400 ns depending on the applied field. A similar time scale is to be expected for changes in the transmission. From (2) we can see that reduction of barrier height (through increased applied bias) results in faster escape times, in agreement with the low intensity data in Figs. 5 and 6. Also, for high intensity, the accumulated carriers would be expected to screen the field so that no change in speed would result, again in agreement with the observed behavior of the InGaAs–InGaP modulators. Similar effects have been observed in InGaAs–InP MQW modulators [11], on a much faster time scale, which agrees with estimates from (2).

We performed simulations using a simple model of the modulator that support the above qualitative reasoning that field screening is the dominant saturation mechanism in these devices.

IV. Model

The model we used to simulate charge build-up is similar to that presented by Wood *et al.* [11]. We consider the reverse bias p-i-n structure as a capacitor with the quantum wells located between the plates. The differential equations governing the areal densities of electrons n and holes p in a quantum well illuminated with an intensity I and subjected to a field F are

$$\frac{\partial n}{\partial t} = \alpha(F)I - Bnp - n/\tau_n \tag{4}$$

$$\frac{\partial p}{\partial t} = \alpha(F)I - Bnp - p/\tau_p. \tag{5}$$

Here $\alpha(F)$ is the field dependent absorption of one well, B is the recombination constant and τ_n (τ_p) is the electron (hole) escape time. The fact that the escape times of electrons and holes are different leads to accumulation of one kind of carrier in the well with the corresponding loss of charge neutrality. We will simulate this effect by the introduction of a layer of charge in the central plane of the quantum well with a charge density given by

$$\sigma = e(p - n). \tag{6}$$

For high incident light intensity, the net positive charge can significantly distort the electric field in the depletion region. When the positive charge is large enough, the potential at one particular well may be reduced until it approaches the Fermi level of the n-type material. Under these conditions, electrons can diffuse from the bulk into that well, effectively reducing the width of the depletion region. In each step of the simulation, we determine the field using Gauss's law and the depletion width d from the boundary condition:

$$V_{bi} + V_e = \int_0^d F(x)dx \tag{7}$$

where V_{bi} and V_e are respectively the built-in and external voltages. The background doping level in the intrinsic material of wells and barriers is assumed negligible for simplicity of the model, which is completed with charge layers at both ends of the depletion region. We number the wells starting from the

TABLE I
PARAMETERS USED IN THE SIMULATION

Temperature	T = 300 K
Bandgap difference[a]	ΔE = 673 meV
Fraction of discontinuity in valence band[b]	Q = 0.6
Effective mass electrons in the well[a,f]	$m_{e,w} = 0.0604 \times m_0$
Effective mass electrons in the barrier[a,f]	$m_{e,b} = 0.119 \times m_0$
Effective mass holes in the well[a,f]	$m_{hw} = 0.471 \times m_0$
Effective mass holes in the barrier[a,f]	$m_{hb} = 0.62 \times m_0$
Recombination constant[c,e]	$B = 10^{-4}$ cm^2/s
Diffusion time constant[d,e]	τ_d = 400 ns
Well width	L_w = 10 nm
Barrier width	L_b = 15 nm
Energy of $n = 1$ level for electrons	E_e = 30.8 meV
Energy of $n = 1$ level for holes	E_h = 26.3 meV
Dielectric constant	ϵ = 12
Area of the device	$A = 360 \times 510\ \mu$m^2
Number of wells	n = 24
Built in voltage	V_{bi} = 1 V
Focal spot radius	$r = 10\ \mu$m

Notes:
a) From [18].
b) From calculations following the procedure in [17].
c) Results in lifetime around 1 ns.
d) Computed from a diffusion constant of 10 cm^2/s.
e) Order of magnitude from GaAs–AlGaAs [19] f) m_0 = electron mass.

one closest to the p region of the diode and assume the light is traveling from p to n.

The numerical values of the parameters used in the simulation are listed in Table I. The field dependent absorption is obtained from low intensity transmission measurements under conditions so as to make charge build-up effects negligible. Besides thermionic emission time, computed using expression (1), the escape time for both electrons and holes also includes tunneling, and diffusion of the carriers in the plane of the wells out of the illuminated area. Although it is negligible for our structure, tunneling was included in order to be able to evaluate different device designs and was computed using formulas given in [3]. The ambipolar diffusion time for a diffusion coefficient of 10 cm^2/s [19] is comparable to thermionic emission when the field is low but, because of its ambipolar nature, it does not contribute to the charge build-up.

We first performed steady state calculations, in which we computed the mutually dependent field and charge distributions in a self consistent manner. Fig. 7 shows the steady state carrier density (a) and the field distribution (b) for the different wells in the structure. These results were obtained for intensities of 16 W/cm^2 and 2.5 kW/cm^2 while the external voltage was kept constant at 5 V. In Fig. 7(a) the circles (triangles) represent the hole (electron) population while the intensity is denoted by the use of empty symbols for high intensity and solid symbols for low intensity. In Fig. 7(b) the result for low intensity is shown by the solid line and that for the high intensity by the dotted line.

In the depletion region, where the field is not zero (Fig. 7(b)), the electrons are efficiently swept out of the wells, and there is accumulation of holes (Fig. 7(a)) due to their

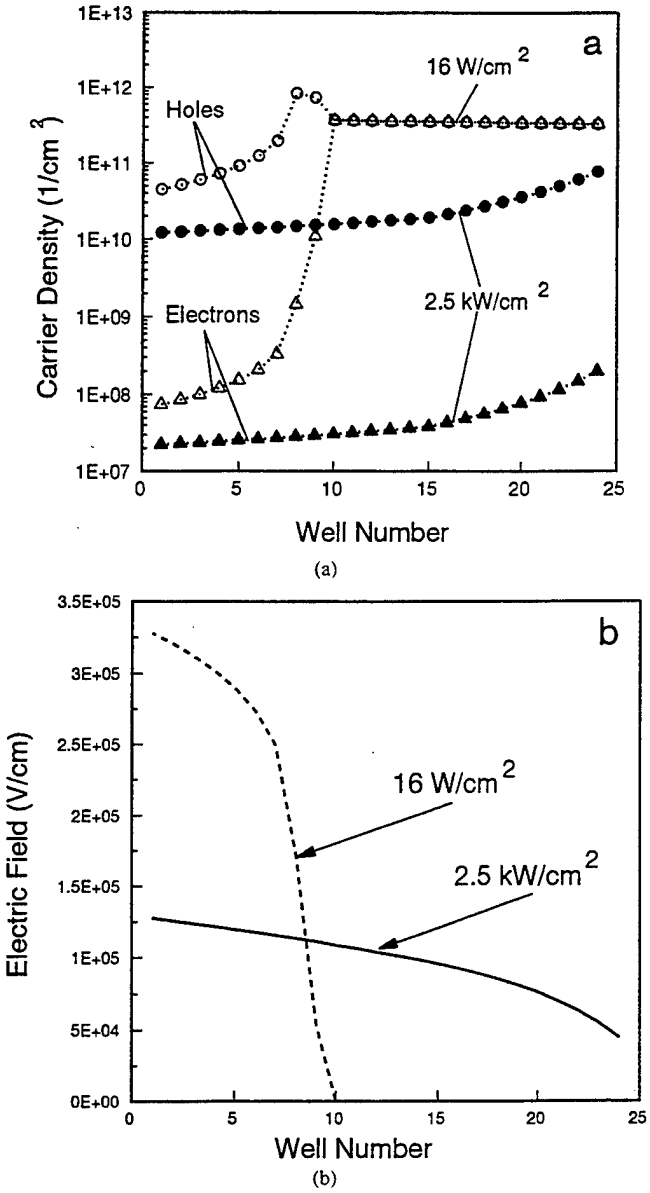

Fig. 7. (a) Computed steady state distribution of electron (triangles) and holes (circles) areal densities with an applied voltage of 5 V for intensities of 16 W/cm^2 (solid symbols) and 2.5 kW/cm^2 (empty symbols). The p region is located to the left of the wells. The light travels from left to right. (b) Computed steady state electric field for the same conditions as in (a). Low intensity data is plotted with solid line, and high intensity data with dashed line.

longer escape time. For 5 V of external bias, and in absence of illumination, all the wells would be subjected to an electric field around 10^5 V/cm. Due to the presence of net charge in the wells, the field is not the same for all the wells and those where the field is lower have higher absorption and longer escape times, leading to higher densities to the right end (n side) of the depletion region in Fig 7. The accumulation of carriers is not very important when the intensity is low, and most of the wells experience a value of the field close to that in the absence of light. Notable changes occur in the charge distribution when the intensity is increased. As the carrier density increases, the charge accumulates and the width of the depletion region varies accordingly. Once a well is out of the depletion region, the field goes to zero with a corresponding

change in transmission and with equal populations of electrons and holes. As shown in Fig. 7(b), at high intensity only few of the wells experience the field, resulting in a reduction of the modulation with respect to the low intensity case. These qualitative results of the model show the same behavior that was observed in the experiment (Fig. 4). In spite of uncertainties in certain material parameters and its simplicity, the model also predicts the modulation with less than 20% error respect to the experimental values for intensities up to the measured I_{sat} (~4 kW/cm^2). At higher intensities, however, the discrepancies are larger and it does not account for all the reduction of modulation that is observed. This difference might be due to effects not included in our model that are nevertheless suggested by the shape of the spectra (Figs. 1 and 4), such as slight saturation of the excitonic absorption or unintentional doping of the material in the intrinsic region. Another possible source of error is inaccuracy associated with the use of (2) to estimate the thermionic escape times.

The simulation of the time response of the modulators starts from the steady state situation for $V_c = 0$ V, and follows the changes produced by an increase of applied voltage with a risetime of 4 ns. In each step of the simulation, the following tasks are performed.

1) An estimate of the external charge flow needed to establish the new voltage across the device is computed. As the flow of carriers external to the MQW structure is much faster than the time scale of the escape from the wells, we assume that the external carriers flow so as to accommodate the internal changes in accordance to the boundary condition (7).
2) The rate of change of the carrier population in all the wells is computed by means of expression (4) and (5) and is used to calculate the new carrier densities after a short time interval dt. The total transmission coefficient of the structure is also computed.
3) The external charge is recomputed to meet the boundary condition (7) taking into account the new internal charge distribution. This is usually a small correction of the values calculated in step 1. Also in this step the width of the depletion region is modified when the new internal charge distribution makes it necessary.

Typical results of the simulation are plotted in Fig. 8, which shows the simulated temporal evolution of the transmission of the device for different conditions of incident intensity and bias voltage. All curves have been normalized to the steady state modulation for ease of comparison. Curves a and b correspond to 50 W/cm^2 of incident intensity, while curves c and d were computed using 2.5 kW/cm^2. The applied voltage changes from 0 to 10 V (a,c) and 0 to 4 V (b,d) with a risetime of 4 ns. As can be seen by comparing these results with the corresponding experimental curves shown in Fig. 6, the model reproduces qualitatively the temporal changes in transmissivity observed in the experiment. At low intensity (a and b), an increase in bias voltage is accompanied by a decrease in switching time, in agreement with the data in Figs. 5 and 6, while at high intensity (c and d) that change is much less noticeable, also in agreement with the experiment.

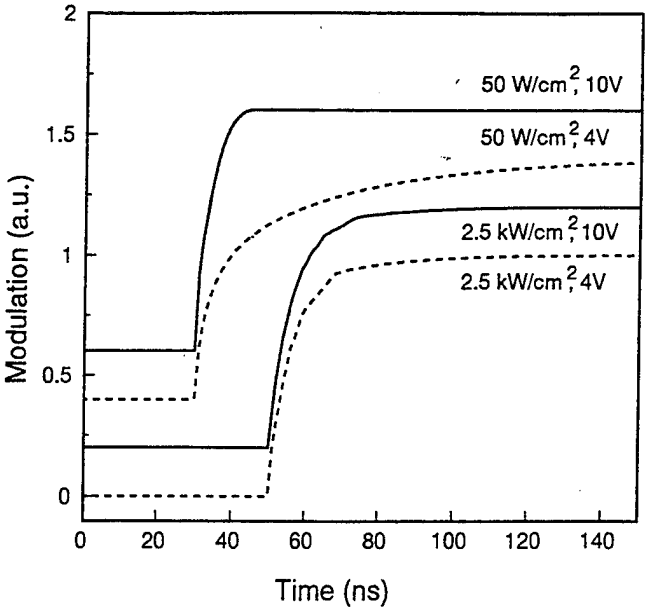

Fig. 8. Simulated temporal evolution of the transmission of the device normalized to the steady state modulation. The conditions of the simulation are the same as those of the experiment in Fig. 6.

The switching time for 10 V bias at high intensity is slower than that of 10 V at low intensity. The origin of this effect is the change in depletion width with voltage. As can be seen from the steady state data in Fig. 7(a), most of the carriers are accumulated near the end of the depletion region. A sudden increase of voltage moves the boundary of the depletion region closer to the n region, leaving several wells in a situation out of equilibrium with low field and consequently ((1)) long time to reach the new steady state situation.

While the simulation gives numerical values for the risetime which do not match exactly those obtained experimentally, this difference is again to be expected given the simplicity of the model and the fact that some of the parameters used are only estimates. Nevertheless, the results of the model give solid support to the qualitative reasoning presented in the previous section leading to the conclusion that field screening due to carrier build-up is the most important effect determining the observed saturation of the modulation in the InGaAs–InGaP modulators investigated. We also ran our simulation for a different structure, with barriers of 7.5 nm thickness. This change makes tunneling the dominant escape mechanism, and produces approximately a tenfold increase in saturation intensity and switching speed limited by the risetime of the electrical pulse. Although the simplicity of the model does not allow a detailed prediction, it shows the possibility of increase both the saturation intensity and speed of the device by means of changes in the structure.

V. Conclusion

We performed a detailed study of the performance of InGaAs–InGaP multiple quantum well modulators under different conditions of incident intensity and operating voltage. We found that the saturation intensity is relatively constant with a value of (1.3±0.1) kW/cm^2 up to ~6 V bias where the saturation begins to increase linearly with

voltage to reach (3.7±0.1) kW/cm^2 at 10 V bias. Spectra at different powers and applied voltages show that the decrease of modulation with power is not due to saturation of the excitonic absorption. We performed measurements on the time response of the devices, which not only characterizes the modulation speed of the device, but also confirm that the most important cause of the saturation is field screening due to charge build-up. The obtained switching times ranging between 10 and 90 ns are not limited by the capacitance of the device, but by the escape time of the photogenerated carriers from the wells. In the devices studied the escape time was dominated by thermionic emission, which is slower than in other material systems due to the larger difference in band gap between the well and barrier materials. In order to improve the speed of InGaAs–InGaP devices while keeping the advantage of a transparent substrate, the structure must be carefully engineered to accelerate the escape of the carriers from the wells, for example by using thinner barriers that would allow tunneling. We performed simulations using a simple model of the modulator which includes field screening effects that confirm field screening to be the dominant physical mechanism governing the saturation and time response of these devices.

REFERENCES

[1] T. H. Wood, C. A. Burrus, D. A. B. Miller, D. S. Chemla, T. C. Damen, A. C. Gossard, and W. Wiegmann, "High-speed optical modulation with GaAs/GaAlAs quantum wells in a p-i-n diode structure," *Appl. Phys. Lett.*, vol. 44, pp. 16–18, 1984.

[2] T. K. Woodward, L. M. F. Chirovsky, A. L. Lentine, L. A. D'Asaro, E. J Laskowski, M. Focht, G. Guth, S. S. Pei, F. Ren, G. J. Przybylek, L. E. Smith, R. E. Leibenguth, M. T. Asom, R. F. Kopf, J. M. Kuo, and M. D. Feuer, "Operation of a fully integrated GaAs-AlxGa1-xAs FET-SEED: A basic optically addressed integrated circuit," *IEEE Photon Technol. Lett.*, vol. 4, pp. 614–617, 1992.

[3] A. M. Fox, D. A. B. Miller, G. Livescu, J. E. Cunningham, and W. Y. Jan, "Quantum well carrier sweep out: Relation to electroabsorption and exciton saturation," *IEEE J. Quantum Electron.*, vol. 27, pp. 2281–2294, 1991.

[4] B. Pezeshki, S. M. Lord, and J. S. Harris, Jr., "Electroabsorptive modulators in InGaAs/AlGaAs," *Appl. Phys. Lett.*, vol. 59, pp. 888–890, 1991.

[5] L. Buydens, P. Demeester, Z. Yu, and P. Van Daele, "High contrast/low voltage normally-on InGaAs/AlGaAs asymmetric Fabry-Perot modulator," *IEEE Photon. Technol. Lett.*, vol. 3, pp. 1104–1106, 1991.

[6] D. Mahgerefteh, C. M. Yang, L. Chen, K. Hu, W. Chen, E. Garmire, and A. Madhukar, "Picosecond time-resolved measurements of electroabsorption in an InGaAs/GaAs multiple quantum well p-i-n modulator," *Appl. Phys. Lett.*, vol. 61, pp. 2592–2594, 1992.

[7] Li Chen, K. C. Rajkumar, and A. Mahukar, "Optical absorption behavior of strained InxGa1-xAs/GaAs(100)(x<0.25) multiple quantum well structures grown via molecular beam epitaxy," *Appl. Phys. Lett.*, vol. 57, pp. 2478–2480, 1990.

[8] G. Ji, D. Huang, U. K. Reddy, T. S. Henderson, R. Houdre, and H. Morkoc, "Optical investigation of highly strained InGaAs/GaAs multiple quantum wells," *J. Appl. Phys.*, vol. 62, pp. 3366–3373, 1987.

[9] J. E. Cunningham, K. W. Goosen, M. Williams, and W. Y. Jan, "Pseudomorphic InGaAs/GaAsP quantum well modulators on GaAs," *Appl. Phys. Lett.*, vol. 60, pp. 727–729, 1992.

[10] J. W. Kim, C. W. Chen, T. J. Vogt, L. M. Woods, G. Y. Robinson, and D. L. Lile, "Strained layer InxGa1-xAs/GaAs and InxGa1-xAs/InyGa1-yP multiple-quantum-well optical modulators grown by gas-source MBE," *IEEE Photon. Technol. Lett.*, vol. 5, pp. 987–989, 1993.

[11] T. H. Wood, J. Z. Pastalan, C. A. Burrus, B. C. Johnson, B. I. Miller, J. L. de Miguel, U. Koren, and M. G. Young, "Electric field screening by photogenerated holes in multiple quantum wells: A new mechanism for absorption saturation," *Appl. Phys. Lett.*, vol. 57, pp. 1081–1083, 1990.

[12] J. A. Cavaillès, D. A. B. Miller, J. E. Cunningham, P. Li Kam Wa, and A. Miller, "Simultaneous measurements of electron and hole sweep-out from quantum wells and modeling of photoinduced field screening dynamics," *IEEE J. Quantum Electron.*, vol. 28, pp. 2486–2497, 1992.

[13] T. Sizer II, R. E. LaMarche, and T. K. Woodward, "Point source heating effects in multiple quantum well modulators," *Appl. Phys. Lett.*, vol. 61, pp. 420–422, 1992.

[14] K. W. Goossen, J. E. Cunningham, M. B. Santos, and W. Y. Jan, "Measurement of modulation saturation intensity in strain-balanced, undefected InGaAs/GaAsP modulators operating at 1.064 μm," *Appl. Phys. Lett.*, vol. 63, pp. 515–517, 1993.

[15] K. W. Goossen, L. M. F. Chirovsky, R. A. Morgan, J. E. Cunningham, and W. Y. Jan, "High-power extremely shallow quantum-well modulators," *IEEE Photon. Technol. Lett.*, vol. 3, pp. 448–450, 1991.

[16] H. Schneider and K. v. Klitzing, "Thermionic emission and gaussian transport of holes in a GaAs/AlGaAs multiple quantum well structure," *Phys. Rev. B*, vol. 38, pp. 6160–6165, 1988.

[17] G. Van de Walle, "Band line up and deformation potential in the model-solid theory," *Phys. Rev. B*, vol. 39, pp. 1871–1883, 1989.

[18] H. C. Casey Jr. and M. B. Panish, *Heterostructure Lasers*. New York: Academic, 1978.

[19] A. Miller, R. J. Manning, P. K. Milsom, D. C. Hutchings, D. W. Crust, and K. Woodbridge, "Transient grating studies of excitonic optical nonlinearities in GaAs/AlGaAs multiple-quantum-well structures," *J. Opt. Soc. Amer. B*, vol. 6, pp. 567–578, 1988.

M. E. Watson was born in Great Bend, KS on October 20, 1969. He received the B.S.E.E. and M.S.E.E. degrees from Colorado State University, Fort Collins, CO, in 1992 and 1995, respectively.

He is a member of the Optoelectronics Computing Systems Center. The work in this paper was for partial fulfillment of his Masters degree.

J. L. A. Chilla was born in Lomas de Zamora, Argentina in 1960. He received the degrees of Licenciado en Fisica in 1988 and Doctor en Fisica in 1991 from the Universidad de Buenos Aires. He was awarded the 1993 Fundacion Ciencias Exactas y Naturales Prize for the most outstanding doctoral dissertation in the department of Physics.

From 1987 to 1992, he was on a doctoral fellowship with the Comision Nacional de Energia Atomica in Argentina, where he worked on the measurement of ultrashort light pulses in amplitude and phase. In 1992, he joined the Electrical Engineering Department at Colorado State University. His areas of research interest include: lasers, ultrafast phenomena and measurement techniques and the physics behind optoelectronic devices.

J. J. Rocca, photograph and biography not available at the time of publication.

J.-W. Kim, photograph and biography not available at the time of publication.

D. L. Lile, photograph and biography not available at the time of publication.

T. J. Vogt, photograph and biography not available at the time of publication.

G. Y. Robinson (S'66–M'69–SM'93) received the B.E.S. degree at the University of Texas, Austin in 1965 and the M.S. degree in 1967 and the Ph.D. degree in 1969, both at the University of California, Berkeley.

From 1970 to 1984, he was an Assistant Professor, Associate Professor, and Professor of Electrical Engineering at the University of Minnesota, Minneapolis where he conducted research on electrical and metallurgical characterization of metal-semiconductor contacts on Si and the III–V semiconductors. During 1980, he was on sabbatical leave at Perkin-Elmer Corporation conducting research in molecular beam epitaxy (MBE). In 1984, he started a new research group at Colorado State University, where he is currently a Professor of Electrical Engineering and involved in the growth of III–V heterostructures by gas-source MBE.

Dr. Robinson is a member of the AVS, has taught short courses in the USA and Europe, and has served on organizing committees for numerous conferences on the III–V semiconductors.

Journal of Electronic Materials, Vol. 23, No. 11, 1994

Regular Issue Paper

Photoluminescence and Interface Abruptness in InGaAsP/InGaAsP Quantum Wells

L.M. WOODS, P. SILVESTRE, P. THIAGARAJAN, G.A. PATRIZI, and G.Y. ROBINSON

Department of Electrical Engineering, Colorado State University, Fort Collins, CO 80523

K.M. JONES and M. AL-JASSIM

National Renewable Energy Laboratory, Golden, CO 80401

Quantum well (QW) structures consisting of InGaAsP wells and InGaAsP barriers grown by gas-source molecular beam epitaxy have been examined by low temperature photoluminescence (PL) in order to evaluate the contributions of compositional fluctuations in the quaternary alloy and of interface roughness to the PL linewidth. The well material was InGaAsP with a bandgap corresponding to a wavelength of 1.3 μm and the barrier material was InGaAsP of 1.15 μm. The theory for QW excitonic linewidths as a function of well thickness L_z due to fluctuations in alloy composition has been extended to include the case of the quaternary InGaAsP barrier. If the interfaces are atomically abrupt, the linewidth is dominated by compositional fluctuations in the well at large L_z and compositional fluctuations in the barrier at small L_z. The theory predicts a weak dependence of the linewidth on L_z since the composition of the well and barrier are similar. For rough heterointerfaces, the theory indicates the usual increase in linewidth with decreasing L_z. Photoluminescence measurements at 13K in arrays of single InGaAsP/InGaAsP QWs with L_z from 1.0 to 6.0 nm show only a weak variation of the full width at half maximum (FWHM) with L_z, in agreement with the theory for smooth interfaces. Furthermore, the lowest measured FWHM of 8.9 meV was found for a narrow well of L_z = 1.8 nm, indicating the InGaAsP/InGaAsP interfaces are smooth and that the PL linewidth is dominated by compositional fluctuations.

Key words: Gas source molecular beam epitaxy (GSMBE), InGaAsP, photoluminescence

INTRODUCTION

The III-V materials system $In_{1-x}Ga_xAs_yP_{1-y}$ grown epitaxially on InP has been used extensively in quantum well (QW) optoelectronic and transport devices. The wide range of bandgap energies available in InGaAsP alloys, by varying the alloy composition x and y, allows the device designer great flexibility in optimizing the device for maximum performance. For example, low threshold QW lasers operating at the wavelength of 1.3 μm utilize InGaAsP wells of one composition and InGaAsP barrier and separate confinement layers of different compositions.[1] In optical modulators using the quantum confined Stark effect, the contrast ratio can be maximized and the applied bias minimized by using InGaAsP wells and InGaAsP barriers of the appropriate compositions.[2] The abruptness of QW heterointerfaces can greatly influence the properties of heterostructure devices derived from quantum-size effects. Previous studies have examined the interface abruptness of InGaAsP/InP QWs,[3-5] and InGaAs/InP QWs,[5-7] but there appears to be little information about the abruptness of InGaAsP/InGaAsP heterointerfaces.

We report here the results of a study of a InGaAsP/InGaAsP QW interface using the photoluminescence characterization technique. The InGaAsP structures were grown by gas source molecular beam epitaxy (GSMBE) on InP and utilized two lattice-matched quaternaries: $In_{0.7}Ga_{0.3}As_{0.6}P_{0.4}$ as the well material

(Received May 3, 1994)

with a room temperature bandgap emission at a wavelength of approximately 1.3 μm (here referred to as 1.3Q), and $In_{0.83}Ga_{0.17}As_{0.37}P_{0.63}$ as the barrier material with emission at 1.15 μm (1.15Q). Quantum wells of these compositions are widely used in optical devices operating at 1.3 μm, but determination of the atomic abruptness of the interface is difficult by the usual methods of transmission electron microscopy (TEM) and x-ray diffraction; the contrast between the well and barrier materials is small since the compositions are so similar. However, the low temperature photoluminescence (PL) linewidth for excitons in quantum wells with well thickness less than about 3.0 nm depends strongly on interface abruptness. If other contributions to the linewidth are properly accounted for, the PL linewidth can be used to estimate the heterointerface abruptness. Here, the theory of PL linewidth for interface roughness was extended to include the contributions from compositional fluctuations in both the well and barrier InGaAsP layers. A comparison of the experimental and theoretical PL linewidths as a function of well width was then used to ascertain the interface roughness in InGaAsP(1.3Q)/InGaAsP(1.15Q) QWs.

THEORY

Low temperature PL, under low power excitation, of QW samples with sharp interfaces and uniform composition yields narrow luminescence peaks. Quantum wells can be dominated by excitons which have an intrinsic emission spectrum of a lifetime broadened delta function. Thus, the linewidth of a purely excitonic transition is very narrow making its peak ideal for monitoring small inhomogeneous contributions to the linewidth. The inhomogeneous contributions can result from compositional variations, and disordered and/or graded heterointerfaces in the QW structure. These statistical mechanisms act to randomize the discrete level of quantum confinement, thus spreading out the energy of luminescence and adding to the width of the luminescence peak.

What follows is an analysis that reviews the contributions to the photoluminescence linewidth of QW excitons, so that the contribution from interface roughness can be identified and characterized. If we let Γ be the full width at half maximum (FWHM) of the PL exciton peak, then

$$\Gamma^2 = \Gamma_T^2 + \Gamma_0^2 \qquad (1)$$

where Γ_T is the homogeneous part and Γ_o is the inhomogeneous part of Γ. Linewidths can be added in this fashion if each component is approximated as a Gaussian distribution and is statistically independent. Γ_T is temperature dependent and can be considered to result from two contributions:

$$\Gamma_T^2 = \Gamma_{phT}^2 + \Gamma_{LB}^2 \qquad (2)$$

where Γ_{phT} is the contribution from longitudinal optical phonon assisted broadening and Γ_{LB} is the contribution from carrier lifetime broadening. The room temperature Γ_{phT} value has been determined from measurements of exciton absorption peaks at 300K by Sugawara et al. as 8.9 meV for 1.33 μm InGaAsP.[3] Here the value of Γ_{phT} at 10K was estimated to be 0.5 meV by using

$$\Gamma_{phT}(T) = \Gamma_{ph} / \left[\exp(\hbar\omega_{LO}/kT) - 1\right] \qquad (3)$$

where Γ_{ph} is a proportionality constant determined from the exciton absorption measurements and $\hbar\omega_{LO}$ is the longitudinal optical phonon energy of 32 meV for InGaAsP(1.3Q).[8,9]

Carrier lifetime broadening is due to the time it takes to re-establish the carrier distribution function within the energy bands after a recombination event. This process does not take place instantaneously, as represented by a nonzero lifetime of the final state.[10] The lifetime has been found to be as small as 500 ps for InGaAs/InP and InGaAsP/InP QWs less than 20.0 nm in thickness.[11] Using Heisenberg's uncertainty principle and a lifetime of 500 ps, the maximum value for Γ_{LB} is estimated to be 0.01 meV for InGaAsP/InGaAsP QWs.

Then using Eq. (2), we estimate $\Gamma_T = 0.50$ meV at low temperatures. But the measured PL FWHM values for QWs of InGaAs and InGaAsP are typically 5 meV or larger.[3-7] Hence, the homogeneous contributions to the PL linewidth can be neglected.

The inhomogeneous linewidth, Γ_o in Eq. (1), is statistical in nature and is due to random variation in the QW structure from point to point. It can also be taken to consist of two independent contributions

$$\Gamma_0^2 = \Gamma_1^2 + \Gamma_2^2 \qquad (4)$$

where Γ_1 is the contribution due to the bandgap variation from localized fluctuations in alloy composition, and Γ_2 is the contribution from quantum size effects due to interface roughness.

Γ_1 is the linewidth at absolute zero temperature that results from random spacial fluctuations in the InGaAsP composition. These spacial composition fluctuations result in a broadening of the PL emission energy due to the corresponding fluctuation of the bandgap energy. The fluctuations occur on a microscopic scale because of the random arrangement of the In and Ga atoms on the group-IIII lattice sites and the As and P atoms on group-V sites. Thus, even an epitaxial layer of uniform average composition will exhibit compositional broadening in PL. A theory for compositional fluctuations has been developed by Schubert et al.[12] for bulk ternary alloys, and we have extended the theory to QWs with quaternary wells and quaternary barriers by using the theory of random variables with joint probability distributions and a covariance of zero.[13] The compositional fluctuations are evaluated over the excitonic volume, which is approximated as an ellipsoid and given by:

$$V_{ex} = 4\pi Z_{ex}\rho_{ex}^2/3 \qquad (5)$$

where ρ_{ex} and Z_{ex} are the lateral extension and perpendicular extension, respectively, of the exciton wavefunction relative to the plane of the QW. This volume is quantum mechanical in nature and thus,

there is a nonzero probability of finding the exciton in the barrier material. Schubert et al.[12] showed that the linewidth is proportional to the product of the rate of change of bandgap with composition and the standard deviation of the compositional fluctuations. Here we take the standard deviations of composition fluctuations in V_{ex} to be weighted according to the probability of the exciton being in the barrier, P_b, or the well, $P_w = 1 - P_b$. Thus, the exciton emission linewidth due to alloy fluctuations in $In_{1-x}Ga_xAs_yP_{1-y}$ QW structures can be written as

$$\Gamma_1 = 2.36\left[\left(\frac{dE_t}{dx}\right)^2 \frac{x_w(1-x_w)P_w}{KV_{exc}} + \left(\frac{dE_t}{dy}\right)^2 \frac{y_w(1-y_w)P_w}{KV_{exc}} + \left(\frac{dE_{gb}}{dx}\right)^2 \frac{x_b(1-x_b)P_b}{KV_{exc}} + \left(\frac{dE_{gb}}{dy}\right)^2 \frac{y_b(1-y_b)P_b}{KV_{exc}}\right]^{1/2} \quad (6)$$

In Eq. (6), E_{gb} is the bandgap energy of the barrier, $K = 4a_o^{-3}$ is the cation or anion density in the zinc-blende lattice with lattice constant a_o, and x_w, y_w, x_b, y_b are the Ga and As concentrations in the well and barrier, respectively. The PL peak is located at the energy

$$E_t = E_{gw} + E_{n,e} + E_{m,hh} - E_B \quad (7)$$

Here E_{gw} is the bandgap energy of the well, $E_{n,e}$ and $E_{m,hh}$ are the quantum confined levels of the electrons and heavy holes, respectively, and E_B is the quasi-two-dimensional exciton binding energy. The dependence of E_{gw}, $E_{n,e}$, and $E_{m,hh}$ on x and y were found from the InGaAsP bandgap data of Moon et al.[14] along with the solution to Schrodinger's equation for a finite potential well of depth ΔE_c for the electron and ΔE_v for the heavy hole, where ΔE_c is the conduction band offset energy and ΔE_v is the valence band offset energy for the heterojunction. The value of dE_t/dx (or dE_t/dy) was then evaluated by differentiating each of the terms in Eq. (7) with respect to x (or y), neglecting the exciton binding energy dependence with composition.

Equation (6) has been used to calculate the dependence of Γ_1 on well width L_z for ground-state excitons in InGaAsP(1.3Q)/InGaAsP(1.15Q) QWs, and the results are shown by the dashed curve in Fig. 1. For this combination of alloy compositions, we used $\Delta E_c = 58$ meV and $\Delta E_v = 88$ meV assuming ΔE_c: ΔEv = 40:60,[15] and the values of effective masses from Restorff et al.[16] The parameters P_b, P_w, ρ_{ex}, and Z_{ex} have been calculated as a function of well width for InGaAs/InP QWs by Herman et al.[17] and approximated here to be the same for the quaternary system in Fig. 1. Γ_1 varies from the bulk value of the well material (3.4 meV) for wide wells, to the bulk value of the barrier material (4.2 meV) as the exciton wavefunction penetrates into the barrier for very narrow wells. The peak in Γ_1 that occurs at about $L_z = 2$ nm is when the contributions to the linewidth from both the well and barrier are comparable.

Next consider Γ_2, the contribution to the inhomogeneous linewidth due to interface roughness or variation in well thickness. Individual monolayer steps at the interface will act to randomize the thickness of the well, L_z, thus randomizing the quantum confined levels and increasing the linewidth. Theoretically,[18]

$$\Gamma_2 \approx \Delta L_z\left[\frac{dE_{n,e}}{dL_z} + \frac{dE_{m,hh}}{dL_z}\right] \quad (8)$$

where ΔL_z is the width of the interface. The dependence of the exciton binding energy E_B with L_z has been ignored in Eq. (8). The solid curves in Fig. 1 show the variation in Γ_2 as a function of well width for the InGaAsP(1.3Q)/InGaAsP(1.15Q) QW system, with ΔL_z varying from 0.5 monodiatomic layers (ml) to 3.0 ml. For L_z greater than 1 nm, the linewidth decreases with increasing well width in the usual manner, and for L_z less than about 1 nm, the linewidth begins to decrease for decreasing L_z as a result of the finite depth of the electron and hole wells.

Based on the above theory, we can expect the measured linewidth Γ to be due to Γ_1, Γ_2, or both. For narrow wells (i.e., L_z less than about 1.5 nm), $\Gamma \approx \Gamma_2$ and the linewidth is dominated by interface roughness if $\Delta L_z > 1$ ml. For wide wells (L_z greater than about 5 nm), $\Gamma \approx \Gamma_1$ and the linewidth is primarily due to composition fluctuations and is relatively insensitive to interface roughness.

EXPERIMENTAL PROCEDURE

The samples were grown by GSMBE on (100) SI InP substrates at approximately 500°C with elemental Ga and In and thermally cracked AsH_3 and PH_3 as source materials.[19] Growth was paused at each heterointerface for 20 s, to allow the surface to anneal in the group-V molecular beams and to allow stabilization of the gas flows before starting growth of the next layer. Double crystal x-ray diffraction and photoluminescence of companion samples were used to check lattice mismatch ($<5 \times 10^{-4}$) and alloy composition.

Two samples were analyzed; each consisted of an

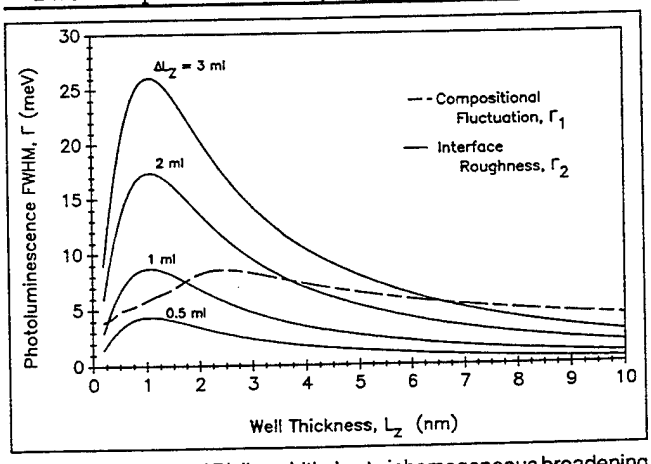

Fig. 1. The theoretical PL linewidth due to inhomogeneous broadening from compositional fluctuations, Γ_1, and interface roughness, Γ_2, as a function of well width, L_z for ground state excitons in InGaAsP(1.3Q)/InGaAsP(1.15 Q) QWs. ΔL_z is the heterointerface roughness.

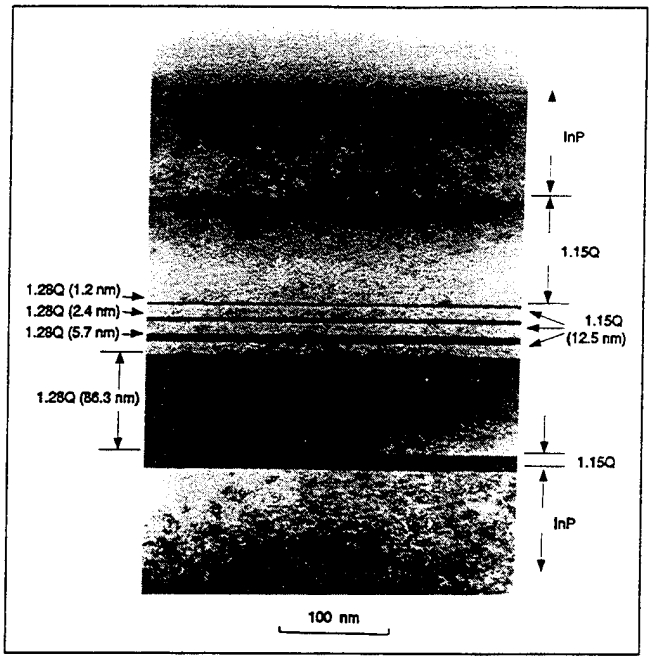

Fig. 2. Transmission electron (200) dark field micrograph of the cross section of an array of InGaAsP/InGaAsP single QWs lattice matched to InP. The wells are InGaAsP(1.28Q) and the barriers are InGaAsP(1.15Q).

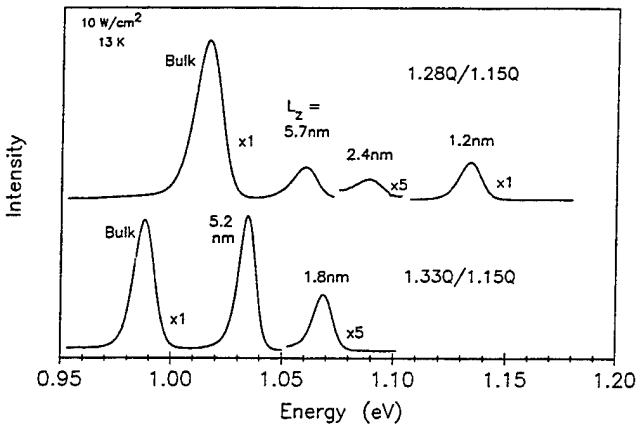

Fig. 3. Photoluminescence spectra at 13K of single QWs in two samples with InGaAsP(1.15Q) barriers: one with three InGaAsP(1.28Q) wells and the other with two InGaAsP(1.33Q) wells. The exciton peaks for each QW are labeled with the corresponding well width.

array of single QWs with InGaAsP wells of nominal 1.3Q composition separated by 1.15Q barriers of 12.5 nm thickness, a thick "bulk" layer of the 1.3Q alloy, and an InP cap layer. A TEM (200) dark field micrograph of a cross section the first sample is shown in Fig. 2. The sample contains three QWs with InGaAsP composition of 1.28Q and thicknesses of 1.2 ± 0.6, 2.4 ± 0.6, and 5.7 ± 0.3 nm. The "bulk" or reference layer is 86.3 nm thick. The low contrast resulting from the similar compositions of 1.28Q and 1.15Q made it difficult to resolve individual atomic layers at the heterointerfaces in high resolution lattice imaging with TEM. Thus, measurements of the interface abruptness in this mode could not be obtained. However, all the QWs are clearly resolvable in Fig. 2 including the 1.2 nm well. Rough measurements of

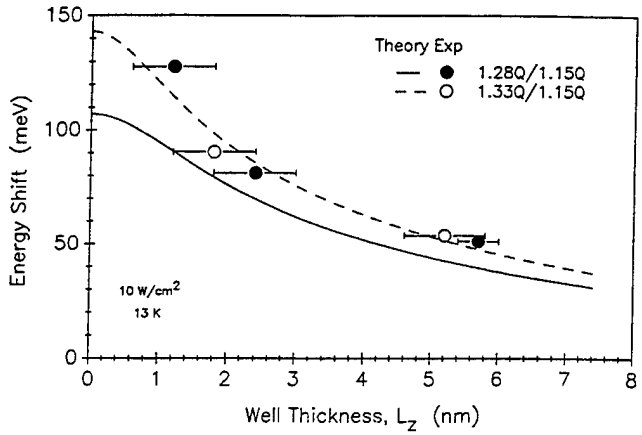

Fig. 4. The shift in QW peak energies with respect to the bulk layer as a function of well width, L_z, from PL measurements at 13K. Also shown is the theory for (solid line) InGaAsP(1.28Q)/InGaAsP(1.15Q) and (dashed line) InGaAsP(1.33Q)/InGaAsP(1.15Q) QWs.

the lateral uniformity from dark field TEM images provided an estimate of a lateral uniformity of the interfaces of about 2 ml (0.6 nm) or less over a lateral distance of about 50.0 nm. The sample in Fig. 2 will be referred to as the 1.28Q/1.15Q sample.

The second sample consisted of two QWs of 1.8 ± 0.6 and 5.2 ± 0.6 nm thickness and a reference layer of 99.9 nm thickness. The InGaAsP composition in the wells was found to be 1.33Q and the layer thicknesses were estimated from the growth conditions. This sample will be referred to as the 1.33Q/1.15Q sample.

Photoluminescence measurements were made with excitation provided by the 488 nm line of an Ar ion laser with incident power of about 10 W/cm² at the sample. At this power level, broadening of the PL peak due to band filling was found to be insignificant. The InGaAsP QW samples were mounted inside a closed cycle refrigerator for measurement in the temperature range of 10–300K. The luminescence wavelength selection was accomplished with a 0.5 m monochrometer, and the intensity detected with LN_2-cooled Ge diode and processed using a lock-in amplifier and computer. Using 1 mm slit widths, the total instrument line broadening (3.4 meV) resulted primarily from the monochrometer and was deconvolved from the measured PL linewidths.

RESULTS

The PL spectra at 13K for the two samples are shown in Fig. 3. The exciton peaks for each QW are labeled with the corresponding well width and the free carrier recombination peak for the bulk layer is indicated. As the temperature of the measurement was increased, the peaks shifted to lower energies in a manner consistent with the dependence of the bandgap of the well material on temperature.[20] At 300K, only the bulk peak was resolvable in both samples, with a FWHM of 60.5 meV for the 1.28Q/1.15Q sample and 42.7 meV for the 1.33Q/1.15Q sample.

The shift in QW peak energies with respect to the bulk layer peak as a function of width L_z are plotted

along with the theory in Fig. 4. Although the 1.33Q/1.15Q sample should exhibit a larger shift than the 1.28Q/1.15Q sample, the observed shift is about the same for both samples. However, the general agreement of the calculated curves with the data confirms the presence of quantum confinement and the large energy shift for the 1.2 nm QW is indicative of a square-like well, as the quantum shift changes very rapidly with well width for narrow wells. Note the 1.2 nm well produces an energy shift of over 90% of the maximum possible.

The FWHM linewidths of the QW peaks measured at 13K have been plotted as a function of well thickness in Fig. 5. Also shown in Fig. 5 is the theoretical inhomogeneous linewidth using the contributions from composition fluctuation Γ_1 and interface roughness Γ_2 calculated in Fig. 1. Although there is appreciable scatter in the data, it is apparent that there is little variation in the FWHM with L_z over the range measured, in agreement with the theoretical trend for smooth heterointerfaces. In particular, for small L_z where the FWHM is most sensitive to the interface roughness, the measured linewidths are less than 10 meV, indicating less than 1 ml roughness at the InGaAsP/InGaAsP interfaces for the smallest QWs. The smallest FWHM was 8.9 meV at L_z = 1.8 nm.

CONCLUSIONS

The interface abruptness between InGaAsP(1.3Q) and InGaAsP(1.15Q) has been studied using PL of QW structures grown by gas source MBE. The strong quantum shift in energy measured for the narrow wells was indicative of square-like wells with abrupt interfaces. This was further confirmed by TEM cross-sectional images that showed good uniformity and values of the well thicknesses that correlated with the growth conditions. The PL linewidth was studied as a function well size for contributions from alloy compositional variations and interface roughness. It was determined that the linewidth was dominated by alloy compositional variations and the contribution from interface roughness was small. For an interface roughness of 2 ml or larger, we would expect a large increase in the linewidth for the narrower wells. This was not observed and the linewidth for the narrow wells in fact decreased, consistent with alloy composition variations dominating the PL linewidth and smooth interfaces of 1 to 2 monolayer in roughness.

ACKNOWLEDGMENTS

The authors would like to acknowledge the help of M.J. Hafich and conversations with H. Temkin. This research was supported by the Hanscom Lab and ARPA (AF contract F 19628-93-K-0022) and the U.S. Air Force Office of Scientific Research (contract F 49620-93-1).

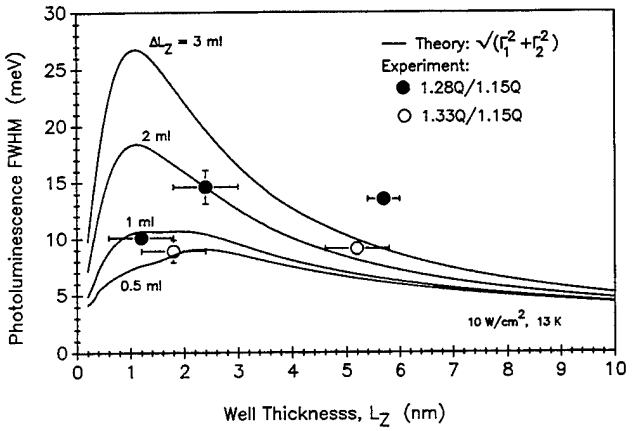

Fig. 5. Photoluminescence linewidths at 13K as a function of well width, L_z. Also shown is the total theoretical inhomogeneous linewidth, Γ_0 using the contributions from composition fluctuations Γ_1, and interface roughness Γ_2 of Fig. 1.

REFERENCES

1. D. Coblentz, T. Tanbun-Ek, R.A. Logan, A.M. Sergent, S.N. Chu and P.S. Davisson, *Appl. Phys. Lett.* 59 (4), 405 (1991).
2. F. Devaux, F. Dorgeuille, A. Ougazzaden, F. Huet, M. Carre, A. Carenco, M. Henry, Y. Sorel, J.-F. Kerdiles and E. Jeanney, *IEEE Photon. Tech. Lett.* 5(11), 1288 (1993).
3. M. Sugawara, T. Fujii, M. Kondo, K. Kato, K. Domen, S. Yamazaki and K. Nakajima, *Appl. Phys. Lett.* 53 (23), 2290 (1988).
4. M. Kondo, S. Yamazaki, M. Sugawara, H. Okuda, K. Kato and K. Nakajima, *J. of Cryst. Growth* 93, 376 (1988).
5. M.J. Ludowise, D. Biswas and P.K. Bhattacharya, *Appl. Phys. Lett.* 56 (10), 958 (1990).
6. H. Kamei and H. Hayashi, *J. Cryst. Growth* 107, 567 (1991).
7. J. Pamulapati and M. Dutta, *Properties of Lattice-Matched and Strained Indium Gallium Arsenide*, ed. P. Bhattacharya, EMIS Datareviews Series No. 8, INSPEC, London (1993), p. 206.
8. D.S. Chemla, D.A. Miller, P.W. Smith, A.C. Gossard and W. Wiegmann, *IEEE J. Quantum Elect.* 20 (3), 265 (1984).
9. Appendix in *GaInAsP Alloy Semiconductors*, ed. T.P. Pearsall (New York: John Wiley and Sons, 1982), p. 456.
10. J. Christen and D. Bimberg, *Phys. Rev. B* 42 (11), 7213 (1990).
11. T. Amand, X. Marie, B. Dareys, J. Barrau, M. Brousseau, D. Dunstan, J. Emery and L. Goldstein, *J. Appl. Phys.* 72 (5), 2077 (1992).
12. E.F. Schubert, E.O. Gobel, Y. Horikoshi, K. Ploog and H.J. Queisser, *Phys. Rev. B* 30 (2), 813 (1984).
13. R.E. Walpole and R.H. Myers, *Probability and Statistics for Engineers & Scientists, 2nd ed.* (New York: MacMillan Publishing Co. Inc., 1978), p. 71.
14. R.L. Moon, G.A. Antypas and L.W. James, *J. Electron. Mater.* 3 (3), 635 (1974).
15. J.D. Lambkin, *Properties of InP*, EMIS Data reviews Series No. 6, INSPECT, (London and New York: The Institution of Electrical Engineers, 1991), p. 318.
16. J.B. Restorff, B. Houston and R.S. Allgaier, *J. Appl. Phys.* 51 (4), 2277 (1980).
17. M.A. Herman, D. Bimberg, and J. Christen, *J. Appl. Phys.* 70 (2), R1 (1991).
18. D.F. Welch, G.W. Wicks and L.F. Eastman, *Appl. Phys. Lett.* 46 (10), 991 (1985).
19. P. Silvestre, M.J. Hafich, T. Vogt, A. Nanda, G.Y. Robinson, J.J. Dudley, J.E. Bowers, K.M. Jones and M.M. Al-Jassim, *J. Vac. Sci. Tech. B* 10 (2), 956 (1992).
20. H. Temkin, V.G. Keramides, M.A. Pollack and W.R. Wagner, *J. Appl. Phys.* 52 (3), 1574 (1981).

A low drive voltage electroabsorption modulator using an InGaAs/InP superlattice

C. W. Chen, J. W. Kim, P. Silvestre, M. J. Hafich, L. M. Woods, G. Y. Robinson, and D. L. Lile
Center for Optoelectronic Computing Systems and Department of Electrical Engineering, Colorado State University, Fort Collins, Colorado 80523

(Received 1 April 1993; accepted for publication 25 July 1993)

Spectral transmission, reflection, and photocurrent absorption data obtained on gas-source molecular beam epitaxy grown InGaAs/InP multiple quantum well (MQW) and superlattice *p-i-n* diode structures demonstrate, for the first time in this materials system, that similar modulation to MQW structures can be achieved using superlattices, but at significantly lower operating voltages. Specifically, we have observed photocurrent absorption changes of as much as 58%, transmission changes of 8.2%, and reflection changes of 32% for applied biases of only 4 V, in nonresonant modulators operating at a wavelength ~ 1.5 μm. These results encourage the possibility of employing such devices in fast, high density optical modulator arrays operating over the 1.3–1.6 μm range.

High speed III-V semiconductor light modulators are of considerable interest for a variety of applications including low chirp external laser modulators, photonic switching fabrics, optical logic circuits, and smart pixel arrays.[1] Most work on such devices has concentrated on the use of the quantum confined Stark effect (QCSE)[2] to modify the spectral characteristics of multiple quantum well (MQW) stacks of various material combinations resulting in voltage controlled modulation of either transmitted or reflected optical signals. Absolute changes in reflectivity as high as 77% have been achieved using asymmetric Fabry Perot resonator structures in strained InGaAs/AlGaAs[3] for operating voltages in the range of 20 V.

Such large voltages, however, result in very large power dissipation densities when the devices are switched repetitively at high rates. The power P is required to charge and discharge the capacitance C associated with the *p-i-n* diodes and is given by $P=CV^2/2\tau$, where τ is the switching time and V is the switching voltage.[4] Reductions in the operating voltage of such devices below ~ 5 V would be desirable, both to reduce their dynamic power consumption and hence allow their application in high speed dense arrays, as well as provide compatibility with Si complementary metal-oxide semiconductor circuits in hybrid architectures.[5] Attempts to reduce operating voltage have been reported using shallow quantum wells[6] and superlattice (SL) structures,[7] and contrast ratios as high as 40:1 at voltages as low as 4 V have been achieved at 0.76 μm in the AlGaAs/GaAs system.[8] Although superlattice diodes have been fabricated in the transparent substrate and lattice matched InGaAs/InP system,[9] and photocurrent spectra reported,[10] no results have appeared on the use of such structures for optical modulation in the 1.3–1.6 μm range.

In this communication we report the results of experiments designed to demonstrate the reduction in operating voltage that can be achieved in InGaAs/InP *p-i-n* modulator diodes by employing the Wannier–Stark effect in a superlattice stack[11] instead of the more usual QCSE MQW structure. A semiconductor superlattice is a stack of wells and barrier layers thin enough so that the wells are coupled by resonant tunneling. Such a modulator achieves a change in the optical spectrum by misaligning the resonant energy levels in adjacent, and coupled, quantum wells by means of an applied electric field, thereby resulting in localization of the initially delocalized electrons and holes. Such localization occurs when the voltage between adjacent wells is on the order of the width of the delocalized carrier minibands, which is typically $\sim 30 \rightarrow 60$ meV.[11] Since the SL period is usually only $\sim 5 \rightarrow 10$ nm, this means that the necessary applied bias across a 1 μm stack will typically be $\lesssim 6$ V.

Two samples, one a MQW structure and the other a SL, were grown by gas-source molecular beam epitaxy (MBE) on n^+ (100) InP substrates at 500 °C. The gas flow rates were 6 sccm of AsH_3 for an InGaAs growth rate of 0.5 μm/h and 4 sccm of PH_3 for InP growth at 1.0 μm/h. The dopants were Si for n-type and Be for p-type. The MQW structure, consisting of 49.5 periods of undoped ($n \sim 10^{16}$ cm^{-3}) 10 nm InGaAs wells and 10 nm InP barriers, was grown on top of a 500-nm-thick n^+ InP buffer, resulting in an active layer thickness of ~ 1 μm. The structure was completed by growing a 50-nm-thick undoped InP layer and a final 1 μm p^+ (1×10^{18} cm^{-3}) InP contact. The second sample was very similar except that it consisted of 60.5 periods of a 4.2 nm InGaAs well/2 nm InP barrier superlattice, for a total thickness of ~ 0.4 μm, less than half that of the MQW structure, and the final InP p^+ contact layer was 500 nm thick. Such a SL should exhibit a miniband width of ~ 120 meV for the first electron level and a resulting bias of ~ 7 V for full carrier localization. Double crystal x-ray diffraction measurements showed that the well composition in the MQW sample was $In_{0.51}Ga_{0.49}As$ whereas in the SL structure $In_{0.53}Ga_{0.47}As$ was obtained. Devices were fabricated in both samples by wet etching in 1 $NK_2Cr_2O_7$:1HBr:1H_3PO_4 to form mesas of ~ 550 μm $\times 550$ μm. Au-Ti was then e-beam evaporated to define contacts to both the p and n regions. The final step was to polish the substrate back surface and to apply antireflection (AR) coatings of SiO_2 to both surfaces. For

 0021-8979/93/74(9)/5895/3/$6.00

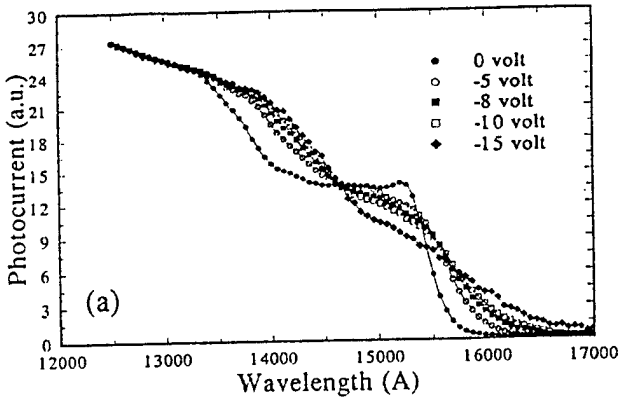

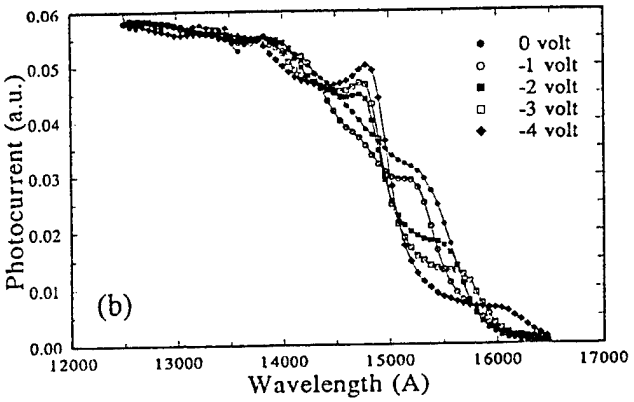

FIG. 1. Photocurrent spectra of a (a) MQW and (b) superlattice diode for various values of reverse bias.

reflection measurements, the AR coating on the back surface was replaced by an evaporated Al mirror. Electrical measurements confirmed good diode characteristics with reverse breakdown voltages ~ 15 V.

Figure 1 shows the photocurrent absorption spectra of the MQW and superlattice devices, normalized to the same value at short wavelength, for various values of reverse bias. In comparison to the MQW results in Fig. 1(a), which clearly show excitonic resonances at zero bias, the spectra in Fig. 1(b), for the SL device, indicate a lack of any significant features at 0 V, consistent with the expectation that the carriers are unlocalized and free to move by tunneling between adjacent wells. Application of reverse bias localizes the carriers in the wells rapidly leading to the appearance of excitons and the staircaselike absorption spectra characteristic of 2D confined carriers, the so-called Wannier–Stark ladder.[11] The positions of the exciton peaks in Fig. 1(a) at ~ 1.52 μm and in Fig. 1(b) at ~ 1.48 μm, using a binding energy of 5 meV, are consistent with the alloy compositions obtained from the x-ray data and the well widths. Of most significance for application of these devices is that the rapid distortion of the optical spectrum for the SL sample occurs at low voltages. Specifically, from Fig. 1(b) we obtain a 58% change in absorption at 1.53 μm for just 4 V of reverse bias corresponding to ~ 80 kV/cm maximum field in the diode. Transmission measurements have shown only a 3.4% absolute change in transmission at the exciton peak position of 1.52 μm in the

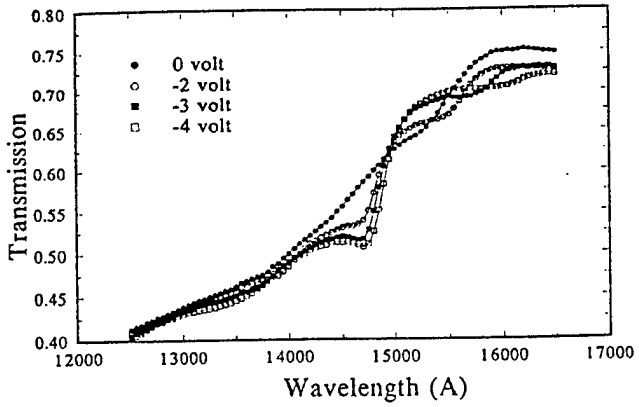

FIG. 2. Transmission spectra for the SL device for various values of reverse bias.

MQW case for as much as 15 V of bias, whereas, in Fig. 2 we show the transmission spectra for the SL that yields an 8.1% change at only 4 V of bias at 1.48 μm, despite the fact that the interaction length in the SL is less than half that in the MQW. In both cases the modulation is close to linear over these applied bias ranges. Voltages $\gtrsim 5$ V across the SL resulted in saturation of the effect, corresponding to full localization of the carriers, and the appearance of the QCSE manifest as a shift in the peaks to longer wavelength and a reduction in the strength of the exciton. In contrast, modulation in the MQW devices continues to increase quadratically to voltages $\gtrsim 15$ V as is shown in Fig. 3, where we have plotted the spectral distribution of the fractional modulation at various biases, defined as the change in signal on application of bias divided by its zero bias value, and measured using a 1 kHz square wave bias signal.

While maintaining low operating voltages, it is well known that increased levels of modulation with little change in spectral bandwidth can be achieved by operating such modulators in reflection, where the signal passes twice through the active region. Figure 4 shows the reflection modulation characteristics of a SL device where the rear AR coating was replaced by an evaporated Al reflector and where the total interaction length for two passes through

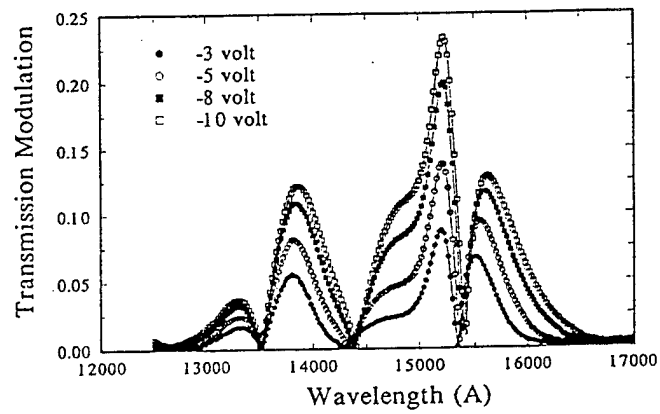

FIG. 3. Fractional transmission modulation measured at 1 kHz for a MQW device.

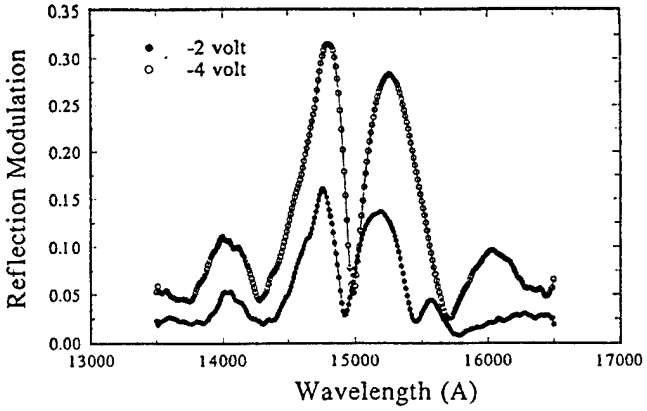

FIG. 4. Fractional reflection modulation measured at 1 kHz for a SL device.

the SL stack is $\sim 0.8\ \mu$m, about the same as for the single pass transmission MQW modulator of Fig. 3. Maximum fractional modulation at 4 V is 32% at 1.48 μm, corresponding to a contrast ratio CR of 1.5:1, which should be compared to the 10% change seen in Fig. 3 for the MQW device at this same bias. The best reflection results we have observed on these nonresonant mode SL devices at this same voltage is a CR of 1.8:1.

Given that the capacitance of these SL structures is ~ 75 pF, we estimate a switching energy at 4 V of 600 pJ and an associated dynamic switching power of 99 W/cm^2 of the active area for switching in 2 ns, a value well within the generally accepted range for continuous nonthermally limited operation.[4] Lower residual doping levels in the SL would result in a reduction in C and a further improvement in power dissipation.

The authors recognize with gratitude financing of this research by the National Science Foundation and the Colorado Advanced Technology Institute, a funding agency of the State of Colorado, through their support of the Optoelectronics Computing Systems Center.

[1] T. K. Woodward, L. M. F. Chirovsky, A. L. Lentine, L. A. D'Asaro, E. J. Laskowski, M. Focht, G. Guth, S. S. Pei, F. Ren, G. J. Przybylek, L. E. Smith, R. E. Leibenguth, M. T. Asom, R. F. Kopf, J. M. Kuo, and M. D. Feuer, IEEE Photon. Technol. Lett. **4**, 614 (1992).
[2] J. Thompson, A. J. Moseley, M. Q. Kearley, C. Meaton, D. J. Robbins, and N. Maung, J. Electron. Mater. **19**, 323 (1990).
[3] B. Pezeshki, S. M. Lord, and J. S. Harris, Jr., Appl. Phys. Lett. **59**, 888 (1991).
[4] H. S. Hinton, IEEE J. Selected Areas Commun. **6**, 1209 (1988).
[5] A. J. Moseley, M. Q. Kearley, R. C. Morris, D. J. Robbins, J. Thompson, and M. J. Goodwin, Electron. Lett. **28**, 12 (1992).
[6] R. A. Morgan, M. T. Asom, L. M. F. Chirovsky, M. W. Focht, K. G. Glogovsky, G. D. Guth, G. J. Przybylek, L. E. Smith, and K. W. Goossen, Appl. Phys. Lett. **59**, 1049 (1991).
[7] E. Bigan, M. Allovon, M. Carré, C. Braud, A. Carenco, and P. Voisin, IEEE J. Quantum Electron. **28**, 214 (1992).
[8] K. K. Law, R. H. Yan, J. L. Merz, and L. A. Coldren, Appl. Phys. Lett. **56**, 1886 (1990).
[9] J. M. Vandenberg, D. Gershoni, R. A. Hamm, M. B. Panish, and H. Temkin, J. Appl. Phys. **66**, 3635 (1989).
[10] C. Starck, F. Mollot, F. Mallecot, J. L. Peyre, and M. Boulou, J. Cryst. Growth **120**, 349 (1992).
[11] J. Bleuse, G. Bastard, and P. Voisin, Phys. Rev. Lett. **60**, 220 (1988).

A2.2 Gas-Source MBE

Gary Y Robinson

A2.2.0 INTRODUCTION

In recent years the use of gaseous feed stocks to replace conventional solid sources in molecular beam epitaxy (MBE) has provided a means of greatly improving the control during growth of III–V semiconductor heterostructures. Several variations of this new technology have appeared, including gas-source MBE (GSMBE) where gaseous hydrides are used for the group V elements, metal-organic MBE (MOMBE) where the metal alkyls are used for the group III elements, and chemical beam epitaxy (CBE) where gases are used for both group III and group V. A review of GSMBE, as applied to the growth of the III–V semiconductors primarily containing phosphorous, is presented here with emphasis on growth mechanisms, vacuum technology and safety. A few III–V materials and their associated heterostructures will be described as illustrations of the GSMBE technique; however, details of how to grow a specific material will be left to section E. A comprehensive description of GSMBE and its application to the InGaAsP/InP materials system and devices can be found in the book by Panish and Temkin [1].

The technique of GSMBE is illustrated by the schematic diagram of figure A2.2.1. As in conventional solid-source MBE, a heated substrate in a UHV chamber is exposed to molecular beams of the group III elements, each beam supplied by a separate effusion oven, called a Knudsen cell. Unlike conventional MBE, however, the group V molecular beam(s) is produced by the thermal dissociation (i.e. cracking) of the appropriate hydride gas as the gas enters the UHV growth chamber. The gases are usually arsine (AsH_3) and phosphine (PH_3), which at the temperatures of 800–1100°C necessary for efficient cracking, produce the dimer molecules As_2 and P_2, respectively. At the usual MBE growth rate of 1 μm hr^{-1}, a significant amount of the by-product H_2 is produced and is removed from the growth chamber by suitable vacuum pumps. Since arsine and phosphine are extremely toxic, great care is exercised in gas handling and storage in order to ensure a safe environment for the crystal grower and the community. Finally, the phosphors deposited in the growth chamber and vacuum pumps can produce hazardous situations and special precautions are exercised during system maintenance. It is these features of GSMBE technology that are unique and will be discussed in more detail in the next section on equipment considerations.

The physical mechanisms controlling film growth in GSMBE are very similar to that operating in solid-source MBE but very different from that in MOMBE and CBE. For example, in the growth of III–III–V ternary alloys, with an excess of the group V flux present, the growth rate and film composition in GSMBE are determined by the rate of arrival of the group III species and largely independent of substrate temperature. Since it is difficult with present technology to control substrate temperature in a reproducible manner, the insensitivity to run-to-run variations in substrate temperature is a major advantage of GSMBE. In MOMBE and CBE, the rates of adsorption, incorporation, and desorption of the metal alkyl molecule are strongly temperature dependent and, thus, the film growth rate and composition can be significantly affected by a modest change in substrate temperature. Thus controlled growth of complex multilayer heteroepitaxial structures is much easier in GSMBE than in MOMBE and CBE. Furthermore, the carbon released by the pyrolysis of the metal alkyls can produce large and undesirable levels of carbon doping during MOMBE and CBE growth, while no carbon by-product is produced during GSMBE. In fact, the molecular fragments produced during cracking of AsH_3 in GSMBE may act to suppress incorporation of low levels of carbon (from CO and other residual gases in the growth chamber) during growth [2].

In comparison to conventional MBE where solid As_4 and P_4 are used in heated effusion cells, GSMBE has several significant advantages. Using a gas source, fast and accurate control of the group V beam is possible. Varying the V/III ratio to check, for example, the transition from an As-stabilized to a Ga-

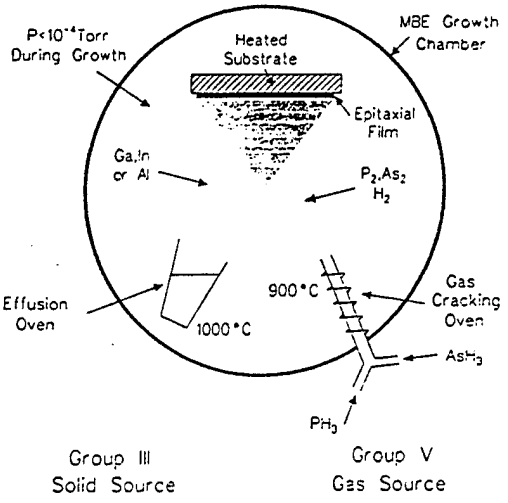

Figure A2.2.1. Schematic diagram showing the major features of gas-source molecular beam epitaxy. The group III molecular beams are supplied by MBE effusion ovens and the group V molecular beams are produced by thermal cracking of the gases PH_3 and AsH_3.

stabilized condition during GaAs growth takes just a few minutes, whereas changing the flux from a large capacity, solid-As_4 oven can take hours. The use of PH_3 rather than solid phosphorus makes the MBE growth of phosphide compounds feasible for the reasons outlined in the next section. The dimer molecules produced in GSMBE have a much larger sticking coefficient than the tetramer molecules produced from the elemental group V materials, and thus more efficient use of source materials is achieved. Feeding the group V source material from outside the UHV chamber can significantly extend the time between venting of the growth chamber since group V effusion cells can be rapidly depleted at the high V/III ratios often needed in MBE growth.

Although the above advantages are also shared with MOMBE and CBE, GSMBE offers some unique advantages relative to MOMBE and CBE. GSMBE avoids the carbon incorporation problem inherent in the use of organic source materials. It is also advantageous to retain from conventional MBE the use of effusion cells for the group III sources since the current generation of commercial effusion cells provides long life, excellent film uniformity, and adequate group III flux stability for most applications. The use of gaseous feed stocks increases the cost and complexity over that of a solid-source MBE system because of the additional equipment needed to control and store the gases. However, a fully automated GSMBE system can be implemented for substantially less cost than a CBE system.

An important advantage of the MOMBE and CBE techniques is the selective-area growth that results from the catalytic decomposition of the metalorganic compounds which can occur on some surfaces. The resulting *in situ* patterning is a promising approach to obtain lateral device definition in highly complex heteroepitaxial structures. GSMBE does not usually exhibit growth selectivity, although selective-area growth of InGaAs/InP has recently been reported by using GSMBE with a high group V flux combined with atomic hydrogen exposure [2].

We have found that the *primary advantage* of GSMBE is the capability to grow with relative ease a wide variety of III–V materials in one growth chamber and retain the precise control of layer thicknesses on the atomic scale characteristic of elemental MBE which is absolutely necessary for modern heteroepitaxial devices. The *primary disadvantage* of GSMBE (and CBE as well) is the extreme toxicity of the hydrides which results in a substantial increase in the cost of equipment, installation, and operation and creates a not insignificant amount of additional stress for the crystal grower. This issue is expected to become less important in the future as less hazardous methods of generating and storing the hydrides on-site are developed and as suitable less toxic, alternative group V source materials become available.

Vacuum deposition using AsH_3 and PH_3 was first reported in 1974 by Morris and Fukui at Bell Laboratories who formed polycrystalline layers of GaAs, GaP, and GaAsP [3]. Panish (1980) was the first to report MBE growth with the gases AsH_3 and PH_3 [4], and a year later Calawa at MIT Lincoln Laboratories reported GaAs with very high electron mobility using AsH_3 instead of elemental As in MBE [5]. Panish pioneered the GSMBE technique by elucidating the mechanisms underlying thermal disassociation of AsH_3 and PH_3 [4], by developing several forms of hydride cracking ovens [6], and by demonstrating that the quaternary alloy InGaAsP could be readily grown using GSMBE [7]. GSMBE has since been used to produce very high quality layers of GaAs [8] and InP [9], and GSMBE heterostructures have been used to fabricate a variety of high performance devices, including InGaAsP/InP lasers [10–12], InGaAs/GaAs/InGaP lasers [13], InGaAs/InP bipolar transistors [14], InGaAsP/InP photodiodes [15], and multiple quantum well optical modulators [16]. The gases AsH_3 and PH_3 have been widely used to produce films of GaAs, InP, GaP, AlP, InGaAs, InGaP, InGaAsP, and InGaAlP, while NH_3 has been used to grow GaN films [17] and GaPN films [18]. Laboratories besides our own now using GSMBE to produce III–V films include ATT Bell Laboratories (USA), British Telecom Research Laboratories (UK), CNET (France), Alcatel Alsthom Recherche (France), Hughes Research Laboratories (USA), Matsushita Research Institute (Japan), Mitsubishi Kasei Co. (Japan), Sharp Laboratories (England), Sophia University (Japan), Tampere University of Technology (Finland), University of California at San Diego (USA), University of Illinois (USA), and University of Minnesota (USA) [19].

A2.2.1 EQUIPMENT CONSIDERATIONS

Generic GSMBE System

An MBE system designed for GSMBE growths is shown in figure A2.2.2 and consists of three UHV chambers and a gas handling system. The UHV system is a standard commercial MBE system (Perkin-Elmer 430) with the single 3-inch wafer capability. The introduction and preparation chambers are used for loading, removal, and *in situ* storage of wafers. The N_2-purged glove box minimizes particulate contamination of the wafer, speeds pump down of the introduction chamber by reducing the noble gases incorporated in the sorption roughing pumps, and provides an extra degree of safety for the operator. The growth chamber contains seven effusion cells and a single gas-cracking oven for both AsH_3 and PH_3, as well as a reflection high energy electron diffraction (RHEED) system for *in situ* characterization of epitaxial surfaces. A quadrapole mass analyser (QMA) is used for determination of AsH_3 and PH_3 cracking patterns as well as for leak checking and residual gas analysis. The gas handling system provides controlled introduction of AsH_3 and PH_3 at low flow rates into the UHV growth chamber from high pressure gas storage cylinders. A single computer provides integrated control of gas flows, effusion cell temperatures, and shutters. All of the effluent from the vacuum pumps and the gas handling system is passed through a gas scrubber for safe removal of toxic gases.

The issues unique to using the gaseous hydrides in a MBE system, including the choice of vacuum pumps, operation of the cracking oven, various schemes for hydride delivery, and safety concerns are discussed in the following sections.

Phosphorus in MBE

The vapour pressure of phosphorus is much higher than that of arsenic and thus control of phosphorus in a UHV MBE system is correspondingly more difficult. To further complicate the situation, there many allotropic forms of solid phosphorus, each with a different dependance of vapour pressure on temperature (see figure A2.2.3) [20, 21]. White phosphorus has a very high vapour pressure (10^2 torr at 200°C), and spontaneously ignites in air producing a dense white smoke that is toxic and corrosive. Red phosphorus has a lower vapour pressure (10^{-2} torr at 200°C), is relatively stable in air at temperatures less than 250°C, and is less reactive than white phosphorus.

Early MBE studies using solid red phosphorus [22, 23] in a conventional effusion cell produced a molecular beam containing primarily P_4 molecules, which have a low incorporation coefficient at the substrate

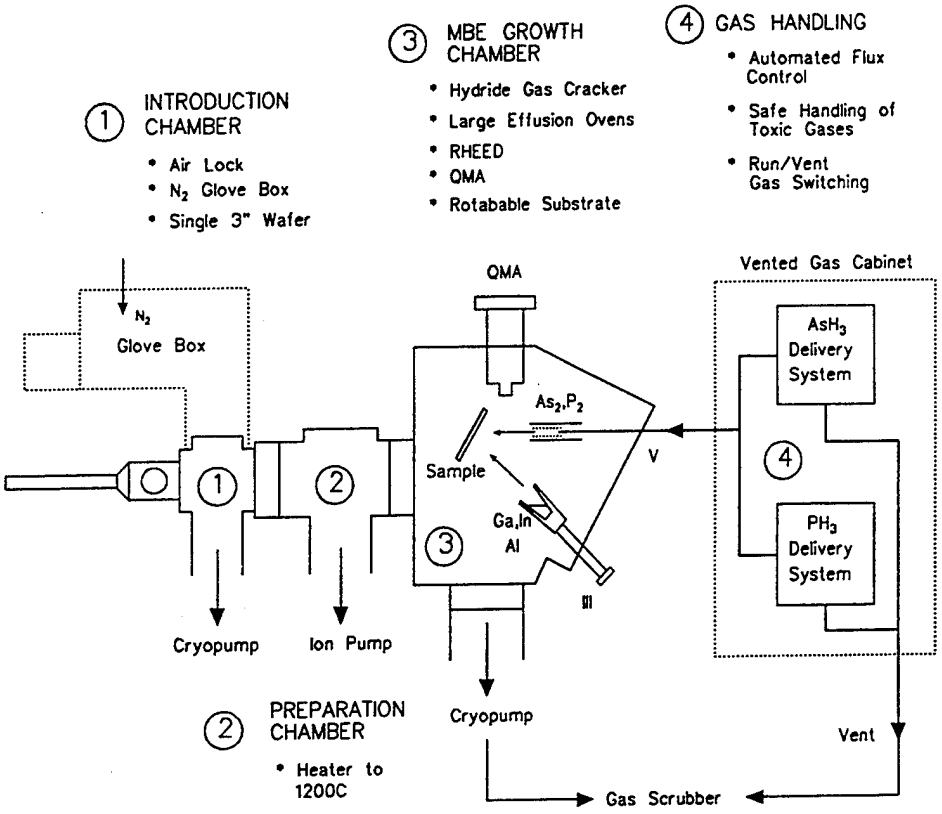

Figure A2.2.2. A GSMBE system with a single growth chamber, two auxiliary UHV chambers, and a gas handling system.

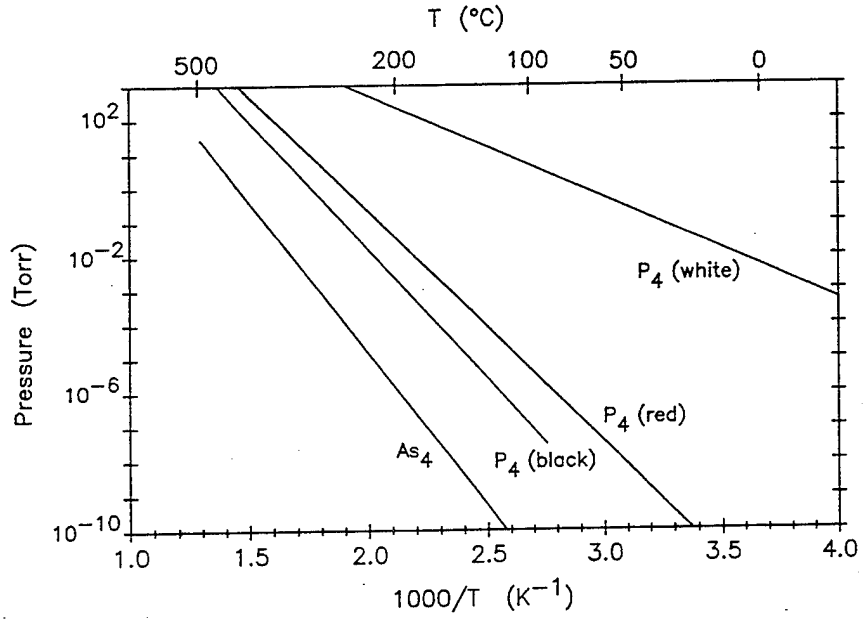

Figure A2.2.3. The vapour pressures as functions of temperature for solid As_4 and the allotropic forms of black, red and white P_4 (based on the vapour pressure curves summarized in [20,21]).

temperatures used in MBE. Thus very high P_4 fluxes are needed for growth and substantial accumulations of phosphorus are deposited on the walls of the MBE chamber. Furthermore, the wall deposits are a mixed phase of red and white phosphorus, with the amount of each varying from run to run. Reproducible growth is very difficult to achieve because of the varying background phosphorus pressure, and the large amount of white phosphorus greatly complicates safe procedures for chamber cleaning. In addition, Panish has pointed out that the molecular flux obtained from heating red phosphorus is expected to depend on the thermal history of the phosphorus effusion cell, and thus achievement of precise control of the phosphorus flux is unlikely [1].

On the other hand, employing a source of P_2 molecules can be a practical means of producing phosphide films in MBE. The P_2 species exhibits a much higher incorporation coefficient s_i than the P_4 species, and thus requires a much lower phosphorus beam flux. We have found that for GSMBE of InP at 520°C and 1 $\mu m\,hr^{-1}$, s_i is about 0.2–0.3 for P_2, which is about 50 times larger than s_i for growth with P_4. Furthermore, P_2 vapour condenses primarily as red phosphorus on the surfaces of the growth chamber, producing a much lower phosphorus background pressure [20]. This permits reproducible, controlled epitaxial growth of phosphide films and the growth of arsenide films (i.e., GaAs, InGaAs) with low phosphorus contamination, in the same growth chamber. The smaller accumulation of white phosphorus deposits extends the time between venting of the system for maintenance and reduces the fire hazard during chamber cleaning.

A P_2 molecular beam can be produced by several methods. Wright and Kroemer [24] have used heated GaP to provide a P_2 beam for MBE growth, but the beam contained Ga and the P_2:Ga flux ratio varied with use. In GSMBE, phosphine is thermally decomposed using special gas cracking ovens, described in a following section, to produce a well controlled P_2 beam. In solid-source MBE, a valved effusion oven for generation of a As_2 beam from solid As_4 has recently been developed [25], and versions of this cracker may make the generation of a P_2 molecular beam from solid phosphorus practical [26, 27]. A large canister of solid red phosphorus, mounted outside the MBE chamber, is heated and the resulting P_4 vapour is passed through a needle valve and then thermally cracked at a higher temperature to produce a P_2 beam. The valve controls the P_2 flux while the canister is kept at a constant temperature. With proper design, the valve can be kept free of clogging, and III–V phosphide films can be grown [27, 28]. The primary advantage of the valved cracking oven is safety; the highly toxic PH_3 is avoided. Although high efficiencies have been reported for a valved cracker [25], the efficiency for creation of dimer molecules from tetramer molecules in a solid-source cracker may not as high as for the hydride-gas cracker discussed below. We have found the As_2/As_4 ratio to be about 6–8 times higher for our hydride-gas cracker than for a solid-source cracker measured under similar conditions.

Vacuum Pumping

During growth, the As_2 and P_2 species are readily pumped, because of their high vapour pressures, by the liquid-nitrogen-cooled panels mounted on the walls of the growth chamber. Thus the primary gas load for the vacuum pumps is the large amount of H_2 produced during hydride cracking. For a typical III–V layer, the pressure at the sample should be less than 1×10^{-4} torr for molecular flow conditions, and for a film growth rate of 1 $\mu m\ hr^{-1}$, a gas flow rate of about 2–10 sccm is needed, depending on the design of the growth chamber. This will produce a gas load of up to 6 litres of H_2 in a 10 hour deposition. The pressure at the nozzle of the gas cracking oven will be about 1×10^{-3} torr, where the pumping rate needed is about 130 l s^{-1}. This rate translates to a pumping speed about 1000 l s^{-1} or more at the vacuum pump, depending on the configuration of the growth chamber. To maintain lower pressures or to operate at higher growth rates requires even higher pumping rates. Also, the group V element is preferentially desorbed from a III–V surface at elevated temperatures and, thus, the maximum substrate temperature is determined by the rate at which the group V molecules can be supplied to replace the lost group V surface atoms. Hence, the pumping rate limits the maximum substrate temperature as well as the maximum growth rate.

Three different types of UHV pumps—diffusion, cryogenic and turbomolecular—have all been used successfully alone or in combination in GSMBE. The diffusion pump offers high pumping rates, low cost and excellent reliability, and large diffusion pumps have been used in GSMBE commercial systems from Vacuum Generators [1] and Perkin-Elmer [29] to grow III–V films of high quality. The major

disadvantages of the diffusion pump are the cold trap which can greatly reduce the pumping speed and the possible contamination of the growth chamber by the pumping fluid. With proper operation, carbon contamination from the diffusion pump can be insignificant. Using a diffusion-pumped GSMBE system, Stillman and co-workers have obtained GaAs with a residual free carrier concentration as low as 9×10^{13} cm^{-3} [29], which is comparable to highest purity GaAs grown by conventional solid-source MBE.

Turbomolecular pumps have high pumping rates for H_2 and the newer turbomolecular pumps are chemically resistant to the metal alkyls used in MOMBE. However, turbomolecular pumps are very expensive and failure of the pump can be catastrophic. If metalorganic gases are to be used, turbomolecular pumps are best suited to the task, but if the only gases to be used are the hydrides, then either diffusion or cryogenic pumps will work well.

Closed cycle He-cooled cyropumps are well suited for GSMBE, since they can provide high pumping rates for H_2 at the required pressures through the use of activated charcoal to adsorb hydrogen. Cyropumps cost substantially less than turbomolecular pumps and produce little or no contamination to the growth chamber. But since the pumped gas is retained, the pump must be frequently regenerated. Figure A2.2.4 shows our GSMBE growth chamber with two CTI model CT-8 cryopumps, each with 2200 l s^{-1} (H_2) pumping rate, that share a single compressor. The pumps are mounted close to the growth region in order to maximize the available pumping speed and in a horizontal position to minimize particle collection on the seat of the UHV gate valves. The pressure relief valves on the CT-8 pumps are vented directly to a gas scrubber. A mechanical pump containing a fluorocarbon fluid (Fomblin) and flushed with N_2 is used for regeneration of the He cryopumps. No in-line traps are used and no evidence of phosphorus accumulation in the roughing pump or lines has been observed in over 600 days of growth. We find we can grow GaAs or InP at 1 μm hr^{-1} using a new CT-8 pump for 3–5 days of growth before regeneration is needed. However, for the growth of InGaAsP alloys where both As_2 and P_2 beams are used at high fluxes, daily regeneration is required. Two pumps then allow uninterrupted growth by alternating pumps between growth and regeneration.

We have found that the H_2 capacity of the CT-8 cryopump degrades considerably with use in our GSMBE

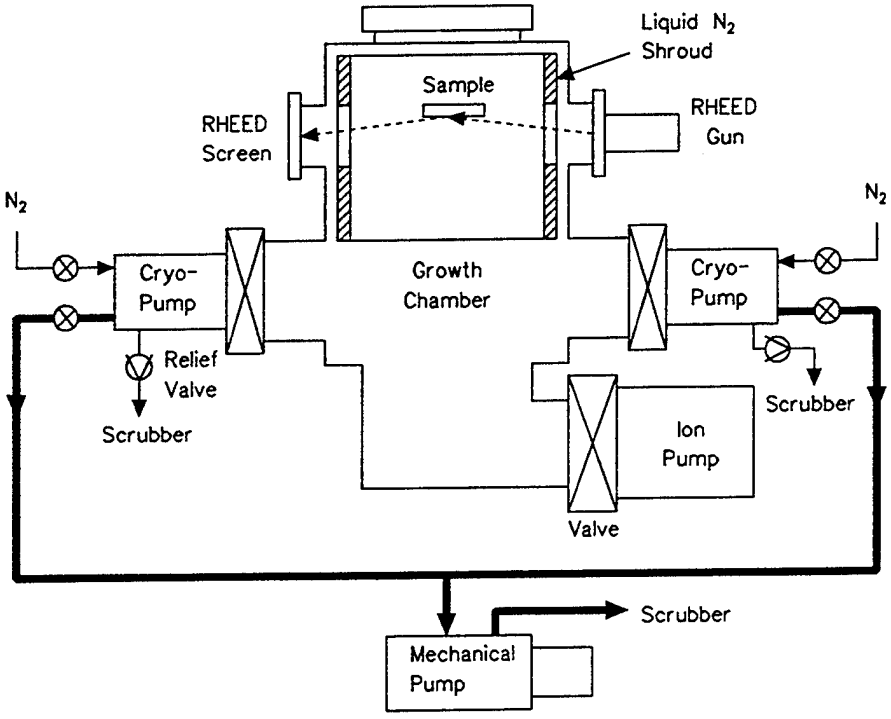

Figure A2.2.4. Vacuum pumping system for GSMBE growth. One cryopump is used during growth while the other can be regenerated. The ion pump is used only during idle periods.

system. As shown in figure A2.2.5, we have measured the pump capacity by noting the H_2 dose where the pressure suddenly increases due to pump regurgitation. The tests were conducted at a constant flow rate of 32 sccm using H_2, not AsH_3 or PH_3, through the gas cracker, and thus do not duplicate the exact conditions present during growth. However, it is apparent that the capacity decreases markedly with use, dropping from over 11 standard litres of H_2 to under 5 litres in about 24 months of use. Replacement of the activated charcoal restores the pumping capacity. Apparently, phosphorus is accumulating on the surfaces of the charcoal and inhibiting H_2 pumping. The replacement of the activated charcoal is a straightforward procedure, costs about 5% of a new cryopump, and does not require opening the growth chamber. Note that care must exercised when growing with a nearly full cryopump. The pressure rises very rapidly when the pump reaches its current capacity, which can result in tripping of pressure-sensitive interlocks that control the main power to the MBE system and damage to the effusion cells during the ensuing abrupt cool down.

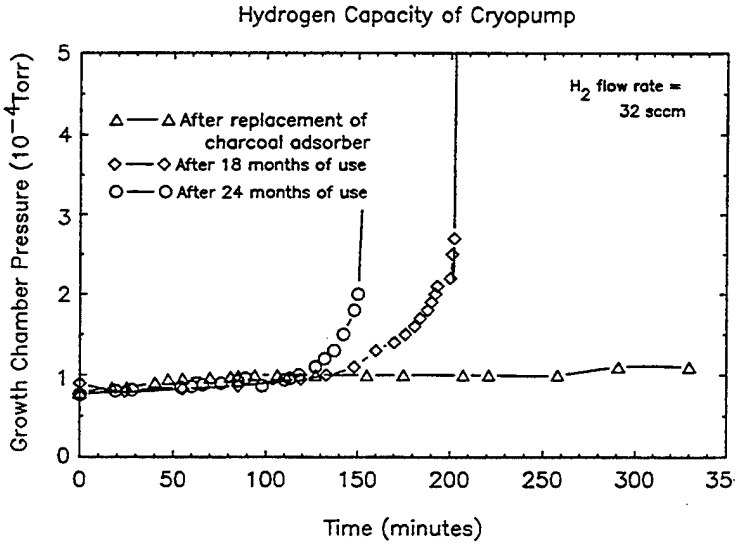

Figure A2.2.5. Measurement of the hydrogen capacity of a CTI CT-8 cryopump with increasing use in a GSMBE system. The time at which the pressure abruptly increases is a measure of the pump capacity.

Hydride Delivery Systems

The flow of the hydride gases can be controlled using either of two methods: mass flow control or pressure control. Mass flow control systems use mass flow controllers based on the temperature change that occurs in a gas flowing through a restricted volume. This approach offers direct control of gas flow rates and precise mixing of AsH_3 and PH_3 for growth of such materials as GaAsP or InGaAsP. The currently available mass flow controllers lack adequate reproducibility at the low flow rates (about 1–2 sccm) used in GSMBE and thus can require frequent recalibration. However, mass flow control systems are relatively simple to implement and have been used in several commercial GSMBE systems.

Pressure control systems employ a precision leak valve to adjust the pressure of a gas which is flowing through a fixed aperture. A pressure transducer (usually a capacitance manometer) and a servo-valve are used to obtain a highly reproducible flow rates over a very wide dynamic range, with very good control at low flow rates. Calibration of the flow rate in terms of the indicated pressure is required for each gas, since the flow rate will depend on the conductance of the gas in the manifold and cracking oven. Pressure control works extremely well for GSMBE and has also been employed in MOMBE for precise control of low vapour pressure gases without the need for a carrier gas [30].

Figure A2.2.6 is a schematic diagram of the pressure-control hydride delivery system in use in our laboratory. Only the components for PH_3 flow control are shown; an identical system for AsH_3 flow

control is mounted in the same cabinet. This system is based on the work of Panish and Sumski at Bell laboratories [7], designed in our laboratory, and assembled by Precision Flow Devices (Beaverton, Oregon). The run/vent valve configuration minimizes flow transients when the P_2 (or As_2) molecular beam is switched on or off by keeping the pressure constant against the conductance of the gas cracking oven in the growth chamber downstream of the run valve and the gas tubing down stream of the vent valve. The cooled sorption pump provides a low pressure to mimic the growth chamber and adequate capacity for temporary storage of any uncracked hydride. At the end of the growth day, the sorption pump is allowed to warm up and the effluent, diluted with N_2, is pumped into a gas scrubber. In this system designed to operate with a low pressure gas cracking oven, an indicated gas pressure of 10 torr corresponds to a flow rate of approximately 10 sccm. The flow rate can controlled with a precision of ± 0.02 sccm.

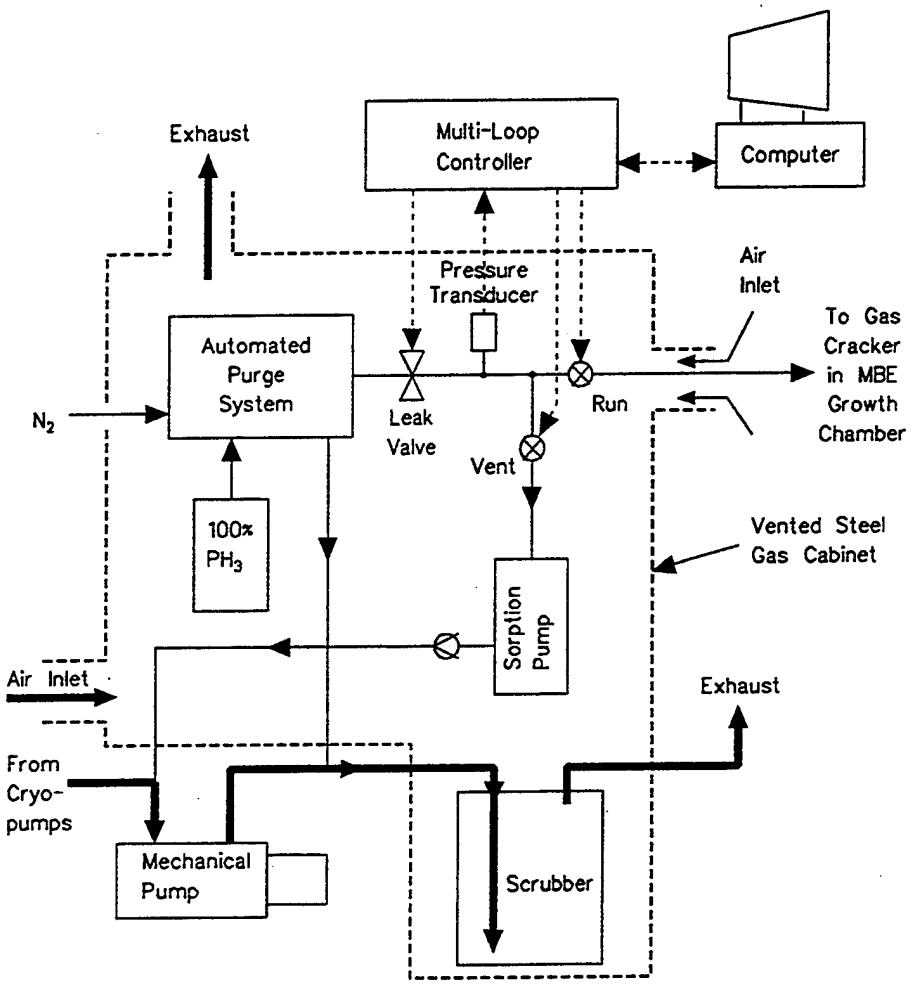

Figure A2.2.6. Schematic diagram of a hydride delivery system for GSMBE growth. A computer controls the opening and closing of the run and vent valves as well as the gas flow rate via the precision leak valve. All components which contain toxic gas at pressures above atmospheric pressure are enclosed in the vented cabinet.

The growth of complex III–V heterostructures with many layers of different composition usually requires the hydride gases to be switched on and off at each heterointerface. In order to achieve rapid gas switching, the volume of the gas lines down stream of the run valve in figure A2.2.6 should be small. Also the conductance of the gas tubing, which depends on the pressure as well as the tube diameter and length, should be large to allow rapid removal of the residual gas via the MBE chamber after the run valve closes and rapid charging of the gas lines after the run valve opens. Furthermore, rapid switching requires the gas cracking oven not to impede gas flow. Using the low pressure gas cracker described below, our system exhibits a gas switching transient of about 4–6 seconds; other GSMBE systems have

achieved gas switching times of less than 1 second [1,31]. It should be noted, however, that in order to obtain atomically abrupt interfaces of InGaAs/InP or InGaP/GaAs, a growth pause of 10 or more seconds is required at each interface [32–35]. Hence, faster gas switching times are not usually needed.

Pressure control can be readily used to grow quaternary alloys of $In_xGa_{1-x}As_yP_{1-y}$ with excellent control of alloy composition. As shown in figure A2.2.7(a), the gases AsH_3 and PH_3 are mixed before entering the MBE system. The flow rate F of each gas is controlled by adjusting the pressure P against the conductances G and kG of the tubing in the gas mixing manifold. Under normal operating conditions, the total flow rate $F_1 + F_2$ is approximately a linear function of the total inlet pressure $P_1 + P_2$, as long as the pressure at node N is larger than the smaller of P_1 or P_2. On the other hand, the flow ratio F_1/F_2, which controls the group V composition of the epitaxial film, is a nonlinear function of the pressure ratio P_2/P_1. For our gas manifold, the conductance ratio k is about 2.0 and the calculated dependance of F_1/F_2 on P_1/P_2 is shown in figure A2.2.7(b) along with the operating points for three different InGaAsP compositions. With this system, we can easily control flow ratios as high as 15:1 with better than ±0.5% reproducibility at a total flow rate of 10 sccm. The *maximum* ratio of As_2/P_2 needed at the surface of the InGaAsP was found to only be about 6:1 under typical growth conditions. High quality InGaAsP layers with band gap emission at wavelengths from 1.15 to 1.67 mm and lattice matched to InP substrates have been obtained in a reproducible manner using this hydride delivery system [36].

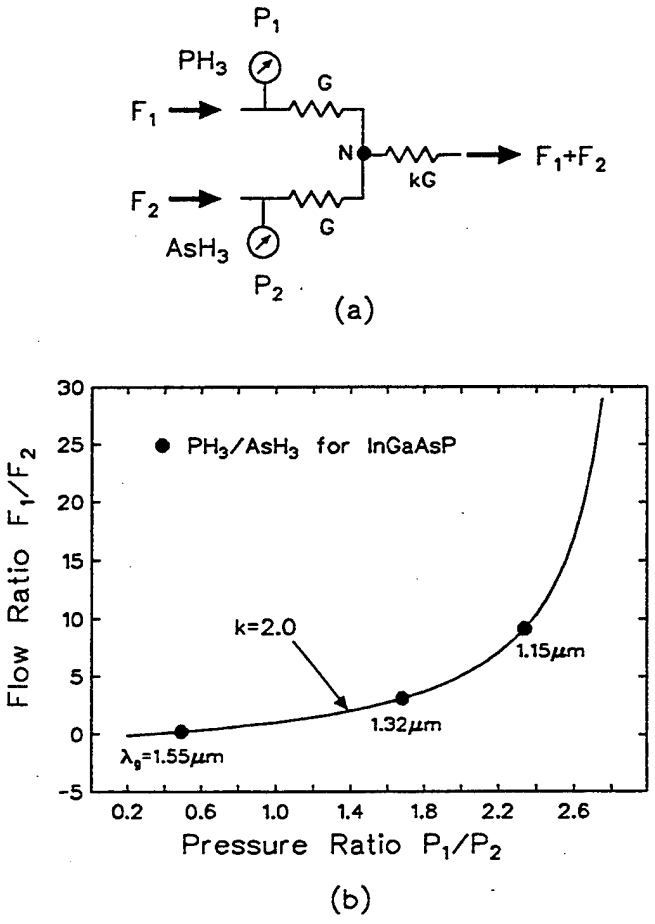

Figure A2.2.7. Pressure control of hydride gas flow in GSMBE. (a) Schematic diagram of gas manifold. (b) Flow ratio as a function of pressure ratio for a manifold with gas conductance ratio of k = 2.0. The operating points for three different InGaAsP compositions are noted for PH_3 as gas 1 and AsH_3 as gas 2.

Hydride Cracker

It is found that the hydrides do not decompose on III–V surfaces during MBE growth, even though the substrate temperatures are typically 500–600°C. Thus, the hydrides are thermally cracked in specially designed high temperature gas cracking oven (i.e. cracker) mounted in the MBE chamber in place of a conventional effusion cell. The ideal cracker should reduce the hydride to a beam containing only elemental group V species and hydrogen in order to avoid introduction of the volatile, toxic hydrides into the vacuum system. As discussed above, the cracker should also produce dimer molecular species, since the incorporation coefficient of the dimers As_2 and P_2 are much higher than the tetramers As_4 and P_4. Furthermore, the use of P_2 minimizes white phosphorus accumulation in the growth chamber.

Two general types of crackers have evolved for use in GSMBE. Panish first used a thermal cracker operating at inlet pressures of 200–1500 torr to thermally decompose AsH_3 and PH_3 at temperatures of 900–1000°C [6]. The cracker contained a high pressure and a low pressure region, separated by a carefully constructed flow constriction in Al_2O_3 tubing as shown in figure A2.2.8(a). By examining the equilibrium thermodynamics for hydride decomposition, Panish showed that in the high pressure region, both AsH_3 and PH_3 should readily form the tetramer molecules As_4 and P_4, but dimerization required the lower pressure region. Both processes take place efficiently at 900–1200°C. A version of the high pressure cracker was manufactured by VG Semicon.

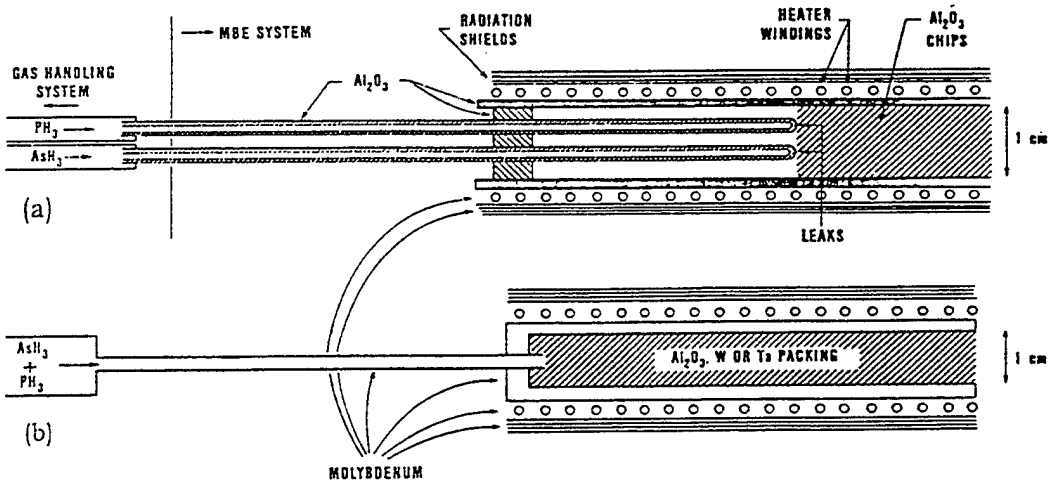

Figure A2.2.8. Gas sources for GSMBE. (a) High-pressure gas cracking oven. (b) Low-pressure gas cracking oven. (Reprinted with permission from [58]).

The second and more widely used type of cracker is the low pressure cracker. Here the inlet pressure varies from 2 mtorr to 10 torr, depending on the design of the cracking region. Early low pressure crackers were constructed of tantalum, since several workers demonstrated that heated Ta acts as a catalysis in the decomposition of AsH_3 and PH_3 [5,7,37]. The use of Ta baffles in the form of crushed foil and pellets can increase the efficiency of cracking and dimerization, albeit at the expense of flow conductance and gas switching speed. A low pressure cracker of this type is shown in figure A2.2.8(b). We have successfully used a low pressure all-Ta-constructed cracker supplied by Ulvac in Japan (model ZB61- 9610) for GSMBE. The cracker consists of a heated region with 11 Ta disks each with several small holes, inside a 12 cm long, 1.5 cm diameter Ta tube. The cracker operates at an inlet pressure of 2–10 torr and at temperatures of 800–1000°C. At cracker temperatures above 1000°C, the total ionized impurity level is found to increase in the sample, apparently as a result of contamination from the hot surfaces in the cracker. Below 800°C, the cracking efficiency falls off rapidly, as evidenced by AsH and AsH_2 molecular species, detected by QMA measurements, produced by the incomplete pyrolysis of AsH_3. We have found that the molecular fragments created by partially decomposed AsH_3 may reduce the incorporation of residual carbon during GSMBE of GaAs [38]. However, the advantage of a lower carbon contamination in the sample is greatly offset by the increased risk of AsH_3 accumulation in the growth chamber during long periods of growth

with the cracker temperature below 800°C. Although an early study [37] indicated that the Ta catalytic action degraded with use through the formation of tantalum phosphide on the surfaces of the cracker, in over six years of operation with our Ulvac cracker using both AsH_3 and PH_3, we have observed no change in the efficiency of cracking or dimerization.

In order to increase the conductance of the low pressure cracker, recent cracker designs have reduced or removed the baffles without appreciable loss of cracking efficiency. Figure A2.2.9 compares the cracking efficiency η_{cr} and dimerization efficiency η_{dim} for Ta- and W-based high conductance hydride crackers used by Jackson and co-workers at the University of Illinois [31]. The efficiencies were measured using a QMA to determine the relative amounts of each molecular species emanating from the cracker. Both crackers approach 100% efficiency at high cracking temperatures, but the Ta-based cracker can operate about 200°C lower in temperature, indicating that, even in a cracker with a straight tube without baffles, the catalytic action of Ta can be very effective. Other high conductance crackers appear to use large-area, inert surfaces without Ta to achieve useful cracking efficiencies, such as the proprietary design by the Intevac Corporation which employs Mo construction. In this type of cracker, an appreciable concentration of monomers may be produced [1]. Recently, As monomers were found to be more readily incorporated than As_2 which in turn was more readily incorporated than As_4, in the GSMBE growth of $GaAs_xP_{1-x}$ alloys [39]. Thus monomer generation via cracked AsH_3 may prove to be very useful.

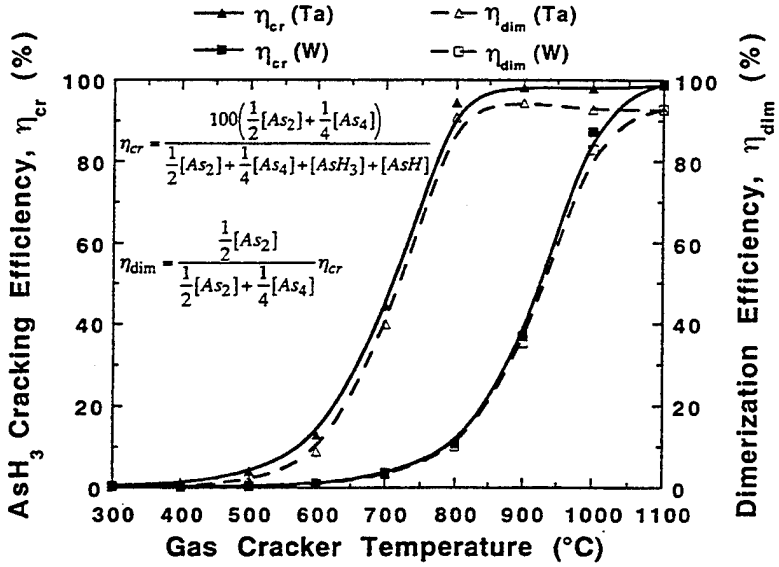

Figure A2.2.9. Comparison of cracking and dimerization efficiencies for Ta-based and W-based crackers using AsH_3. Dashed curves are for dimerization efficiency and solid curves are for cracking efficiency. (Reprinted with permission from [31]).

It should be noted that accurate measurement of the value of the cracking efficiency is fraught with difficulties since the QMA will detect molecular species reflected from hot surfaces in the growth chamber, the QMA can be nonlinear at the pressures used in growth, and the QMA can crack the molecules before they are detected. The comparison of the cracking behaviour in figure A2.2.9 is meaningful since the measurements were carried out in an identical fashion, but the value of the efficiencies given may be in error.

In order to determine the optimum gas switching performance of a gas cracking oven and gas handling system, Jackson *et al* [31] have also have examined the composition depth profiles of InP/InGaAs heterostructures grown under different gas flow conditions. The heterostructures were grown without growth pause at the interfaces in a GSMBE system fitted with a 5000 l s^{-1} He cryopump and a 2200 l s^{-1} turbomolecular pump. Using secondary ion mass spectroscopy (SIMS), the composition-depth profiles of figure A2.2.10 were obtained for two different growths. In figure A2.2.10(a), a single low pressure cracker with Ta baffles was used for both AsH_3 and PH_3 and the gas switching manifold was located about 1 m

from the cracker inlet port. A long P tail is seen to extend into the InGaAs layer and the As appears to penetrate into the InP layer as well. In figure A2.2.10(b), separate high conductance Ta crackers without baffles were used with the run/vent switching valves mounted at the gas inlet flange on the MBE growth chamber. The layer thicknesses and growth conditions were the same as for the sample of figure A2.2.10(a). The P concentration in the InGaAs has dropped to the detection limit of the SIMS instrument and the P and As tails have been greatly reduced. Clearly, in this GSMBE configuration, significant improvement in heterointerface abruptness was achieved by using high conductance hydride crackers, reducing the volume between the gas switching manifold and the cracker, and utilizing separate flow paths for AsH_3 and PH_3.

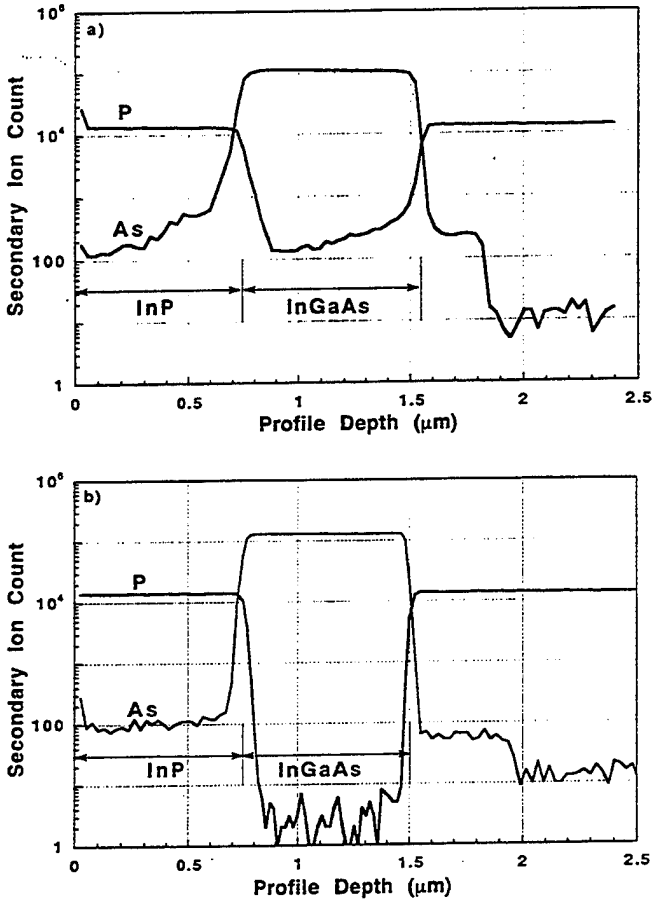

Figure A2.2.10. SIMS depth profiles for InGaAs/InP heterostructures grown by GSMBE. (a) Grown with a single low conductance hydride gas cracker and remotely mounted gas switching manifold. (b) Grown with separate high conductance gas crackers and closely mounted gas switching manifold. (Reprinted with permission from [31]).

System Operation

The placement of the eight sources on the growth flange in our GSMBE is shown in figure A2.2.11. The dopant cells for Be and Si have a maximum capacity of 2 cc while the remaining effusion cells have a maximum capacity of 60 cc each. The inclination of the axis of each cell from the horizontal varies from less than 10 degrees near the top of the flange to 46 degrees at the bottom. In and Ga are used at the highest rate and thus the cells for these elements are positioned near the bottom of the flange to provide to largest usable volume of the cell crucibles without spillage. Two In and two Ga cells are used to allow growth of at least two InGaAsP layers of different group III composition in the same growth run without

changing cell temperatures. The placement of the cells are chosen to minimize the lateral variation of the group III alloy composition across the wafer.

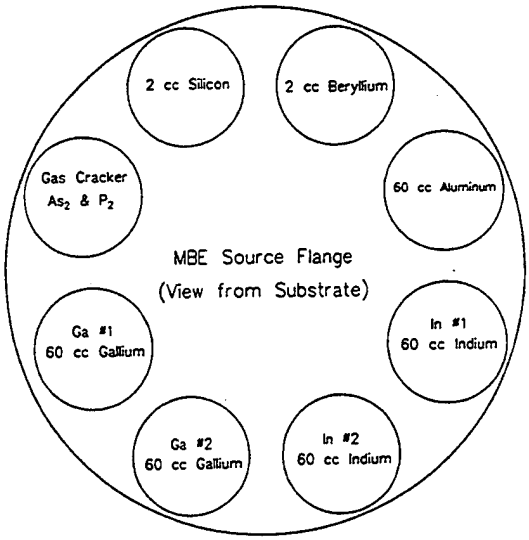

Figure A2.2.11. Placement of effusion ovens and gas cracker on GSMBE source flange.

Each effusion cell exhibits a momentary overshoot followed by a slow decrease in the molecular flux when the mechanical shutter is opened because the melt surface temperature will drop slightly due to radiation loss after shutter opening. The flux transient depends on cell construction as well as on the interval for which the shutter has been closed. The In and Ga cells are used in pairs to match the flux transients and thus minimize changes in layer composition with depth at the start of the growth of alloys such as InGaAs or InGaAsP. However, the growth rate will vary with time and in the growth of the thin layers required in quantum well (QW) heterostructures, the flux transients can significantly alter the layer thickness from that for a constant growth rate [40]. The placement of the cells is chosen to minimize the lateral variation of alloy composition across the finished wafer. The placement of the gas cracker is not critical, since the As_2 and P_2 beams emanate from the same location on the source flange when using a single gas cracker.

During a typical GSMBE growth the chamber pressure is $(2–8)\times10^{-5}$ torr, which is primarily the partial pressure of hydrogen. Chilled water is used to cool the shroud surrounding the effusion cells and liquid nitrogen is used to cool the shrouds on the walls of the growth chamber. The hot filaments in the effusion cells, RHEED, QMA, and ionization gauges operate in the normal fashion. To prolong ionization gauge life, the emission current for the gauge should be kept at its lowest setting. The useful operating life of the electron multiplier in the QMA is about six months. We find the current generation of commercial effusion cells are long lived and provide a stable and reproducible flux even in the H_2 ambient of GSMBE. No adverse effects on the life of the oven heater filaments have been observed, unlike in MOMBE where the metal alkyls can rapidly corrode and destroy hot filaments. However, we have found a white crust forms on the surface of the Be source material over a period of months in our GSMBE system. The crust will eventually prevent the sublimation of the Be and the cell is no longer useable. The Be can be removed, the Be metal etched in $HF:H_2O$ 1:100, and then replaced without the loss of the expensive, high purity Be material. We speculate that the crust is a result of the presence of phosphorus in the growth chamber, but the composition of the crust has not been identified.

Commercial phosphine is currently available with total impurity levels in the range 2–5 ppm. In some applications, higher levels of purity are needed and on-site purification can be used to improve the properties of GSMBE films grown with commercial phosphine [41]. We have used a gas filter consisting of synthetic zeolite molecular sieve to purify 100% PH_3 prior to thermal cracking during the growth of InP, InGaP, and InGaAlP. The filter contained 150 cc of 3A molecular sieve, which has a molecular structure that is particularly effective in trapping water. SIMS data indicated that a major source of oxygen contamination was the as-supplied PH_3 gas. The oxygen had no measurable effect on the InP and very little effect on the

InGaP. However, the addition of only 1% Al to form InGaAlP had the dramatic effect of greatly increasing the oxygen content of the epitaxial layer. The Al was very effective in aiding the incorporation of oxygen in the InGaAlP epitaxial surface during growth. The combination of the Al and oxygen led to a significant decrease in electron concentration in n-type InGaAlP, producing non-conducting material. However, the molecular sieve was found to reduce the oxygen content and permitted the growth of conducting InGaAlP. No tests were conducted to determine the effectiveness of on-site purification on AsH_3.

At end of a day of growth, the temperatures of the effusion cells and the gas cracker are reduced to 200°C, with a slow cooling rate of about 10°C min^{-1} used for the Al cell to avoid breakage of the crucible. The liquid-nitrogen-cooled shrouds are allowed to warm up to room temperature, which produces a pressure increase in the growth chamber from 1×10^{-7} torr to about 1×10^{-4} torr in a period of about one hour. Within about five hours the pressure has dropped to about 1×10^{-6} torr, mostly due to residual P_2, and the system is ready for another day of growth. By cycling the shrouds to room temperature between growth days, the consumption of liquid nitrogen is greatly reduced. The total volume of gas evolved from the wall shrouds is 1–2 sl, which can be a significant fraction of the cryopump capacity, as seen from figure A2.2.5. Thus, the cycling also avoids the large gas load that would accumulate during many days of growth and which could easily exceed the capacity of the He cyropumps, leading to a catastrophic pressure increase during warm up of the wall shrouds. Also, incomplete dimerization of P_4 to P_2 in the gas cracker can lead to a build up of white P_4 on the shrouds, which can produce an increasing background pressure with each growth and lead to unwanted P incorporation in arsenide compounds. Frequent cycling of the shrouds avoids this problem.

For maintenance, the growth chamber is opened to the atmosphere about once in every six months of use. Before opening, the MBE chamber is baked for 4–5 days to a temperature of 180–200°C to stabilize the phosphorus coated walls, reducing the chance of a white- phosphorus fire and minimizing contamination from reaction of the phosphorus with the air. Upon opening, we usually detect toxic gas (e.g. 100 parts per billion) at open ports on the growth chamber; thus, self-contained breathing apparatus must be worn during servicing. The toxic gas levels at the open ports usually drop to below detectable concentrations within about 24 hours if room air is continually drawn through the chamber and exhausted. Maintenance includes cleaning of the RHEED gun and screen, view ports and effusion cell shutters, and replacement of filaments in the ion gauges, RHEED, and QMA. We have found that most of the phosphorus deposited in the growth chamber is on the surfaces of the wall shrouds and is mixed with arsenic deposits. Little phosphorus is found in the He cryopumps and none has been found in the mechanical pump used for cryopump regeneration. After reloading the effusion cells, the chamber is evacuated and again baked for 4–5 days with the pressure held constant at about 3×10^{-6} torr until the wall temperatures reach 180–200°C. Upon cooling, the base pressure is in the 10^{-10} torr range and the system is carefully leak checked before introducing P_2 or As_2. After re-establishing the calibration of the group V and dopant fluxes, the residual free carrier concentration is measured in unintentionally doped material to check the 'purity' of the GSMBE system. We have used this up-to-air procedure for more than 15 openings of the growth chamber, and we find no increase in the residual carrier concentrations in either GaAs (p-type, $p < 2 \times 10^{15}$ cm^{-3}) or InP (n-type, $n < 6 \times 10^{15}$ cm^{-3}). Also, we have found no degradation in the photoluminescence intensity of InGaAsP layers after opening the growth chamber. Thus, with the proper operating and maintenance procedures the quality of the III–V material grown in a phosphorus-based GSMBE system does not deteriorate with system use. Furthermore, the properties of III–V layers are as reproducible as those grown in a arsenic-based solid-source MBE system.

Safety

Arsine and phosphine are extremely toxic and great care must be exercised in the design and operation of a GSMBE laboratory to ensure it is a safe working environment for the laboratory personnel and that the GSMBE facility does not present a major health hazard to the community [21, 42, 43]. Figure A2.2.12 summarizes the critical concentrations of AsH_3 and PH_3 relevant to health hazards; note that even a 30 min exposure to only 30 parts per million (ppm) of AsH_3 can be lethal. The OSHA Permissible Exposure Limit (PEL) and the Total Limit Value (TLV), defined as the maximum concentration that a worker can be exposed to in an 8 hour period in a 40 hour work week, is currently 50 parts per billion (ppb) for AsH_3 and 300 ppb for PH_3 [44]. The gases are stored in pressurized bottles and even a very small leak can

result in concentrations that exceed TLV levels. Thus, to provide a safe environment, the laboratory should be designed so that no gas is allowed to escape and all the AsH_3 and PH_3 that is consumed is converted to a safe form for proper hazardous waste disposal. A sufficient volume of air flow must be provided in the laboratory areas for ventilation and in the room air exhaust system in order to dilute the toxic gases to safe levels in case of a leak in the gas handling system. The hydrides are pyrophoric [21] and toxic PO_x oxides are released during a PH_3 fire; thus, provision for controlling toxic fires must also be made. Hydride gas detectors [45] must be used to continuously monitor the laboratory areas and gas storage cabinets and must be connected to an independent alarm system. Self-contained breathing apparatus must be used during system maintenance and be readily available for use in an emergency. Most importantly, all personnel must be well informed, well trained in the proper operation of the equipment, and well exercised in the emergency procedures in case of an accident [46].

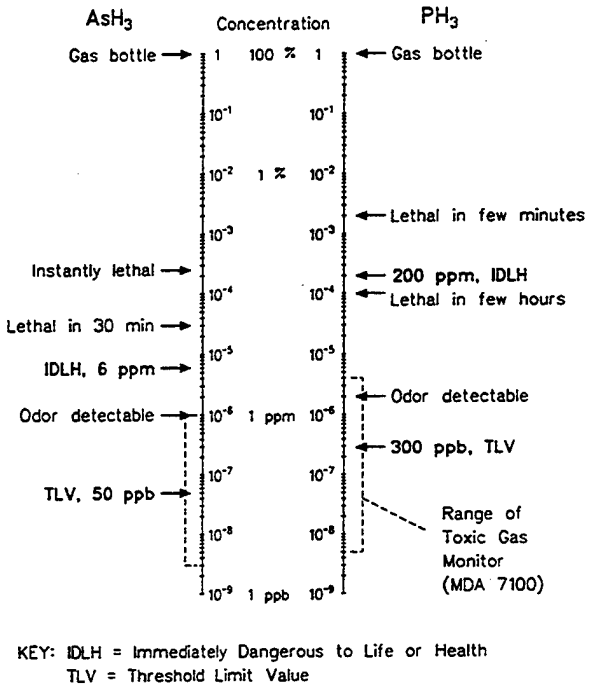

Figure A2.2.12. Critical concentrations of the toxic gases arsine AsH_3 and phosphine PH_3.

In our laboratory the hydride gas bottles and associated gas purge system, the gas handling system of figure A2.2.6, and the gas scrubber are housed in a single vented steel cabinet. The cabinet immediately adjoins the UHV MBE system and the hydride gas lines outside of the cabinet are under vacuum. A minimum amount of gas is stored on site (0.5–1.0 lbs of AsH_3 and 1–2 lbs of PH_3) in the same cabinet. The hydride flow rates are low (typically < 10 sccm) during growth and thus each bottle valve is left closed if there is no limited-flow aperture supplied with the gas bottle, minimizing the loss of toxic gas in case of a leak downstream of the gas bottles. Two toxic gas monitors are permanently connected to an integrated alarm system: a colorimetric paper tape monitor (MDA Scientific, Inc., model 7100) continuously checks the laboratory area and a solid-state sensor (IST Corp, model AG3100) monitors the exhaust air from the gas cabinet. The alarm system also provides an indication of loss of the main electrical power, loss of vacuum in the MBE system, insufficient flow of exhaust air from the room and gas cabinet, fire in the gas cabinet, insufficient nitrogen gas pressure for purging of the toxic gases, and excessive flow of the toxic gases from their storage bottles. The alarm system is connected to an automatic telephone dialing system which can alert key personnel on a 24 hour basis. The functioning of the alarm system is tested periodically. The MDA 7100 monitor and the microcomputer for control of the MBE system receive ac power from an uninterruptible power supply. A separate battery-operated toxic gas monitor (MDA model TLD-1) is used during gas bottle changes and during maintenance of the growth chamber.

All procedures for using the hydride gases, whether for epitaxial growth or for changing the gas bottles,

are carefully documented in a step-by-step procedure. The same procedure is used by each crystal grower at the start of each day of growth to bring the hydride gases into the gas handling system. In normal operation, all AsH_3 and PH_3 is purged from the gas handling system and bottle pressure regulators at the end of each day of growth, leaving the only AsH_3 and PH_3 present in the laboratory contained in the storage bottles. The amount of gas withdrawn from the bottles is noted and used to predict when the gas scrubber will need changing and when to order a replacement AsH_3 or PH_3 bottle. The toxic gas bottles are usually changed every 4–6 months.

The most unpredictable safety hazard of GSMBE is a phosphorus fire. This is most likely to occur during cleaning of the growth chamber or the vacuum pumps connected to the growth chamber. As discussed above, white phosphorus can ignite in air, and the resulting fire produces a dense white smoke which contains toxic PO_x oxides. Thus, each worker must wear self-contained breathing apparatus while the growth chamber is open to air. A fire may start spontaneously, but more likely it will be initiated by mechanical scraping on a phosphorus-coated metal surface. The chance of a phosphorus fire can be minimized by using low P_2 fluxes during growth, baking the growth chamber prior to opening to air, and flushing the chamber with dry cold N_2 gas during repairs. Liquid nitrogen is a very effective and clean fire extinguisher. Large phosphorus fluxes can lead to substantial phosphorus build-up in mechanical vacuum pumps, with fires occurring during pump maintenance [44]. Furthermore, the oxides in the smoke can react with the water in the air to form phosphoric acid, which in turn is highly corrosive. The corrosive smoke can result in serious damage to electronic equipment and adequate air exhaust in the laboratory must be provided to limit smoke damage. An 'elephant's trunk' connected to an exhaust duct can be very effective in removing the smoke (and toxic gases) when placed in the immediate vicinity of the working area or loosely connected to an open port on the growth chamber during repairs.

As shown in figure A2.2.6, a gas scrubber is used to convert vented AsH_3 and PH_3 from the gas handling system and any uncracked AsH_3 and PH_3 from the growth chamber into a stable form for safe disposal. For the small amount of hydrides used in GSMBE, we have found a dry filter containing potassium permanganate $KMnO_4$ to be a simple, cost-effective means of neutralizing the toxic gases. $KMnO_4$ is a dry solid that reacts with the hydrides to form non-volatile oxides. The scrubber consists of 100 lbs of Purafil Chemisorbant ($KMnO_4$ in an alumina binder) placed in a 15 gallon, sealable polyethylene drum which also serves as the final shipping container. The lid of the drum is fitted with two pipes: an inlet pipe for introduction of the effluent from the GSMBE system at the bottom of the Purafil and an outlet pipe near the top of the Purafil Chemisorbant for connection to the exhaust. When the scrubber is full, the pipes are disconnected and the drum is sealed for shipment; no handing of the contaminated Purafil is necessary. We have found the capacity of the Purafil scrubber to be very reproducible, with about 0.5 lbs of hydride adsorbed for every 100 lbs of Purafil. We change the scrubber when the toxic gas monitor first indicates that hydride is present in the exhaust from the scrubber, which occurs at intervals of 6–9 months. The scrubber material is then disposed of in a manner consistent with governmental regulations.

Although only relatively small quantities of AsH_3 and PH_3 are needed for GSMBE, their extreme toxicity presents serious safety issues. The possibility of more stringent environmental regulations could lead to elimination of these gases for commercial purposes in the future. Several, less toxic, direct replacements for the hydrides have appeared recently for use in MOMBE and MOCVD, and methods that reduce the hazards associated with on-site storage of the AsH_3 and PH_3 under pressure have been developed in recent years. The compounds tertiarybutylarsine (TBA) and tertiarybutylphosphine (TBP) are now available as substitutes for arsine and phosphine, respectively [47,48]. Both TBA and TBP are liquids at room temperature and exhibit vapour pressures that make delivery with a carrier gas feasible in both MOMBE and atmospheric MOCVD. Although TBA and TBP are still quite toxic, the spillage of a liquid presents substantially fewer hazards than the release of gaseous AsH_3 and PH_3 from high pressure gas cylinders. The major disadvantage of the organic materials TBA and TBP is carbon contamination of the epitaxial layers and their high cost.

One method to avoid the hazards during the transportation and storage of AsH_3 and PH_3 in pressurized cylinders is to use on-site generation of the hydride gas from less hazardous materials. Buckley *et al* [49] have shown that high purity arsine can be electrochemically generated at the point of use using an arsenic cathode in an aqueous electrolyte. The solid arsenic used in the electrolytic cell is considerably less hazardous than AsH_3 in compressed gas cylinders.

Finally, an alternative method for safer transportation and storage of the hydrides is to use adsorption of the hydrides in a molecular seive at atmospheric pressure [50]. The molecular sieve consists of a synthetic zeolite in a sealed container which is baked prior to absorbing either AsH_3 or PH_3 upon cooling to room temperature. The pressure at room temperature in the container is about one atmosphere and can be safely transported to the point of use. Upon heating to about 200°C, the AsH_3 or PH_3 is released; the recovery can be almost complete and thus little AsH_3 or PH_3 is lost. The zeolite is reusable and adequate volumes of gas can be easily stored [50], making the molecular sieve an attractive method of handing AsH_3 and PH_3. Arsine absorbed on zeolite has been used recently to grow GaAs by GSMBE and MOMBE [51].

Growth Procedure

We have used GSMBE to grow a variety of high quality III–V films on GaAs, GaP, InP, and Si substrates. Preparation of the III–V substrates followed the same procedures as used in conventional solid-source MBE [52]. Both GaAs and InP substrates with 'epi ready' and chemically etched protective oxide layers have been successfully used. Each substrate is mounted with indium solder on a molybdenum block, or in the case of a full 3-inch diameter wafer, mounted in a molybdenum ring without In solder. The protective oxide is then desorbed in the growth chamber by heating the block or ring under the appropriate group V molecular beam. Epitaxial growth then proceeds in a fashion identical to solid-source MBE.

In the case of growth on Si substrates, we have found the use of phosphorus in the growth chamber can influence the procedure for thermal cleaning of Si substrates. (100) Si substrates were etched in 5:1 H_2SO_4:H_2O_2, then transferred to a N_2 atmosphere and briefly etched in a HF:H_2O solution before loading into the MBE system. The substrates could then be cleaned in the growth chamber at 800°C for 20 min, using RHEED to monitor the surface cleanliness. The process was very reproducible and a number of InP-on-Si heterostructures were successfully grown [53, 54]. However, after about one year of growth in the same MBE chamber, it became increasing difficult to obtain a RHEED pattern typical of a clean well ordered Si surface, and the structural quality of the InP epitaxial films deteriorated noticeably. Measurements indicated that a small amount (i.e. a few atomic per cent) of P was being deposited on the hot wafer surface from the walls of the chamber. The P apparently reacted with any oxide on the Si surface to form a thin phosphosilicate layer whose vapour pressure was high enough to prevent adequate sublimation to occur at 800°C. By exposing the surface to a Ga molecular beam at a low flux (about 0.1 μm hr^{-1}) for 30 min at 800°C, a clean Si surface could be produced as evidenced by a well-defined (2×2) RHEED reconstruction pattern. Presumably the Ga decomposes the phosphosilicate layer, producing volatile reaction products at 800°C [55]. The Ga beam cleaning technique has consistently produced atomically clean Si surfaces in our phosphorus-based MBE system.

One advantage of GSMBE over sold-source MBE is the capability to rapidly alter the group V flux and produce abrupt changes in arsenic and phosphorus composition. This capability has been exploited in the growth of several quantum well heterostructures consisting of alternating arsenide and phosphide layers. Examples include QWs of GaAs with barriers of InGaP and QWs of InGaAs with barriers of InP. The growth is usually paused at each heterointerface to increase the smoothness of the growth front and to obtain atomically abrupt interfaces. Because of the high vapour pressure and low sticking coefficients of the group V elements, the switching of the group V molecular beams during the growth pause may produce an interfacial region with a composition that differs significantly from that of the surrounding well and barrier layers. A grading in bandgap and localized strain at the interface can result and can adversely affect device operation. The method of switching the AsH_3 and PH_3 gas flows and the pumping speed in the GSMBE chamber can greatly influence the interfacial compositional abruptness.

A typical example of the sequencing of the molecular beams during the growth of GaAs/InGaP QWs is shown in figure A2.2.13, where the $In_{0.48}Ga_{0.52}P$ alloy composition is chosen to be lattice matched to the GaAs substrate. The growth pause at the InGaP-to-GaAs interface is of duration $t_1 + t_2$ and at the GaAs-to-InGaP interface of duration $t_1' + t_2'$. During the interval t_1 the InGaP growth surface is allowed to anneal in a protective P_2 overpressure. The gases are then switched and growth recommences after interval t_2. A similar sequence is preformed at the GaAs-to-InGaP interface but using different intervals t_1' and t_2'. A systematic study of the effect of varying t_1, t_2, t_1' and t_2' on the structural and compositional abruptness of each interface was carried out using double-crystal x-ray (DCXR) diffraction, transmission

electron microscopy (TEM), photoluminescence (PL), and RHEED [33, 34]. It was found that t_1 = 10 s and t_1' = 30 s were long enough at the growth temperature to provide atomically abrupt interfaces. The InGaP surface required very little annealing, but the smoothness of GaAs surface improved with longer times for t_1'. The time t_2 (or t_2') must be chosen short enough to minimize intermixing on the group V sublattice resulting from incorporation of As (or P), but long enough to allow the residual P_2 (or As_2) to be pumped from the growth chamber and to allow the As_2 (or P_2) flux to stabilize before starting the growth of GaAs (or InGaP). With the pumping system of figure A2.2.4 and the gas handling system of figure A2.2.6, we found $t_2 = t_2'$ = 6 s or less to be suitable. Using this gas switching sequence GaAs/InGaP QWs have been grown in a reproducible manner with interfacial regions of 1–2 ml in thickness and with minimal As–P intermixing [34].

Similar considerations have been applied to the growth of InGaAs/InP QWs by GSMBE, where the $In_{0.53}Ga_{0.47}As$ alloy composition is lattice-matched to InP. Panish and co-workers [32, 56] had previously used a sequence similar to that of figure A2.2.13 where the group V beams are switched under conditions such that a group V overpressure is always present during each growth pause. Pausing for 5–15 s at each interface produced InGaAs-to-InP and InP-to-InGaAs interfaces which exhibited equal and opposite strains. The strained interfacial regions occur as result of asymmetric ordering inherent in the atomic arrangement of perfectly abrupt interfaces. Thus the interfaces obtained were atomically abrupt and ideal-like in composition. Atomically abrupt interfaces in InGaAs/InP heterostructures have also been obtained by Moy *et al* [35] but using a different gas-handling and pumping arrangement and a different gas switching sequence. Here growth is paused for 17–20 s, but P_2 and As_2 is rapidly pumped from the growth chamber and no group V overpressure is provided, except for a 10 s interval prior to recommencing growth of InGaAs. Apparently the lack of protective group V overpressure at the InGaAs-to-InP interface causes no adverse effects as long as the growth pause is kept short, but the As_2 beam prior to growth of InGaAs is needed to obtain an abrupt InP-to-InGaAs interface.

Another important issue is cross contamination of the group V elements during GSMBE growth. For example, P can be incorporated in GaAs as result of incomplete removal of P from the growth chamber by the vacuum pumps and cyropanels or from the evaporation of P from the walls of the growth chamber onto the growth surface. The degree of contamination is strongly dependent on the incorporation coefficient of the unwanted group V element; the design of the growth chamber and associated vacuum pumps, gas delivery system, and gas cracker; and the recent growth history of the MBE system. Figure A2.2.14 is a DCXR spectrum of a GaAs epitaxial film of 1.86 μm in thickness grown on a GaAs substrate one day after InP was grown in the same vacuum chamber and with the same gas cracker. Two peaks are can be resolved in the spectrum: the peak on the left is from the GaAs substrate and the peak on the right is from an epitaxial film of composition $GaAs_{0.999}P_{0.001}$. We have found As contamination in InP is somewhat higher than P in GaAs probably because the incorporation coefficient for As is larger than for P in InGaAsP [36]; the composition is typically $InP_{0.998}As_{0.002}$. For most applications, this level of group V contamination is insignificant.

The degree of cross contamination is undoubtedly higher in layers of heterojunction samples where the group V species from the previous layer has not been completely pumped out of the chamber before growth of the next layer begins. However, with proper sequencing of the AsH_3 and PH_3 gas flows, rapid gas switching, and adequate pumping in the growth chamber, cross contamination can be reduced to acceptable levels. Jackson and coworkers [31] have examined the degree of cross contamination in InGaAs/InP heterostructures and their results are seen in the SIMS depth profiles in figure A2.2.10. No growth pause was employed so that the speed of response of the hydride gas delivery system and gas cracker could be clearly evaluated. For the sample of figure A2.2.10(a), a single low conductance cracker and a slow gas switching system was used. A long P tail penetrates deep in the InGaAs layer and the residual P is substantial (> 0.01%). In figure A2.2.10(b), separate high conductance crackers were used for AsH_3 and PH_3 along with a fast gas switching system. The P tail is greatly reduced and the residual P in the InGaAs is below the SIMS detection limit (< 0.0003%). Thus, cross contamination of the group V elements in heterostructures can be reduced to insignificant levels.

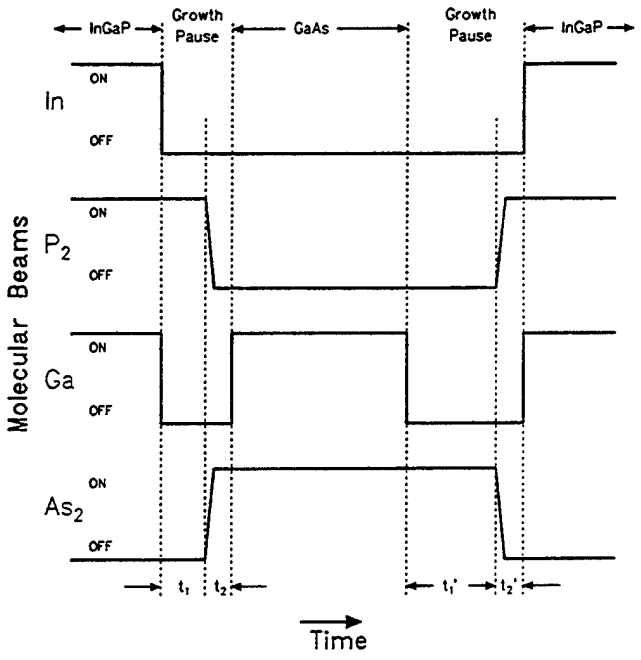

Figure A2.2.13. Sequence of molecular beams during the growth of InGaP/GaAs heterostructures. Growth is interrupted by closing the group III shutters at the InGaP-to-GaAs interface for the period $t_1 + t_2$ and at the GaAs-to-InGaP interface for the period $t_1' + t_2'$. Annealing of the growth front occurs during the intervals t_1 and t_1'.

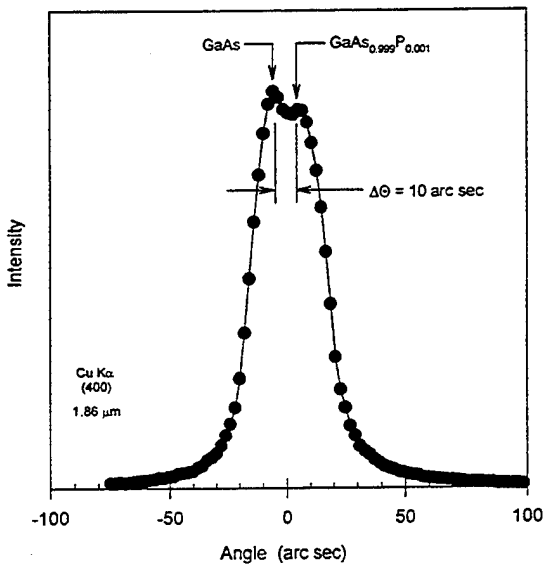

Figure A2.2.14. High resolution double-crystal x-ray rocking curve of a GaAs film grown on a GaAs substrate using a GSMBE growth chamber with residual phosphorus vapour. The composition of the film is determined to be $GaAs_{0.999}P_{0.001}$ from the separation of the film peak and the substrate peak.

A2.2.2 SUMMARY

We have previously stated that the primary advantage of GSMBE is the capability to grow a wide variety of III–V materials in one growth chamber with relative ease. This capability is illustrated in figure A2.2.15 where PL spectra are shown for a variety of III–V samples, all grown in the same GSMBE chamber. Each sample consisted of an epitaxial layer of 1–2 μm in thickness and lattice matched to the appropriate substrate material. The materials range from the InGaAs with emission in the infrared region of the spectrum to alloys of InGaAlP with emission in the visible region. Portions of the spectrum not covered in figure A2.2.15 have been addressed with lattice mismatched (i.e. strained) alloys and QW heterostructures of the same materials. Growth of any of the materials shown can take place in any order and in the same day, without compromising film quality. Thus, GSMBE allows great flexibility in sample design as well as scheduling of growth runs.

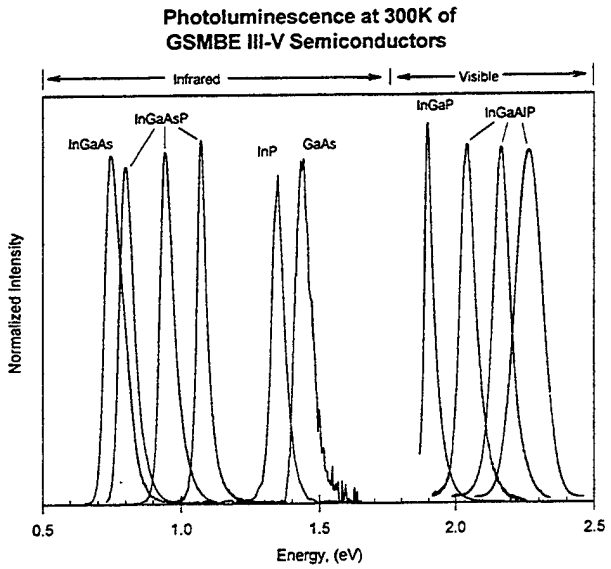

Figure A2.2.15. Photoluminescence spectra of different III–V epitaxial samples grown in the same GSMBE growth chamber. Note the wide range of energies for the emitted light. The InGaAs, InGaAsP, and InP samples were lattice matched to InP substrates, and the InGaP, InGaAlP, and GaAs samples were lattice matched to GaAs substrates.

When combined with the precise control of layer thicknesses on the atomic scale of conventional MBE, GSMBE is a powerful tool for fabricating a wide range of III–V heteroepitaxial devices. This feature is exemplified by the high resolution TEM lattice image in figure A2.2.16 of the cross section of a GaAs/InGaP QW sample grown by GSMBE [57]. Here a film of GaAs only two monolayers (0.57 nm) in thickness is bounded on both sides with thick layers of lattice-matched InGaP. Heterostructures with similar interface abruptness and layer thickness control have been routinely obtained in other III–V material combinations using GSMBE technology

In summary, we have provided the technological details for the design and operation of a GSMBE system when using the hydride gases as source materials for arsenic and phosphorus. With the procedures outlined, reproducible epitaxial growth of complex heterostructures can be achieved in a safe and reliable manner.

Acknowledgements

The development and implementation of GSMBE in our laboratory was largely accomplished by the efforts of M J Hafich and the author gratefully acknowledges his substantial contributions. The author would also like to acknowledge the graduate students and post-doctoral fellows in our MBE laboratory, M D Crook,

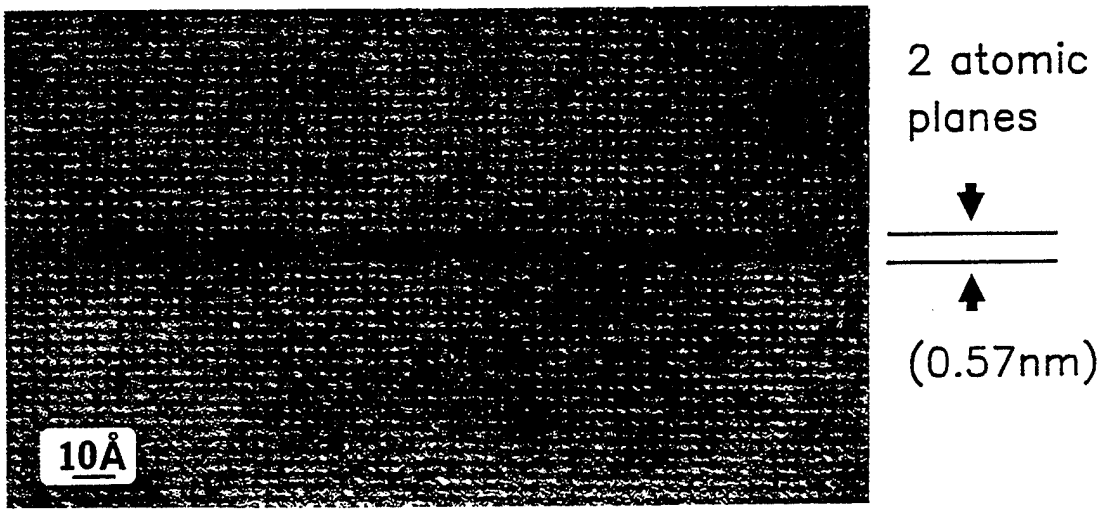

Figure A2.2.16. TEM lattice image of a [010] cross section of a InGaP/GaAs quantum well grown by GSMBE. The GaAs well layer is the thin darker band across the centre of the micrograph. The {200} atomic planes are resolved and the GaAs QW is two monolayers thick with atomically abrupt interfaces. TEM photo by N Otsuka and D Li at Purdue University.

T E Crumbaker, H Y Lee, A Nanda, G A Patrizi, J H Quigley, P Silvestre, R L Stave, P Thiagarajan, T J Vogt, and L M Woods, who have made many valuable contributions to our GSMBE research program. This work was supported by the Air Force Office of Scientific Research, National Science Foundation (including the Optoelectronic Computing Systems Center), Air Force Rome Laboratory, and Advanced Research Projects Agency.

REFERENCES

[1] Panish M B and Temkin H 1993 *Gas Source Molecular Beam Epitaxy* 1st edn (New York: Springer)
[2] Kuroda N, Sugou S, Sakaki T and Kitamura M 1993 *Proc. 5th Int. Conf. on InP and Related Materials (Paris)*
[3] Morris F J and Fukui H 1974 *J. Vac. Sci. Technol.* **11** 506
[4] Panish M B 1980 *J. Electrochem. Soc.* **127** 2729
[5] Calawa A R 1981 *Appl. Phys. Lett* **38** 701
[6] Panish M B and Hamm R A 1986 *J. Crystal Growth* **78** 445
[7] Panish M B and Sumski S 1984 *J. Appl. Phys.* **55** 3571
[8] Cunningham J E, Chiu T H, Timp G, Agyekum E and Tsang W T 1988 *Appl. Phys. Lett.* **53** 1285
[9] Lambert M, Péralès A, Vergnaund R and Stack C 1990 *J. Crystal Growth* **105** 97
[10] Huet D and Lambert M 1986 *J. Electron. Mat.* **15** 37
[11] Panish M B and Temkin H 1984 *Appl. Phys. Lett* **44** 785
[12] Temkin H, Chu S N G, Panish M B and Logan R A1987 *Appl. Phys. Lett* **50** 956
[13] Wu M C, Chen Y K, Chin M A and Sergent A M 1992 *IEEE Photon. Technol. Lett.* **4** 676
[14] Nottenburg R N, Chen Y K, Panish M B, Humphrey D A and Hamm R A 1989 *IEEE Electron. Dev. Lett.* **10** 30
[15] Wey W G, Gibony K S, Bowers J E, Rodwell M J W, Silvestre P, Thiagarajan P and Robinson G Y 1993 *IEEE Photon. Technol. Lett.* **5** 1310
[16] Temkin H, Gershoni D and Panish M B *Appl. Phys. Lett* **50** 1776
[17] Powell R C, Lee N-E and Green J E 1992 *Appl. Phys. Lett* **60** 2505
[18] Baillargeon J N, Cheng K Y, Hofler G E, Pearah P J and Hsieh K C 1992 *Appl. Phys. Lett.* **60** 2540
[19] Pessa M, Hakkarainen T, Keskinen J, Rakennus K, Salokatve A, Zhang G and Asonen H 1990 *Proc. SPIE Int. Conf. on Physical Concepts for Novel Optoelectronic Device Applications (Aachen, 1990)* p 1
[20] Stanley C R, Farrow R F C and Sullivan P W 1985 *The Technology and Physics of Molecular Beam Epitaxy* ed E H C Parker (New York: Plenum) p 275
[21] Corbridge D E C 1978 *Phosphorous: An Outline of Its Chemistry, Biochemistry and Technology* (Amsterdam: Elsevier)
[22] Asahi H, Kawamura Y, Ikeda M and Okamoto H 1981 *J. Appl. Phys.* **52** 2852

[23] Asahi H, Kawamura Y and Nagai H 1982 *J. Appl. Phys.* **53** 4928
[24] Wright S L and Kroemer H 1982 *J. Vac. Sci. Technol.* **20** 143
[25] Miller D L, Bose S S and Sullivan G J 1990 *J. Vac. Sci. Technol.* B **8** 311
[26] Doto M L, Golmayo D and Briones F 1993 *J. Crystal Growth* **127** 619
[27] Johnson F G, Wicks G W, Viturro R E and LaForce R 1993 *J. Vac. Sci. Technol.* B **11** 823
[28] Baillargeon J N, Cho A Y, Fisher R J, Pearah P J and Cheng K Y 1994 *J. Vac. Sci. Technol.* B **12** 1106
[29] McCollum M J, Plano M A, Hasse M, Robbins V M, Jackson S L, Cheng K Y and Stillman G E 1989 *Proc. Int. Conf. on InP and Related Materials (Norman, OK)*
[30] Ishikawa H, Ando H, Kondo K, Sandhu A, Miyauchi E, Fujii T and Hiyamizu S 1990 *J. Vac. Sci. Technol.* A **8** 805
[31] Jackson S L, Baillargeon J N, Curtis A P, Lui X, Baker J E, Malin J I, Hsieh K C, Bishop S G, Cheng K Y and Stillman G E 1993 *J. Vac. Sci. Technol.* B **11** 1045
[32] Vandenberg J M, Chu S N G, Hamm R A, Panish M B and Temkin H 1986 *Appl. Phys. Lett* **49** 1302
[33] Lee H Y, Hafich M J and Robinson G Y 1990 *J. Crystal Growth* **105** 244
[34] Lee H Y, Hafich M J, Mahalingam K, Otsuka N and Robinson G Y 1991 *J. Crystal Growth* **111** 525
[35] Moy A M, Chen A C, Jackson S L, Lui X, Cheng K Y, Stillman G E and Bishop S G 1993 *J. Vac. Sci. Technol.* B **11** 826
[36] Silvestre P, Hafich M J, Vogt T, Nanda A, Robinson G Y, Dudly J J, Bowers J E, Jones K M and Al-Jassim M M 1992 *J. Vac. Sci. Technol.* B **10** 956
[37] Chow R and Chai Y G 1983 *J. Vac. Sci. Technol.* A **1** 49
[38] Hafich M J, Lee H Y, Silvestre P and Robinson G Y 1991 *J. Crystal Growth* **111** 507
[39] Santos M B, Cunningham J E and Jan W Y 1993 *Proc. North American Conf. on Molecular Beam Epitaxy (Stanford, CA, 1993)*
[40] Hafich M J, Lee H Y, Robinson G Y, Li D and Otsuka N 1991 *J. Appl. Phys.* **69** 752
[41] Hafich M J, Woods L M, Kim H S, Patrizi G A and Robinson G Y, 1993 *J. Crystal Growth* **127** 995
[42] McIntyre A J and Sherin B J 1989 *Solid State Technol.* 119–26
[43] Arsine Poisoning in the Workplace 1979 *Current Intelligence Bulletin 32* NIOSH Publication No. 79-142 (Washington, DC: US Department of Health, Education, and Welfare)
[44] Wicks G W, Koch M W, Johnson F G, Varriano J A, Kohnke G E and Colombo P 1993 *Proc. North American Conf. on Molecular Beam Epitaxy (Stanford, CA)* paper IV.7
[45] Korolkoff N O 1989 *Solid State Technol.* **49**
[46] *Proc. American Conf. of Governmental Industrial Hygienists (ACGIH) (Cincinnati, OH, 1986)* 5th edn
[47] Miller G A 1989 *Solid State Technol.* 59–60
[48] FitzGerald M 1991 *Solid State Technol.* 53–5
[49] Buckley D N, Seabury C W, Valdes J L, Cadet G, Mitchell J W, DiGiuseppe M A, Smith R C, Filipe J R C, Bylsma R B, Chakrabarti U K and Wang K-W 1990 *Appl. Phys. Lett* **57** 1684
[50] Sillmon R S and Freitas Jr J A 1990 *Appl. Phys. Lett* **56** 174
[51] Ballingall J M, Mazurowski J S, Martin P A, McManus J and Tom G 1993 *Proc. North American Conf. on Molecular Beam Epitaxy (Stanford, CA)* paper X.6
[52] Herman M A and Sitter H (eds) 1989 *Molecular Beam Epitaxy: Fundaments and Current Status* (New York: Springer)
[53] Crumbaker T E, Lee H Y, Hafich M J and Robinson G Y 1989 *Appl. Phys. Lett.* **54** 140
[54] Crumbaker T E, Lee H Y, Hafich M J, Robinson G Y, Al-Jassim M M and Jones K M 1990 *J. Vac. Sci. Technol.* B **8** 261
[55] Wright S and Kroemer H 1980 *Appl. Phys. Lett* **36** 210
[56] Vandenberg J M, Panish M B, Temkin H and Hamm R A 1988 *Appl. Phys. Lett.* **53** 1920
[57] Hafich M J, Quigley J H, Owens R E, Robinson G Y, Li D and Otsuka N 1989 *Appl. Phys. Lett* **54** 2686
[58] Panish M B, Temkin H and Sumski S 1985 *J. Vac. Sci. Technol.* B **3** 657

